12-2016

# Model Predictive Control of a Nonlinear Aeroelastic System Using Volterra Series Representations

Wai Leuk Law

# MODEL PREDICTIVE CONTROL OF A NONLINEAR AEROELASTIC SYSTEM USING VOLTERRA SERIES REPRESENTATIONS

by

Wai Leuk Law

A Thesis Submitted to the College of Engineering and the Department of Aerospace Engineering in Partial Fulfillment of the Requirements for the Degree of

Master of Science in Aerospace Engineering

December 2016

Embry-Riddle Aeronautical University

Daytona Beach, Florida

MODEL PREDICTIVE CONTROL OF A NONLINEAR AEROELASTIC SYSTEM USING VOLTERRA SERIES REPRESENTATIONS

by

Wai Leuk Law

A Thesis prepared under the direction of the candidate's committee chairman, Dr. Richard Prazenica, Department of Aerospace Engineering, and has been approved by the members of the thesis committee. It was submitted to the School of Graduate Studies and Research and was accepted in partial fulfillment of the requirements for the degree of Master of Science in Aerospace Engineering.

THESIS COMMITTEE

Chairman, Dr. Richard Prazenica

Member, Dr. Mark Balas

Member, Dr. Troy Henderson

Graduate Program Coordinator, Dr. Magdy Attia — Date: 11·28·2016

Associate Dean of College of Engineering, Dr. Yi Zhao — Date: 11/28/2016

Vice Chancellor, Academic Support, Dr. Christopher Grant — Date: 11/29/16

## ACKNOWLEDGMENTS

I would like to express my gratitude to my advisor Dr. Richard Prazenica for his invaluable guidance, encouragement and support not only for my Masters research but over the course of my five years of education here at Embry-Riddle Aeronautical University. I would also like to thank the rest of my thesis committee: Dr. Mark Balas and Dr. Troy Henderson for their assistance and share of knowledge throughout this memorable journey as a graduate student.

Last but not least, I would like to thank my parents and friend for all the help and support received throughout my studies. They have worked tirelessly and made sacrifices to give me the best chance to attend and pursue my dream and for that I am forever thankful. Without their guidance, encouragement and unconditional love I would not be completing this thesis and graduating with the degree of Master of Science in Aerospace Engineering.

TABLE OF CONTENTS

Page

LIST OF TABLES . . . . . vi

LIST OF FIGURES . . . . . x

SYMBOLS . . . . . xvii

ABBREVIATIONS . . . . . xviii

ABSTRACT . . . . . xix

1 Introduction . . . . . 1
- 1.1 Model Predictive Control . . . . . 1
- 1.2 The Evolution of MPC . . . . . 2
- 1.3 Concept, Procedures and Objectives of MPC . . . . . 7
- 1.4 MPC Applications . . . . . 12
- 1.5 Introduction on Volterra Series . . . . . 19
- 1.6 Motivation and Objective . . . . . 20

2 Prototypical Aeroelastic Systems and Simulation Setup . . . . . 23
- 2.1 Texas A&M Nonlinear Aeroelastic Testbed . . . . . 23
- 2.2 Open-Loop Response of the Aeroelastic System . . . . . 29
- 2.3 Classical Linear Quadratic Regulator (LQR) Control . . . . . 33

3 Volterra Modeling & MPC Algorithm . . . . . 37
- 3.1 Volterra Series Representations . . . . . 37
- 3.2 Volterra Kernel Identification . . . . . 38
- 3.3 Volterra-Based Model Predictive Control Algorithm . . . . . 43

4 Controller Implementation on a Linear Aeroelastic System . . . . . 49
- 4.1 Classical LQR Baseline Controller . . . . . 49
  - 4.1.1 Continuous-Time LQR: Free-stream Velocity at 6 m/s . . . 52
  - 4.1.2 Continuous-Time LQR: Free-stream Velocity at 12.5 m/s . . 57
  - 4.1.3 Discrete-Time LQR: Free-stream Velocity at 6 m/s . . . . . 61
  - 4.1.4 Discrete-Time LQR: Free-stream Velocity at 12.5 m/s . . . . 65
- 4.2 LMPC Stability . . . . . 69
  - 4.2.1 Method 1: Terminal Constraint . . . . . 69
  - 4.2.2 Method 2: Terminal Cost Term . . . . . 72
- 4.3 LQR Fixed Horizon Controller . . . . . 75
- 4.4 Linear Volterra-Based MPC . . . . . 80

Page

4.4.1 LMPC: Free-stream Velocity at 6 m/s . . . . . 80
4.4.2 LMPC: Free-stream Velocity at 12.5 m/s . . . . . 86

5 Controller Implementation on a Nonlinear Aeroelastic System . . . . . 92
5.1 Classical LQR Baseline Controller . . . . . 92
5.1.1 Discrete-Time LQR: Free-stream Velocity at 6 m/s . . . . . 94
5.1.2 Discrete-Time LQR: Free-stream Velocity at 12.5 m/s . . . . 98
5.2 NMPC Stability . . . . . 102
5.2.1 Method 1: Tuning Design Parameters . . . . . 102
5.2.2 Method 2: Modify Constraints Requirement . . . . . 103
5.2.3 Method 3: Quasi-Infinite Horizon NMPC Scheme . . . . . 104
5.3 Nonlinear Volterra-Based MPC . . . . . 108
5.3.1 NMPC: Free-stream Velocity at 6 m/s . . . . . 108
5.3.2 The Effect of Control Discretization and Predictive Model . 109
5.3.3 The Effect of Control Horizon . . . . . 124
5.3.4 The Effect of Volterra Kernel Padding . . . . . 128
5.3.5 The Effect of Cost Function Weighting . . . . . 132
5.3.6 NMPC Design Summary at U = 6 m/s . . . . . 136
5.4 NMPC: Free-stream Velocity at 12.5 m/s . . . . . 141
5.4.1 Regulator Case . . . . . 142
5.4.2 Tracking Case . . . . . 148

6 Conclusion and Future Work . . . . . 151
6.1 Conclusion . . . . . 151
6.2 Future Work . . . . . 152

REFERENCES . . . . . 154

A Numerical Values of A and B Matrices for the Aeroelastic System . . . . 160

# LIST OF TABLES


| Table | | Page |
|---|---|---|
| 1.1 | MPC academic research with industry, MPC type and years. | 13 |
| 2.1 | Parameters values for the pitch-plunge aeroelastic system. | 26 |
| 2.2 | Eigenvalues for the linear aeroelastic system. | 29 |
| 4.1 | Maximum value for each state in $Q$ using method 1 for the continuous-time LQR controller at 6 m/s. | 50 |
| 4.2 | Maximum value for each state in $Q$ using method 1 for the continuous-time LQR controller at 12.5 m/s. | 50 |
| 4.3 | Maximum value for each state in $Q$ using method 2 for the continuous-time LQR controller at 6 m/s. | 50 |
| 4.4 | Maximum value for each state in $Q$ using method 2 for the continuous-time LQR controller at 12.5 m/s. | 51 |
| 4.5 | Maximum value for each state in $Q$ using method 1 for the discrete-time LQR controller at 6 m/s. | 51 |
| 4.6 | Maximum value for each state in $Q$ using method 1 for the discrete-time LQR controller at 12.5 m/s. | 51 |
| 4.7 | Maximum value for each state in $Q$ using method 2 for the discrete-time LQR controller at 6 m/s. | 52 |
| 4.8 | Maximum value for each state in $Q$ using method 2 for the discrete-time LQR controller at 12.5 m/s. | 52 |
| 4.9 | RMSE and control effort for LQR controller using method 1 to determine the $Q$ matrix at 6 m/s. | 54 |
| 4.10 | RMSE and control effort for LQR controller using method 2 to determine the $Q$ matrix at 6 m/s. | 55 |
| 4.11 | RMSE and control effort for LQR controller using method 1 to determine the $Q$ matrix at 12.5 m/s. | 57 |
| 4.12 | RMSE and control effort for LQR controller using method 2 to determine the $Q$ matrix at 12.5 m/s. | 59 |

Table Page

4.13 RMSE and control effort for discrete-time LQR controller using method 1 to determine the $Q$ matrix at 6 m/s. . . . . 61

4.14 RMSE and control effort for discrete-time LQR controller using method 2 to determine the $Q$ matrix at 6 m/s. . . . . 63

4.15 RMSE and control effort for discrete-time LQR controller using method 1 to determine the $Q$ matrix at 12.5 m/s. . . . . 65

4.16 RMSE and control effort for discrete-time LQR controller using method 2 to determine the $Q$ matrix at 12.5 m/s. . . . . 67

4.17 RMSE and control effort for LMPC regulator case on the linear aeroelastic system at 6 m/s. . . . . 82

4.18 RMSE and control effort comparison between chosen controllers at U = 6 m/s. . . . . 84

4.19 RMSE and control effort for tracking case using LMPC on the linear aeroelastic system at 6 m/s. . . . . 86

4.20 RMSE and control effort for regulator case using LMPC on the linear aeroelastic system at 12.5 m/s. . . . . 88

4.21 RMSE and control effort comparison between chosen controllers at U = 12.5 m/s. . . . . 90

4.22 RMSE and control effort for tracking case using LMPC on the linear aeroelastic system at 12.5 m/s. . . . . 90

5.1 Maximum value for each state in $Q$ using method 1 for tuning the LQR controller at 6 m/s. . . . . 93

5.2 Maximum value for each state in $Q$ using method 1 for tuning the LQR controller at 12.5 m/s. . . . . 93

5.3 Maximum value for each state in $Q$ using method 2 for tuning the LQR controller at 6 m/s. . . . . 93

5.4 Maximum value for each state in $Q$ using method 2 for tuning the LQR controller at 12.5 m/s. . . . . 94

5.5 RMSE and control effort for the discrete-time LQR controller using method 1 to determine the $Q$ matrix on the nonlinear aeroelastic system at U = 6 m/s. . . . . 96

5.6 RMSE and control effort for the discrete-time LQR controller using method 2 to determine the $Q$ matrix on the nonlinear aeroelastic system at U = 6 m/s. . . . . 96

Table Page

5.7 RMSE and control effort for the discrete-time LQR controller using method 1 to determine the $Q$ matrix on the nonlinear aeroelastic system at U = 12.5 m/s. . . . . 98

5.8 RMSE and control effort for the discrete-time LQR controller using method 2 to determine the $Q$ matrix on the nonlinear aeroelastic system at U = 12.5 m/s. . . . . 100

5.9 RMSE and control effort for Linear MPC regulator case with $T_H = 4$ *sec* and $T_C = 2$ *sec* for various control discretizations ($\Delta T_D$). . . . . 111

5.10 RMSE for Linear MPC tracking case at $T_H = 4$ *sec* and $T_C = 2$ *sec* with various control discretizations ($\Delta T_D$). . . . . 113

5.11 RMSE and control effort for second- and third-order NMPC regulator case with $T_H = 2$ *sec* and $T_C = 2$ *sec* with various control discretizations ($\Delta T_D$). . . . . 114

5.12 RMSE and control effort for second- and third-order NMPC tracking cases with $T_H = 2$ *sec* and $T_C = 2$ *sec* with various control discretizations ($\Delta T_D$). . . . . 120

5.13 RMSE and control effort for nonlinear regulator case using NMPC with varying control time horizon. . . . . 124

5.14 RMSE and control effort for nonlinear tracking case using NMPC with varying control time horizon. . . . . 126

5.15 RMSE and control effort for nonlinear regulator and tracking cases using NMPC with padded and non-padded Volterra kernels. . . . . 129

5.16 RMSE and control effort for nonlinear regulator case with various combinations of pitch and control weighting factors. . . . . 134

5.17 RMSE for tracking case with various combinations of pitch and control weighting factors. . . . . 135

5.18 NMPC final design parameters with quantitative analysis results for both nonlinear regulator and tracking cases. . . . . 136

5.19 RMSE and control effort comparison between chosen controllers at U = 6 m/s. . . . . 141

5.20 RMSE and control effort for regulator case at 12.5 m/s. . . . . 144

5.21 RMSE and control effort for regulator case at U = 12.5 m/s with various combinations of weights. . . . . 146

Table Page

5.22 RMSE and control effort comparison between chosen controllers at U = 12.5 m/s. . . . . 148

5.23 RMSE and control effort for tracking case at U = 12.5 m/s. . . . . 148

# LIST OF FIGURES


| Figure | | Page |
|---|---|---|
| 1.1 | Evolutionary tree for MPC technology development (Qin & Badgwell, 2003). | 2 |
| 1.2 | Conventional vs. MPC structure on hierarchy control system in processing plants (Deshmukh & Sawarkar, 2015). | 4 |
| 1.3 | Relationship between process transfer function matrix and degrees of freedom (J. B. Froisy, 1994). | 6 |
| 1.4 | MPC controller block diagram (Seborg, Mellichamp, Edgar, & Doyle III, 2010). | 8 |
| 1.5 | Basic concept of MPC and receding horizon strategy (Dai, Mahmoud, Fu, & Xia, 2012). | 10 |
| 1.6 | MPC technology in different industrial areas (Qin & Badgwell, 2003). | 12 |
| 1.7 | The use of MPC techniques in US industries (Bemporad, 2015). | 13 |
| 1.8 | McDonnell Douglas AV-8B Harrier II performing VTOL on an aircraft carrier (Abyss, 2016). | 15 |
| 2.1 | Schematic of the Texas A&M Nonlinear Aeroelastic Testbed Apparatus (NATA) with airfoil and control surface (W. Silva, Strganac, & Hajj, 2005). | 23 |
| 2.2 | Aeroelastic system simulation setup in Simulink. | 28 |
| 2.3 | Open-loop plunge response for both linear and nonlinear aeroelastic systems at 6 m/s. | 31 |
| 2.4 | Open-loop pitch response for both linear and nonlinear aeroelastic systems at 6 m/s. | 31 |
| 2.5 | Open-loop plunge response for both linear and nonlinear aeroelastic systems at 12.5 m/s. | 32 |
| 2.6 | Open-loop pitch response for both linear and nonlinear aeroelastic systems at 12.5 m/s. | 32 |
| 2.7 | Linear aeroelastic system with LQR controller in Simulink. | 36 |
| 2.8 | Nonlinear aeroelastic system with LQR controller in Simulink. | 36 |

Figure Page

3.1 Identified first- and second-order pitch and plunge Volterra kernels at $U =$ 6 m/s (Prazenica, 2014). . . . . 42

3.2 Optimization function *fmincon* routine in flowchart form. . . . . 47

3.3 MPC routine in flowchart form. . . . . 48

4.1 Pitch response for LQR baseline controller on the linear aeroelastic system with $Q$ chosen using method 1 at 6 m/s. . . . . 53

4.2 Control effort for LQR baseline controller on the linear aeroelastic system with $Q$ chosen using method 1 at 6 m/s. . . . . 53

4.3 Pitch response for LQR baseline controller on the linear aeroelastic system with $Q$ chosen using method two. . . . . 56

4.4 Control effort for LQR baseline controller on the linear aeroelastic system with $Q$ chosen using method two. . . . . 56

4.5 Pitch response for LQR baseline controller on the linear aeroelastic system at U = 12.5 m/s with $Q$ chosen using method one. . . . . 58

4.6 Control effort for LQR baseline controller on the linear aeroelastic system at U = 12.5 m/s with $Q$ chosen using method one. . . . . 58

4.7 Pitch response for LQR baseline controller on the linear aeroelastic system at U = 12.5 m/s with $Q$ chosen using method two. . . . . 60

4.8 Control effort for LQR baseline controller on the linear aeroelastic system at U = 12.5 m/s with $Q$ chosen using method two. . . . . 60

4.9 Pitch response for discrete-time LQR baseline controller on the linear aeroelastic system with $Q$ chosen using method 1 at 6 m/s. . . . . 62

4.10 Control effort for discrete-time LQR baseline controller on the linear aeroelastic system with $Q$ chosen using method 1 at 6 m/s. . . . . 62

4.11 Pitch response for discrete-time LQR baseline controller on the linear aeroelastic system with $Q$ chosen using method two. . . . . 64

4.12 Control effort for discrete-time LQR baseline controller on the linear aeroelastic system with $Q$ chosen using method two. . . . . 64

4.13 Pitch response for discrete-time LQR baseline controller on the linear aeroelastic system at U = 12.5 m/s with $Q$ chosen using method one. . 66

4.14 Control effort for discrete-time LQR baseline controller on the linear aeroelastic system at U = 12.5 m/s with $Q$ chosen using method one. . . . . 66

Figure Page

4.15 Pitch response for discrete-time LQR baseline controller on the linear aeroelastic system at U = 12.5 m/s with $Q$ chosen using method two. . 68

4.16 Control effort for discrete-time LQR baseline controller on the linear aeroelastic system at U = 12.5 m/s with $Q$ chosen using method two. . . . . 68

4.17 Diagonal value of $P$ within the fixed horizon at 6 m/s with Q matrix defined using method 1. . . . . 76

4.18 Comparison between infinite and fixed horizon LQR controller at 6 m/s with Q matrix defined using method 1. . . . . 78

4.19 Comparison between infinite and fixed horizon LQR controller at 6 m/s with Q matrix defined using method 2. . . . . 78

4.20 Comparison between infinite and fixed horizon LQR controller at 12.5 m/s with Q matrix defined using method 1. . . . . 79

4.21 Comparison between infinite and fixed horizon LQR controller at 12.5 m/s with Q matrix defined using method 2. . . . . 79

4.22 Regulator case pitch response for LMPC on the linear aeroelastic system at 6 m/s. . . . . 81

4.23 Regulator case control effort for LMPC on the linear aeroelastic system at 6 m/s. . . . . 81

4.24 Pitch response comparison between open-loop, discrete-time LQR and LMPC on the linear system at free-stream velocity of 6 m/s. . . . . 83

4.25 Control effort comparison between the discrete-time LQR and LMPC on the linear system at free-stream velocity of 6 m/s. . . . . 83

4.26 Tracking case pitch response using LMPC on the linear aeroelastic system at 6 m/s. . . . . 85

4.27 Tracking case control effort using LMPC on the linear aeroelastic system at 6 m/s. . . . . 85

4.28 Regulator case pitch response using LMPC on the linear aeroelastic system at 12.5 m/s. . . . . 87

4.29 Regulator case control effort using LMPC on the linear aeroelastic system at 12.5 m/s. . . . . 87

4.30 Pitch response comparison between open-loop, discrete-time LQR and LMPC for the linear system at U = 12.5 m/s. . . . . 89

4.31 Control effort comparison between the discrete-time LQR and LMPC controllers on the linear system at U = 12.5 m/s. . . . . 89

Figure Page

4.32 Tracking case pitch response using LMPC on the linear aeroelastic system at 12.5 m/s. . . . . 91

4.33 Tracking case control effort using LMPC on the linear aeroelastic system at 12.5 m/s. . . . . 91

5.1 Pitch response for discrete-time LQR baseline controller on the nonlinear aeroelastic system with $Q$ chosen using method 1 at U = 6 m/s. . . . . 95

5.2 Control effort for discrete-time LQR baseline controller on the nonlinear aeroelastic system with $Q$ chosen using method 1 at U = 6 m/s. . . . . 95

5.3 Pitch response for discrete-time LQR baseline controller on the nonlinear aeroelastic system with $Q$ chosen using method 2 at U = 6 m/s. . . . . 97

5.4 Control effort for discrete-time LQR baseline controller on the nonlinear aeroelastic system with $Q$ chosen using method 2 at U = 6 m/s. . . . . 97

5.5 Pitch response for the discrete-time LQR baseline controller on the nonlinear aeroelastic system with $Q$ chosen using method 1 at U = 12.5 m/s. 99

5.6 Control effort for the discrete-time LQR baseline controller on the nonlinear aeroelastic system with $Q$ chosen using method 1 at U = 12.5 m/s. 99

5.7 Pitch response for the discrete-time LQR baseline controller on the nonlinear aeroelastic system with $Q$ chosen using method 2 at U = 12.5 m/s. 101

5.8 Control effort for the discrete-time LQR baseline controller on the nonlinear aeroelastic system with $Q$ chosen using method 2 at U = 12.5 m/s. 101

5.9 Pitch response for nonlinear regulator case using the linear predictive model with different control discretizations with $T_H = 4$ *sec* and $T_C = 2$ *sec*. . . . . 110

5.10 Control effort for nonlinear regulator case using the linear predictive model with different control discretizations with $T_H = 4$ *sec* and $T_C = 2$ *sec*. . 110

5.11 Pitch response for nonlinear tracking case using the linear predictive model with different control discretizations with $T_H = 4$ *sec* and $T_C = 2$ *sec*. . 112

5.12 Control effort for nonlinear tracking case using the linear predictive model with different control discretizations with $T_H = 4$ *sec* and $T_C = 2$ *sec*. . 112

5.13 Pitch response for nonlinear regulator case using the second-order nonlinear predictive model with different control discretizations with $T_H = 2$ *sec* and $T_C = 2$ *sec*. . . . . 115

Figure Page

5.14 Control effort for nonlinear regulator case using the second-order nonlinear predictive model with different control discretizations with $T_H = 2$ *sec* and $T_C = 2$ *sec*. . . . . 115

5.15 Pitch response for nonlinear regulator case using the third-order nonlinear predictive model with different control discretizations with $T_H = 2$ *sec* and $T_C = 2$ *sec*. . . . . 116

5.16 Control effort for nonlinear regulator case using the third-order predictive model with different control discretizations with $T_H = 2$ *sec* and $T_C = 2$ *sec*. . . . . 116

5.17 Pitch response for nonlinear tracking case using the second-order nonlinear predictive model with different control discretizations with $T_H = 2$ *sec* and $T_C = 2$ *sec*. . . . . 118

5.18 Control effort for nonlinear tracking case using the second-order nonlinear predictive model with different control discretizations with $T_H = 2$ *sec* and $T_C = 2$ *sec*. . . . . 118

5.19 Pitch response for nonlinear tracking case using the third-order nonlinear predictive model with different control discretizations with $T_H = 2$ *sec* and $T_C = 2$ *sec*. . . . . 119

5.20 Control effort for nonlinear tracking case using the third-order nonlinear predictive model with different control discretizations with $T_H = 2$ *sec* and $T_C = 2$ *sec*. . . . . 119

5.21 Pitch response comparison of different predictive models for nonlinear regulator case with 0.5 second and 0.25 second control discretizations. . . 121

5.22 Control effort comparison of different predictive models for nonlinear regulator case with 0.5 second and 0.25 second control discretizations. . . 122

5.23 Pitch response comparison of different predictive models for nonlinear tracking case with 1 second and 0.5 second control discretizations. . . . 123

5.24 Control effort comparison of different predictive models for nonlinear tracking case with 1 second and 0.5 second control discretizations. . . . . 123

5.25 Nonlinear regulator case pitch response with $\Delta T_D = 0.5$ second at different control time horizons ($T_c$). . . . . 125

5.26 Nonlinear regulator case control effort with $\Delta T_D = 0.5$ second at different control time horizons ($T_c$). . . . . 125

5.27 Nonlinear tracking case pitch response with $\Delta T_D = 1$ *sec* with different control time horizons ($T_c$). . . . . 127

Figure Page

5.28 Nonlinear tracking case control effort with $\Delta T_D = 1$ *sec* with different control time horizons ($T_c$). . . . . 127

5.29 Nonlinear regulator case pitch responses with padded and non-padded NMPC at $T_C = 2$ *sec*. . . . . 130

5.30 Nonlinear regulator case control effort with padded and non-padded NMPC at $T_C = 2$ *sec*. . . . . 130

5.31 Nonlinear tracking case pitch responses with padded and non-padded NMPC at $T_C = 2$ *sec*. . . . . 131

5.32 Nonlinear tracking case control effort with padded and non-padded NMPC at $T_C = 2$ *sec*. . . . . 131

5.33 Regulator case pitch response with various combinations of weighting factors. . . . . 133

5.34 Regulator case control effort with various combinations of weighting factors. . . . . 133

5.35 Nonlinear tracking case pitch response with various combinations of weighting factors. . . . . 134

5.36 Nonlinear tracking case control effort with various combinations of weighting factors. . . . . 135

5.37 Pitch response from nonlinear regulator case NMPC controller with specific parameter values. . . . . 137

5.38 Control effort from nonlinear regulator case NMPC controller with specific parameter values. . . . . 138

5.39 Pitch response from nonlinear tracking case NMPC controller with specific parameter values. . . . . 138

5.40 Control effort from nonlinear tracking case NMPC controller with specific parameter values. . . . . 139

5.41 Nonlinear pitch response comparison between open-loop, DLQR and NMPC controllers at free-stream velocity of 6 m/s. . . . . 140

5.42 Control effort comparison between DLQR and NMPC controllers at free-stream velocity of 6 m/s. . . . . 140

5.43 Regulator case pitch response for nonlinear aeroelastic system using the linear MPC controller with different control input discretizations. . . . 143

5.44 Regulator case control effort for nonlinear aeroelastic system at using the linear MPC controller with different control input discretizations. . . . 143

Figure Page

5.45 Regulator case pitch response for the nonlinear aeroelastic system using the linear MPC controller with different combinations of weights. . . . 145

5.46 Regulator case control effort for the nonlinear aeroelastic system using the linear MPC controller with different combinations of weights. . . . . 145

5.47 Nonlinear pitch response comparison between open-loop, DLQR and NMPC controllers at free-stream velocity of U = 12.5 m/s. . . . . 147

5.48 Control effort comparison between DLQR and NMPC controllers at free-stream velocity of U = 12.5 m/s. . . . . 147

5.49 Tracking case pitch response for the nonlinear aeroelastic system using the linear MPC controller with different control input discretizations. . . . 149

5.50 Tracking case control effort for the nonlinear aeroelastic system at using the linear MPC controller with different control input discretizations. . 149

# SYMBOLS

| | |
|---|---|
| $\rho$ | Air density |
| $C_{l_\alpha}$ | Coefficient of lift due to angle of attack |
| $C_{l_\beta}$ | Coefficient of lift due to control surface deflection |
| $C_{m_\alpha}$ | Coefficient of moment due to angle of attack |
| $C_{m_\beta}$ | Coefficient of moment due to control surface deflection |
| $\beta$ | Control surface deflection |
| $U$ | Free stream velocity |
| $L$ | Lift |
| $m$ | Mass |
| $M$ | Moment |
| $I_\alpha$ | Moment of inertia about the elastic axis |
| $\alpha$ | Pitch angle |
| $c_\alpha$ | Pitch damping coefficient |
| $k_\alpha$ | Pitch stiffness coefficient |
| $c_h$ | Plunge damping coefficient |
| $h$ | Plunge displacement |
| $k_h$ | Plunge stiffness coefficient |
| $b$ | Semi-chord |
| $x_\alpha$ | Static unbalance |

# ABBREVIATIONS

| | |
|---|---|
| AFRL | Air Force Research Laboratory |
| AIAA | American Institute of Aeronautics and Astronautics |
| CVs | Controlled Variables |
| DMC | Dynamic Matrix Control |
| DMPC | Decentralized Model Predictive Control |
| DVs | Disturbance Variables |
| FIR | Finite Impulse Response |
| GUI | Graphical User Interface |
| HIECON | Hierarchical Constraint Control |
| ICT | Information and Communication Technologies |
| IDCOM | Identification and Command |
| LBMPC | Learning Based Model Predictive Control |
| LMPC | Linear Model Predictive Control |
| LQG | Linear Quadratic Gaussian |
| LQR | Linear Quadratic Regulator |
| LTV | Linear Time Varying |
| MIMO | Multiple Input Multiple Output |
| MPC | Model Predictive Control |
| MPHC | Model Predictive Heuristic Control |
| MVs | Manipulated Variables |
| NATA | Nonlinear Aeroelastic Testbed Apparatus |
| NMPC | Nonlinear Model Predictive Control |
| PCT | Predictive Control Technology |
| PEGs | Pursuit Evasion Games |
| QDMC | Quadratic Dynamic Matrix Control |
| QP | Quadratic Program |
| RHC | Receding Horizon Control |
| RMPC | Robust Model Predictive Control |
| RMPCT | Robust Multivariable Predictive Control Technology |
| RMSE | Root-Mean-Square Error |
| SISO | Single Input Single Output |
| SMCA | Setpoint Multivariable Control Architecture |
| SMOC | Shell Multivariable Optimizing Controller |
| TVC | Thrust Vector Control |
| UAVs | Unmanned Aerial Vehicles |
| V/STOL | Vertical/ Short Take-off and Landing |

# ABSTRACT

Law, Wai Leuk, MSAE, Embry-Riddle Aeronautical University, December 2016.

MODEL PREDICTIVE CONTROL OF A NONLINEAR AEROELASTIC SYSTEM USING VOLTERRA SERIES REPRESENTATIONS.

The purpose of this study is to investigate the potential effectiveness of using a Volterra-based Model Predictive Control strategy to control a nonlinear aeroelastic system. Model Predictive Control (MPC), also known as Receding Horizon Control (RHC), entails computing optimal control inputs over a finite time horizon, applying a portion of the computed optimal control sequence, and then repeating the process over the next time horizon. The Volterra series provides input-output models of a dynamical system in terms of a series of integral operators of increasing order, where the first-order Volterra operator models the linear dynamics and the higher-order operators model the nonlinear dynamics. In this thesis, Volterra-based Model Predictive Control is applied to simulated linear and nonlinear pitch-plunge aeroelastic systems. A linear MPC controller based on a first-order Volterra model is used to control the linear aeroelastic system, and the results are compared to those obtained using a standard LQR controller and a LQR-based MPC strategy. The controller is implemented for regulator and tracking cases for a free-stream velocity of 6 m/s, a condition for which the open-loop linear system is stable, and a free-stream velocity of 12.5 m/s, which corresponds to an unstable flutter condition. Nonlinear MPC controllers, using second- and third-order Volterra models, are then used to control the nonlinear aeroelastic system for regulator and tracking cases at the stable flight condition. The stability and performance of the linear and nonlinear Volterra-based MPC strategies are discussed, and a detailed analysis of the effect of different parameters such as the optimization horizon, control horizon and control discretization, is provided. The results show that the linear MPC controller is able to successfully track a reference input for the stable condition and stabilizes the system at the unstable flutter condition. It is also shown that the incorporation of the second- and third-order Volterra kernels in the nonlinear MPC controller provides superior performance on the nonlinear aeroelastic system compared to the results obtained using only a linear model.

# 1. Introduction

## 1.1 Model Predictive Control

Anticipation is the process of visualizing a future event or state (*Anticipation*, 2016). In other words, anticipation is the same as prediction. Humans make use of their anticipation ability in their daily life, examples of which include driving a vehicle, pouring a cup of coffee, playing a tennis match, etc (Rossiter, 2014). While we are pouring a cup of coffee into an empty cup, we anticipate how fast the cup is filling up and adjust the flow rate to ensure the coffee does not overflow.

Based on humans' ability to anticipate, engineers in the 1970s created a class of control algorithms known as Model Predictive Control (MPC). MPC, also known as Receding Horizon Control (RHC) (Mayne, Rawlings, Rao, & Scokaert, 2000) or Moving Horizon Optimal Control (Bemporad & Morari, 1999), uses an explicit dynamic model to predict the future reaction of the plant to an optimal control sequence over a given control horizon (Holkar & Waghmare, 2010a). MPC technology was originally developed for slow process plants, such as plug and papers, petroleum refineries, and power plants. In recent years, MPC technology can be found in a wide variety of industries like automotive, food processing, aerospace and more (Qin & Badgwell, 2003).

## 1.2 The Evolution of MPC

The history of MPC dates back to the 1960s. Figure 1.1 presents the development of MPC algorithms in an evolutionary tree representation, which clearly shows the relationship and evolution between each generation of MPC algorithms.

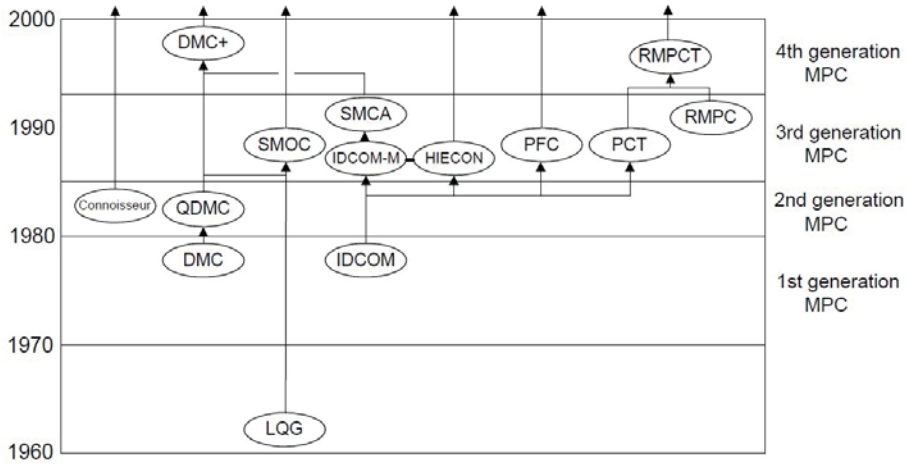


Figure 1.1. Evolutionary tree for MPC technology development (Qin & Badgwell, 2003).

Two papers, *Contribution to the Theory of Optimal Control* (Kalman, 1960a) and *A New Approach to Linear Filtering and Prediction Problems* (Kalman, 1960b), both written in 1960, represent the origins of MPC algorithms. The first paper is related to linear quadratic feedback control, which sets the stage for the well-known Linear Quadratic Regulator (LQR) control. The second paper discussed the importance of controllability and observability as key tools in analyzing least-squares control problems over an infinite horizon. These two papers form the basis of Linear Quadratic Gaussian (LQG) control. LQG control with infinite prediction horizon has

powerful stabilizing properties. LQG control will stabilize a linear plant, provided that it is stabilizable, as long as the Q and R matrices in the objective function are positive semidefinite and positive definite respectively (Qin & Badgwell, 2003). A survey estimated that there are thousands of real-world applications of LQG in a wide variety of industries (Goodwin, Graebe, & Salgado, 2001). However, LQR control theory is limited in that it does not handle constraints, nonlinearities and uncertainties in the process model (Garcia, Prett, & Morari, 1989; Richalet, Rault, Testud, & Papon, 1976).

The first generation of MPC technology is represented by Model Predictive Heuristic Control (MPHC) and Dynamic Matrix Control (DMC), which were established in the 1970s. The software used to solve the MPHC control problem was named Identification and Command (IDCOM). IDCOM allows verification of input and output constraints and uses a trial and error approach to solve the control problem. As the algorithm has the ability to utilize self-educating techniques such as feedback to improve performance (*Heuristic*, 2016), Richalet et al. (1976) referred to this control algorithm as heuristic. Figure 1.2 represents a comparison between conventional control structure and MPC structure of a hierarchy control system in a typical processing plant. The objective of IDCOM is to drive the predicted future output trajectory as closely as possible to the reference trajectory. The desired closed-loop response speed and aggressiveness of the algorithm can be set by tuning the time constant term in the reference trajectory. As the value of the time constant increases, it yields a slower and more robust controller.

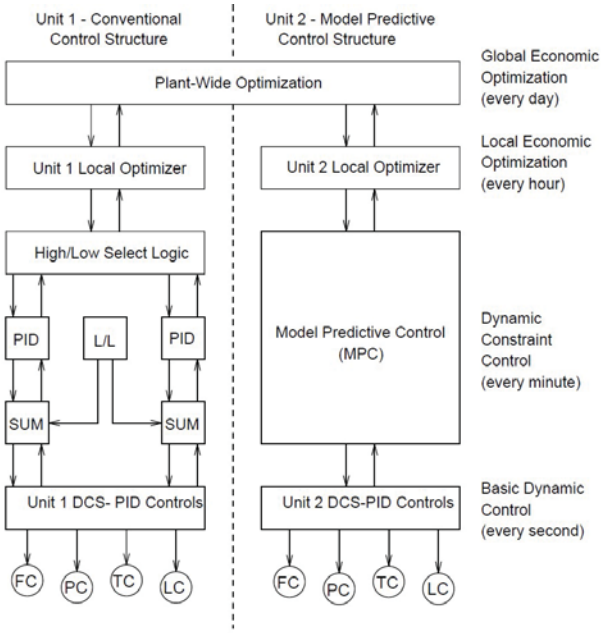


Figure 1.2. Conventional vs. MPC structure on hierarchy control system in processing plants (Deshmukh & Sawarkar, 2015).

DMC is an unconstrained multivariable control algorithm developed by Shell Oil's engineers in the early 1970s with its initial application in 1973. The objective of DMC is to drive the control variables (CVs) as close to the set point as possible in a least-squares sense with penalty on the manipulated variables (MVs). The control inputs yield a less aggressive output response as the value of the MVs gets smaller (C. R. Cutler & Ramaker, 1980). Using a set point instead of a reference trajectory in MPHC allowed DMC to have an extra degree of robustness to modeling error.

DMC provided excellent control of unconstrained multivariable process models only. To address this weakness, engineers at Shell Oil treated the DMC algorithm as a Quadratic Program (QP) by rewriting the DMC objective function into a standard QP (C. Cutler, Morshedi, & Haydel, 1983), which Cutler et al. referred to as

Quadratic Dynamic Matrix Control (QDMC). QP has the ability to include multivariable constraints and it results in a relatively simple optimization problem. Quadratic programming is defined as follows:

$$\min_{x} \quad \frac{1}{2}x^T P x + f^T x \tag{1.1}$$

$$\text{subject to} \quad Ax \leq b, \quad x \in \mathbb{R}^n$$

A global minimum solution exists if the P matrix is positive semidefinite because a positive semidefinite P will lead to a convex optimization problem (Bemporad, 2015).

MPC controllers gained wide acceptance in the industry at the same time control problems became more complex. Although the QDMC algorithm provides a systematic way to include hard input and output constraints, it does not provide a method to handle infeasible solutions. In practice, process input and output signals can be lost due to hardware failures resulting in dynamic changes on the structure and degrees of freedom of the controller (Qin & Badgwell, 2003).

The relationship between the problem structure and degrees of freedom is illustrated in Figure 1.3. There are three general cases for the process transfer function matrix. The square plant case is the ideal situation and it will lead to a unique solution. The fat plant case is commonly seen in practice, where there are more MVs than CVs. This case results in extra degrees of freedom in the objective function, causing the plant to move closer to an optimal operating point. When there are more CVs than MVs, the thin plant case, it is not possible to meet all the control objectives (J. B. Froisy, 1994).

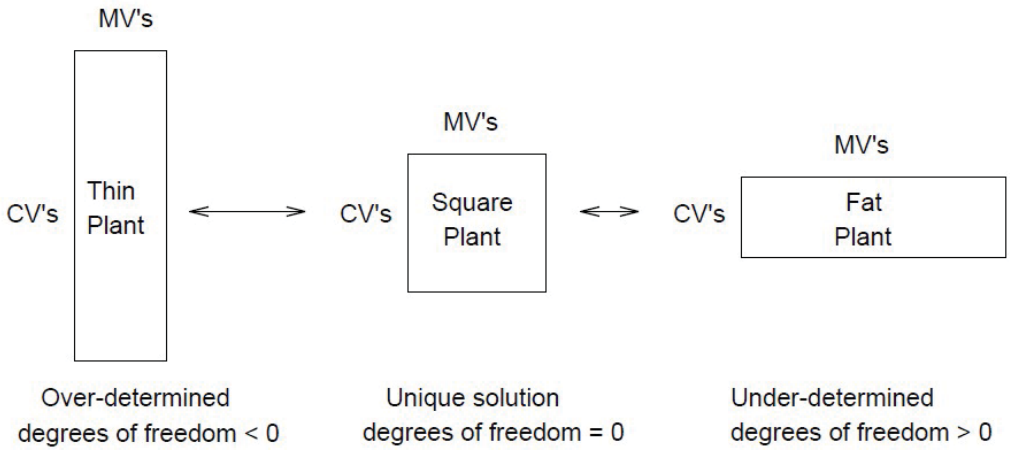


Figure 1.3. Relationship between process transfer function matrix and degrees of freedom (J. B. Froisy, 1994).

Furthermore, it is hard to convert control requirements into relative weights, such as values for output set point violations, output soft constraint violations and optimal input target violations, for a single objective function. For larger control problems, the processes will be more complex and sometimes it is impossible to express all requirements in a single objective function.

With these problems, engineers were motivated to develop more advanced MPC algorithms. The IDCOM-M algorithm by Setpoint first appeared in 1988 (Grosdidier, Froisy, & Hammann, 1988) and a summary of its application on the Shell Fundamental Control Problem was provided in 1990 (J. Froisy & Matsko, 1990). It uses two separate objective functions, one for outputs and another one for inputs if there is an extra degree of freedom. A quadratic output objective function is optimized subject to hard input constraints. The output value is driven closely to the desired value at a single point in time, which is known as the coincidence point. The basic tuning

parameters are used to define the reference trajectory, namely the coincidence point and the closed-loop response time.

During the late 1980s, engineers at Shell Research in France developed the Shell Multivariable Optimizing Control (SMOC) algorithm, which they described as the bridge between MPC algorithms and state-space systems (Marquis & Broustail, 1988; Yousfi & Tournier, 1991). The SMOC algorithm basically solves the LQR control problem with constraints on a finite horizon; however, it does not inherit the strong stabilizing properties of the LQR algorithm (Rawlings & Muske, 1993; Scokaert & Rawlings, 1998).

## 1.3 Concept, Procedures and Objectives of MPC

In MPC application, process outputs are referred to as controlled variables (CVs), while the process inputs are called manipulated variables (MVs). If disturbances are modeled, the measured disturbance variables are called DVs or feed-forward variables (Seborg et al., 2010). The ideas behind MPC are discussed in a journal article and are as follows (Holkar & Waghmare, 2010b):

- Explicit use of a model to predict the CVs along a future time horizon;

- Calculation of an optimal control sequence by solving an objective function (Linear or Quadratic) to optimize a desired performance index;

- Use of a receding horizon strategy: At each instant of time the horizon is moved towards the future and the first control signal of the optimal control sequence is implemented on the system.

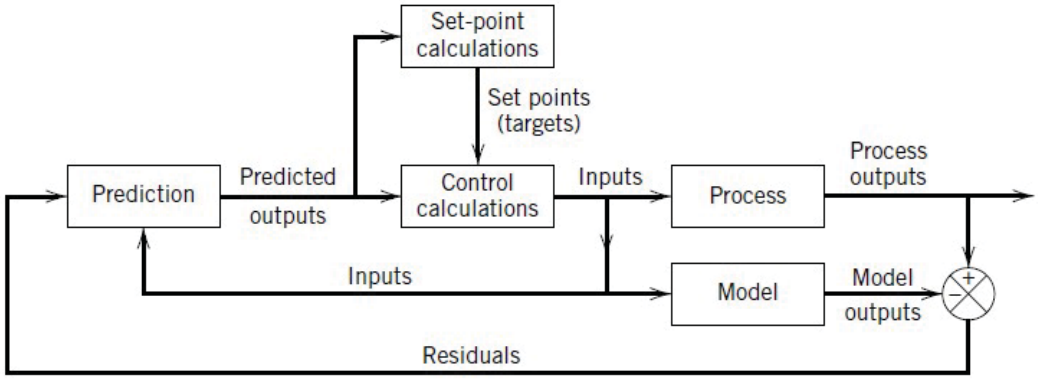


Figure 1.4. MPC controller block diagram (Seborg et al., 2010).

A block diagram of the MPC controller system is shown in Figure 1.4. The process block is used to predict the current values of the output variables, which are called process outputs. The residuals are calculated by taking the difference between the predicted outputs (model outputs) and actual outputs (process outputs), which are then passed into the prediction block as feedback signals. The predicted outputs are used in two calculations that are performed at each time instant, namely control calculation and set point calculation. Inequality constraints for input and output variables can be included in either calculation. Set points for control calculation are also called targets; they are calculated from an economic optimization perspective based on the steady-state model of the process. The types of optimization include: minimizing a cost function, maximizing a profit function or maximizing a production

function. The optimal value for set points changes frequently due to different process conditions and changes in inequality constraints. Thus, set point values need to be recalculated every time control calculations are performed (Seborg et al., 2010).

MPC controllers are designed to drive the process from one constrained steady state to another. The objectives for MPC controllers are listed as follows, in order of importance (Qin & Badgwell, 2003):

- Prevent violation of input and output constraints;
- Drive the CVs to their steady-state optimal values (Dynamic output optimization);
- Drive the MVs to their steady-state optimal values using remaining degrees of freedom (Dynamic input optimization);
- Prevent aggressive control inputs (MVs) in the optimal control sequence;
- Control as many process variables as possible when a sensor or actuator is not available.

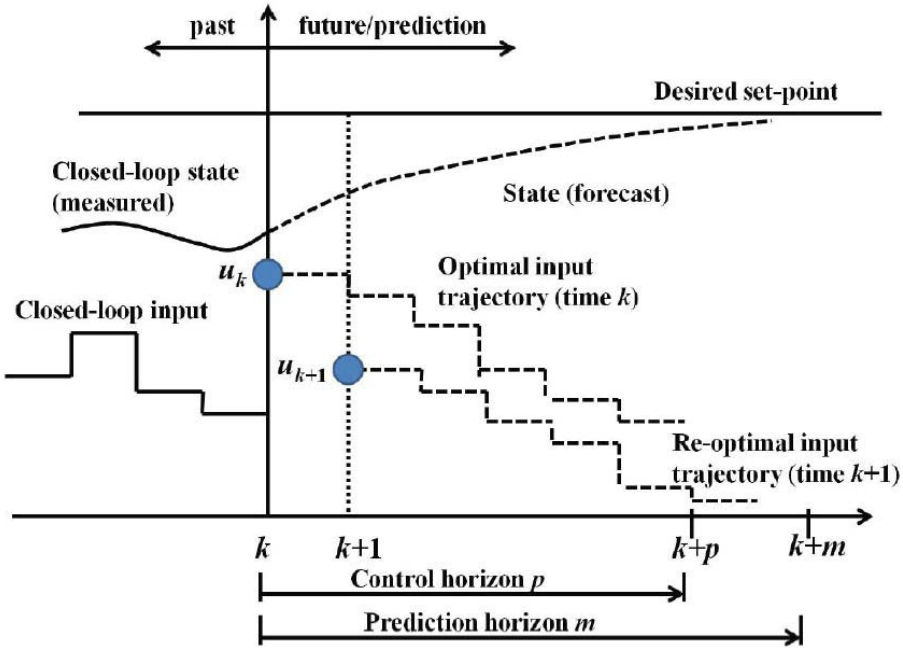


Figure 1.5. Basic concept of MPC and receding horizon strategy (Dai et al., 2012).

The receding horizon strategy used in MPC controllers was first proposed in the 1960s by a Russian engineer (Propoi, 1963). The idea is the end points of the prediction and control horizon move to the future time. The basic concept of MPC and receding horizon strategy are shown in Figure 1.5. The MPC procedure is summarized as follows (Holkar & Waghmare, 2010b):

**Step 1**

The process model is used to predict the state for the entire prediction horizon ($m$) at each time instant ($k$). The prediction state depends on the previous measured closed-loop state and the closed-loop inputs up until the current time instant ($k$).

**Step 2**

The optimal input trajectory ($u_k$) is calculated for the entire control horizon ($p$) at time $k$ by minimizing a cost function.

**Step 3**

Only the current control signal ($u_{k|k}$) is applied to the process. At the next time step ($k+1$), the closed-loop state is measured and Step 1 of the procedure is then repeated, all sequences are updated and the current optimal input trajectory ($u_{k+1|k+1}$) is calculated.

MPC is an important advanced control algorithm to the industry. The objectives and methods used by the controller to solve difficult multivariable control problems offer several important advantages compared to other control algorithms (Seborg et al., 2010):

- The process model captures the dynamic and static interaction between input, output and disturbance variables;
- Constraints on inputs and outputs are considered in a systematic manner in both SISO and MIMO control problems;
- Control calculations can be coordinated with the calculation of optimum set points;
- Accurate model predictions can provide early warnings of potential problems.

## 1.4 MPC Applications

Qin and Badgwell (2003) gave an overview of commercially available MPC technology with data provided by the vendors. A survey of MPC applications in various industries was conducted in the mid-1900's, and the results are tabulated in Table 1.6. Oil refining is clearly one of the major industries that utilizes MPC technology, while the aerospace/ defense industry had only 0.2% of MPC applications at that time. The percentage increased to 0.7% for the aerospace industry in a survey performed in 2005 by the ARC Advisory Group, which is shown in Figure 1.7. The oil refining industry is still the leading industry in MPC technology application (Bemporad, 2015).

| Area | Aspen Technology | Honeywell Hi-Spec | Adersa[b] | Invensys | SGS[c] | Total |
|---|---|---|---|---|---|---|
| Refining | 1200 | 480 | 280 | 25 | | 1985 |
| Petrochemicals | 450 | 80 | — | 20 | | 550 |
| Chemicals | 100 | 20 | 3 | 21 | | 144 |
| Pulp and paper | 18 | 50 | — | — | | 68 |
| Air & Gas | — | 10 | — | — | | 10 |
| Utility | — | 10 | — | 4 | | 14 |
| Mining/Metallurgy | 8 | 6 | 7 | 16 | | 37 |
| Food Processing | — | — | 41 | 10 | | 51 |
| Polymer | 17 | — | — | — | | 17 |
| Furnaces | — | — | 42 | 3 | | 45 |
| Aerospace/Defense | — | — | 13 | — | | 13 |
| Automotive | — | — | 7 | — | | 7 |
| Unclassified | 40 | 40 | 1045 | 26 | 450 | 1601 |
| Total | 1833 | 696 | 1438 | 125 | 450 | 4542 |
| First App. | DMC:1985<br>IDCOM-M:1987<br>OPC:1987 | PCT:1984<br>RMPCT:1991 | IDCOM:1973<br>HIECON:1986 | 1984 | 1985 | |
| Largest App. | 603 × 283 | 225 × 85 | — | 31 × 12 | — | |

Figure 1.6. MPC technology in different industrial areas (Qin & Badgwell, 2003).

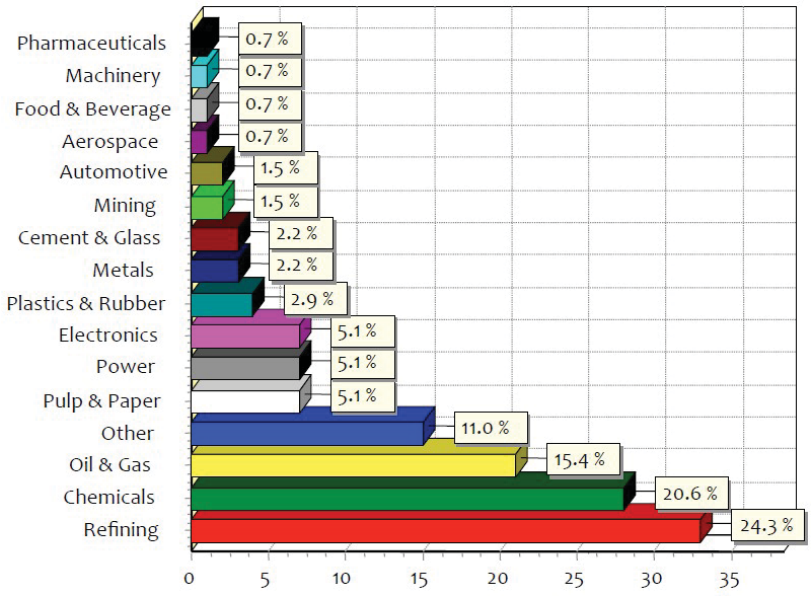


Figure 1.7. The use of MPC techniques in US industries (Bemporad, 2015).

Table 1.1. MPC academic research with industry, MPC type and years.

| **Industry Type** | **MPC Type** | **Years** |
|---|---|---|
| Process Control | Linear/ Nonlinear | 1980-2000 |
| Automotive Control | Explicit & Hybrid | 2001-2010 |
| Aerospace System and UAVs | Linear Time-Varying (LTV) | >2005 |
| Information and Communication Technologies (ICT) | Distributed/ Decentralized | >2005 |
| Energy, Finance & Automotive | Stochastic | >2010 |

Academic research on MPC technology is driven by industry needs. As hardware and software have advanced in the past decade, the amount of research and applications of MPC technology have increased, which can be seen in industries that utilize fast response models. Dr. Alberto Bemporad, a professor from the Institute for Advance Studies Lucca, has summarized academic research for different types of MPC

with their corresponding application industry and year (Bemporad, 2015), which is presented in Table 1.1.

In recent years, more applications of MPC can be seen in the aerospace field due to advancement in the computational power of modern computers. The increase in computational power allowed MPC to be implemented on fast dynamic processes, such as aeroelastic systems and Unmanned Aerial Vehicles (UAVs), for online optimization.

Campbell et al. applied a MPC algorithm on a highly flexible micro air vehicle (MAV) with baseline geometry provide by the U.S. Air Force Research Laboratory (AFRL) to counteract disturbances and drive the plant to the target states. Two different MAV designs were investigated. The first design utilized passive wing morphing, where the position of the morphing wing depends solely on aerodynamic and connection constraint forces and moments. The second design utilized active wing morphing, where the MPC algorithm controls certain wing properties to improve the MAV's maneuverability (Campbell & Maciejowski, 2009).

Development of a high altitude long endurance aircraft often features a high aspect ratio, flexible wing to improve aerodynamic efficiency. This type of aircraft wing poses challenges in design and control due to large deformations during flight operation. Wang et al. designed a MPC controller that suppresses wing oscillations in response to atmospheric gusts and other disturbances that the flexible wing might encounter during flight (Wang, Wynn, & Palacios, 2016).

Flutter analysis and control is another important research area, as wing flutter can lead to catastrophic failure due to wing structural fatigue. Prazenica investi-

gated the feasibility of using Volterra-based MPC strategies to control a simulated nonlinear aeroelastic system corresponding to the Texas A&M Nonlinear Aeroelastic Testbed. The controller is used to compute trailing edge flap deflection commands for controlling the pitch response of the system at different free-stream velocities, which included a flight condition where the underlying linear aeroelastic system is in an unstable flutter condition (Prazenica, 2014).

Figure 1.8. McDonnell Douglas AV-8B Harrier II performing VTOL on an aircraft carrier (Abyss, 2016).

Thrust vectoring, also known as Thrust Vector Control (TVC) is an ability that some aircraft, rockets and missiles have to maneuver by manipulating the direction of the thrust produced from the engine. Benefits of TVC are Vertical/ Short Take-off and Landing (V/STOL) and high maneuverability. The McDonnell Douglas AV-8B Harrier II, shown in Figure 1.8, is a well-known operational fighter jet with V/STOL

capabilities. Dunbar et al. applied a MPC controller to the Caltech ducted fan, a thrust-vectored flight experimental testbed designed for research and development of nonlinear flight guidance and control techniques for Uninhabited Combat Aerial Vehicles (UCAVs), where actuation and spatial constraints are present. The ducted fan is a scale model of the longitudinal axis of the flight vehicle. One of their papers showed that the MPC controller is able to stabilize a step disturbance (Dunbar, Milam, Franz, & Murray, 2002), for example.

In recent years, UAVs have been widely used by the military, academic researchers and Radio Control hobbiests. UAVs are aerial vehicles that operate without a human pilot on board (Newcome, 2004). Their flight path is either controlled autonomously by on-board or ground computers, or remotely controlled by a human operator at a ground station (Luukkonen, 2011).

In order to achieve a high degree of operational flexibility, it is often required for UAVs to be deployed and recovered anywhere in the world without the support of proper infrastructure such as a runway. To help meet these operational requirements, Mathisen et al. suggested the use of deep stall landings. The UAV approaches deep stall when the angle of attack of the vehicle is beyond the stall angle, after which the vehicle will lose altitude rapidly. The NMPC controller is used to determine the optimal control sequence that guides a model of a fixed wing UAV into a deep stall and then lands the UAV at a given location and path angle with minimum speed. Results from a simulation on a 3-DOF model (Mathisen, Fossen, & Johansen, 2015) and a 6-DOF model (Mathisen, Gryte, Fossen, & Johansen, 2016) were presented.

Du et al. proposed using a MPC method for controlling a small scale unmanned helicopter, where limitations of the actuators and rotors were taken into consideration during the controller design for position hold (Du et al., 2008). Slegers et al. applied nonlinear model predictive control (NMPC) to a parafoil and glider. The controller computes a closed form solution for the optimal control input that is able to expand both the output and control in a truncated Taylor series, where the expansion term can be used to indirectly penalize control action (Slegers, Kyle, & Costello, 2006). A linear controller applied to a nonlinear system is most effective when the system operates close to the linearized operating conditions. Chen et al. proposed using a MPC controller with cascaded structure, which has the ability to maintain the state variables within the vicinity of a given operating condition by imposing operational constraints. They verify their findings by implementing the controller on a quadrotor UAV (X. Chen & Wang, 2013).

In UAV navigation and trajectory tracking applications, Kang and Hedrick designed and implemented a NMPC controller with cost function that minimizes the tracking error of a fixed wing UAV from a desired line or trajectory, while Subbarao et al. implemented NMPC controllers on a quadcopter platform (Subbarao, Tule, & Ru, 2015). The single line tracking cost function is also extended to allow the tracking of multiple line segments with obstacle avoidance capabilities (Kang & Hedrick, 2006). Shekhar et al. introduced a new formulation of MPC for robust trajectory guidance of UAVs, which they named Robust Model Predictive Control (RMPC). The controller generalized the concept of waypoints to waysets in order to provide robustness

to bounded state disturbances in the presence of obstacles. The results showed how wayset guidance combined with constrained tightening guaranteed robust recursive feasibility and finite time completion of a control maneuver (Shekhar, Kearney, & Shames, 2015).

The military uses UAVs for missions such as target tracking and orbiting a target. Hafez et al. implemented a decentralized Learning Based Model Predictive Control (LBMPC) on a group of multiple cooperative UAVs in a desired geometrical formation pattern while tracking an aerial target. LBMPC is a new control technique that combines statistical learning along with control engineering providing guarantees on safety, robustness and convergence (Hafez, Givigi, Ghamry, & Yousefi, 2015). Encirclement is a military strategic tactic that is performed by a team of UAVs to neutralize a target by restricting its movement and maintaining awareness in close proximity at all times. Iskandarani et al. implemented a Linear Model Predictive Control (LMPC) strategy on a Qball-X4 quadrotor aircraft to perform this tactic (Iskandarani, Givigi, Rabbath, & Beaulieu, 2013). On the other hand, Marasco et al. proposed using a Decentralized Model Predictive Control (DMPC) method (Marasco, Givigi, & Rabbath, 2012). Eklund et al. applied a NMPC algorithm on a fixed wing UAV for the purpose of pursuit evasion games (PEGs) against a piloted F-15 aircraft (Eklund, Sprinkle, & Sastry, 2005).

Cooperative behavior for multiple UAVs is used to enhance capabilities to share information and complete different operations, such as intelligence surveillance, reconnaissance and wide area search or destroy. These operations are usually performed

by a group of UAVs in formation flight (H. Chao, Cao, & Chen, 2010). Line abreast, triangular and cross formation are common formations for a group of UAVs and Iskandarani et al. accomplishes these formations using a high-level LMPC algorithm on the Qball-X4 quadrotors (Iskandarani, Givigi, Fusina, & Beaulieu, 2014). NMPC provides a framework to solve optimal control sequences for a nonlinear system under state constraints and input saturation. Shim et al. implemented the controller on multiple autonomous helicopters in a complex environment, which combined stabilization of vehicle dynamics and trajectory generation. The cost function of the controller also included information about other moving obstacles or vehicles (Shim, Kim, & Sastry, 2003). Chao et al. designed a collision free formation flight control in the framework of NMPC, where obstacle and anti-vehicle collision avoidance is guaranteed by the cost function (Z. Chao, Zhou, Ming, & Zhang, 2012). Singh and Fuller described a NMPC control scheme for autonomous trajectory generation and flight control of an UAV in urban terrain (Singh & Fuller, 2001).

## 1.5 Introduction on Volterra Series

The Volterra series was developed by Vito Volterra, an Italian mathematician, in the late 1800s (Volterra, 1887) and it provided a convenient method to represent a large class of nonlinear dynamical systems. Volterra series representations are widely used to model nonlinear dynamical systems in different fields, for instance, biological (Chon, Chen, Holstein-Rathlou, & Marmarelis, 1998; French, Sekizawa, Höger, & Torkkeli, 2001) and aeroelastic (Marzocca, Librescu, & Silva, 2002; W. A. Silva,

1993; Prazenica, 2014) systems. In the electrical engineering field, Volterra filters are used to compensate for signal distortion from nonlinear disturbances (Cherry & Snelgrove, 1998; Borys, 2001).

The Volterra series is equivalent to the Taylor series with memory. A Taylor series represents a system that instantaneously maps the input signals to the output signals, while the output signals in a Volterra series depend on past input signals (Mathews & Sicuranza, 2000). Furthermore, the Volterra theory applies to a wide range of dynamical systems with system output(s) expressed in terms of a set of analytic ordinary differential equations (ODEs) and systems with fading memory. The fading memory requirement states that the influence of present inputs must diminish to zero in a finite period of time. For example, impacting a cantilever beam with a hammer exhibits fading memory, as the impulse response cause by the hammer will disappear after the beam stops vibrating (Prazenica, 2014).

## 1.6 Motivation and Objective

The main objective of this study is to investigate the effectiveness of using a Volterra-based model predictive control strategy to control a nonlinear aeroelastic system. The advantages of such an approach include the potential ability to perform online nonlinear system identification from input-output data, providing the ability to update the model as the flight condition changes throughout the operational flight envelope. The use of Volterra series representations provides the opportunity to model unknown weak nonlinearities that may exist in the system, such as structural nonlin-

earities or control surface freeplay, without requiring explicit knowledge of the form or nature of the nonlinearities. Because MPC is performed over a finite time horizon, it is straightforward to incorporate updated Volterra models, based on evolving flight conditions, into the control algorithm.

In this thesis, Volterra-based model predictive control is applied to simulated linear and nonlinear pitch-plunge aeroelastic systems. A linear MPC controller based on a first-order Volterra model is used to control the linear aeroelastic system, and the results are compared to those obtained using a standard LQR controller and a LQR-based MPC strategy. The controller is implemented for regulator and tracking cases for a free stream velocity of 6 m/s, a condition for which the open-loop linear system is stable, and a free stream velocity of 12.5 m/s, which corresponds to an unstable flutter condition. Nonlinear MPC controllers, using second- and third-order Volterra models, are then used to control the nonlinear aeroelastic system for regulator and tracking cases at the stable flight condition. The stability and performance of the linear and nonlinear Volterra-based MPC strategies are discussed, and a detailed analysis of the effect of different parameters such as the optimization horizon, control horizon, and control discretization, is provided. This work represents an extension of results presented in a related conference paper (Prazenica, 2014).

The thesis is organized into six chapters. Chapter 1 presents a literature review of MPC along with the motivation and objectives of this thesis. Chapter 2 defines the linear and nonlinear aeroelastic systems, presents the open-loop response of the system at different free-stream velocities and discusses the setup of a classical LQR

controller, which serves as a baseline for evaluating the performance of the Volterra-based MPC strategies. Chapter 3 discusses the Volterra models used in the MPC controllers and the Volterra-based MPC algorithms used in this study. Chapters 4 and 5 present simulation results and analysis using the linear and nonlinear MPC controllers implemented on the linear and nonlinear aeroelastic systems respectively. Finally, Chapter 6 provides conclusions and suggestions for future work.

# 2. Prototypical Aeroelastic Systems and Simulation Setup

## 2.1 Texas A&M Nonlinear Aeroelastic Testbed

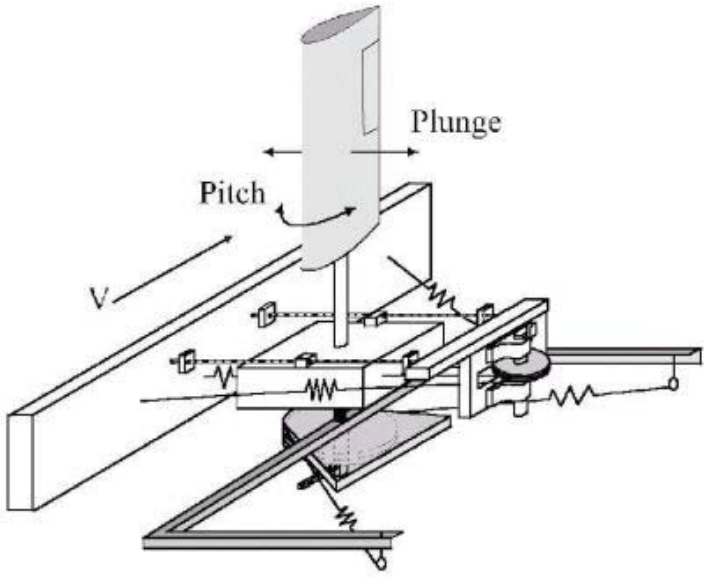


Figure 2.1. Schematic of the Texas A&M Nonlinear Aeroelastic Testbed Apparatus (NATA) with airfoil and control surface (W. Silva et al., 2005).

The simulated nonlinear aeroelastic system used in this case study corresponds to a model of the Texas A&M Nonlinear Aeroelastic Testbed (Strganac, Ko, & Thompson, 2000). The testbed consists of an airfoil section with plunge and pitch degrees of freedom and a trailing edge flap for control actuation.

The equations of motion for the NATA can be modeled as a pair of coupled second-order differential equations as follows:

$$\begin{bmatrix} m & mbx_\alpha \\ mbx_\alpha & I_\alpha \end{bmatrix} \begin{bmatrix} \ddot{h} \\ \ddot{\alpha} \end{bmatrix} + \begin{bmatrix} c_h & 0 \\ 0 & c_\alpha \end{bmatrix} \begin{bmatrix} \dot{h} \\ \dot{\alpha} \end{bmatrix} + \begin{bmatrix} k_h & 0 \\ 0 & k_\alpha(\alpha) \end{bmatrix} \begin{bmatrix} h \\ \alpha \end{bmatrix} = \begin{bmatrix} -L \\ M \end{bmatrix} \tag{2.1}$$

where the following variables are defined:

| | |
|---|---|
| $m$ | Mass |
| $b$ | Semi-chord |
| $h$ | Plunge displacement |
| $\alpha$ | Pitch angle |
| $x_\alpha$ | Static unbalance |
| $I_\alpha$ | Moment of inertia about the elastic axis |
| $c_h$ | Plunge damping coefficient |
| $c_\alpha$ | Pitch damping coefficient |
| $k_h$ | Plunge stiffness coefficient |
| $k_\alpha$ | Pitch stiffness coefficient |
| $L$ | Lift |
| $M$ | Pitch moment |

The terms on the left-hand side of the equation represent the structural dynamics of the system, while the right-hand side defines quasi-steady aerodynamic forces and

moments. The quasi-steady lift (L) and pitch moment (M) of the system are modeled by the following equations:

$$L = \rho U^2 b C_{l_\alpha} \left[ \alpha + \frac{\dot{h}}{U} + \frac{b\dot{\alpha}}{U} \left( \frac{1}{2} - a \right) \right] + \rho U^2 b C_{l_\beta} \beta \tag{2.2}$$

$$M = \rho U^2 b^2 C_{m_\alpha} \left[ \alpha + \frac{\dot{h}}{U} + \frac{b\dot{\alpha}}{U} \left( \frac{1}{2} - a \right) \right] + \rho U^2 b^2 C_{m_\beta} \beta \tag{2.3}$$

where

| | |
|---|---|
| $\rho$ | Air density |
| $U$ | Free stream velocity |
| $\beta$ | Control surface deflection |
| $C_{l_\alpha}$ | Coefficient of lift due to angle of attack |
| $C_{l_\beta}$ | Coefficient of lift due to control surface deflection |
| $C_{m_\alpha}$ | Coefficient of pitch moment due to angle of attack |
| $C_{m_\beta}$ | Coefficient of pitch moment due to control surface deflection |

Defining $\underline{z} = [h \;\; \alpha]^T$, Eq.(2.1) can be written in the form

$$\bar{M}\ddot{\underline{z}} + \bar{C}\dot{\underline{z}} + \bar{K}\underline{z} = \bar{F}_1\dot{\underline{z}} + \bar{F}_2\underline{z} + \bar{B}\beta \tag{2.4}$$

where

$$\bar{M} = \begin{bmatrix} m & mbx_\alpha \\ mbx_\alpha & I\alpha \end{bmatrix} \qquad \bar{C} = \begin{bmatrix} c_h & 0 \\ 0 & c_\alpha \end{bmatrix} \qquad \bar{K} = \begin{bmatrix} k_h & 0 \\ 0 & k_\alpha(\alpha) \end{bmatrix}$$

$$\bar{F}_1 = \begin{bmatrix} \rho U b C_{l_\alpha} & \rho U b^2 C_{l_\alpha}(\frac{1}{2} - a) \\ \rho U b^2 C_{m_\alpha} & \rho U b^3 C_{m_\alpha}(\frac{1}{2} - a) \end{bmatrix} \quad \bar{F}_2 = \begin{bmatrix} 0 & \rho U^2 b C_{l_\alpha} \\ 0 & \rho U^2 b^2 C_{m_\alpha} \end{bmatrix} \quad \bar{B} = \begin{bmatrix} \rho U^2 b C_{l_\beta} \\ \rho U^2 b^2 C_{m_\beta} \end{bmatrix}$$

The system has a single input, the trailing edge flap deflection ($\beta$), and two outputs corresponding to the pitch angle ($\alpha$) and plunge displacement ($h$). The pitch-plunge system is nonlinear due to the $k_\alpha(\alpha)$ term, the polynomial torsional spring stiffness, which generates a nonlinear restoring moment as a function of pitch angle. The polynomial torsional spring stiffness can be described using the following equation:

$$k_\alpha(\alpha) = k_{\alpha_1} + k_{\alpha_2}\alpha \tag{2.5}$$

The spring stiffness function in Eq.(2.5) was chosen to emphasize the contribution of the second and third-order Volterra kernels in the nonlinear response. An underlying linear system can be obtained by setting $k_{\alpha_2} = 0$, which result in a linear spring stiffness. MATLAB/Simulink is used to simulate the pitch-plunge system with the parameters show in Table 2.1.

Table 2.1. Parameters values for the pitch-plunge aeroelastic system.

| | | | | | | | | |
|---|---|---|---|---|---|---|---|---|
| $m$ | = | 12.387 $kg$ | $x_\alpha$ | = | 0.2466 | $C_{m_\alpha}$ | = | -0.628 |
| $I_\alpha$ | = | 0.065 $m^2kg$ | $c_h$ | = | 27.43 $kg/s$ | $C_{m_\beta}$ | = | -0.635 |
| $\rho$ | = | 1.225 $kg/m^3$ | $c_\alpha$ | = | 0.180 $m^2kg/s$ | $k_h$ | = | 2844.4 $N/m$ |
| $a$ | = | -0.6 | $C_{l_\alpha}$ | = | 6.28 | $k_{\alpha_1}$ | = | 2.82 $N \cdot m$ |
| $b$ | = | 0.135 $m$ | $C_{l_\beta}$ | = | 3.358 | $k_{\alpha_2}$ | = | 14.1 $N \cdot m$ |

It is important to note that the behavior of the aeroelastic system varies significantly with the free-stream velocity (U) experienced by the airfoil. The studies provided in this thesis consider the case where U = 6 m/s and U = 12.5 m/s. At U

= 6 m/s, the nonlinear system and the underlying linear system are stable. At U = 12.5 m/s, the nonlinear system enters a limit cycle oscillation while the linear system is in an unstable flutter condition.

In order to develop a simulation environment the linear aeroelastic system can be expressed in the following state-space form, where $x = \{h, \alpha, \dot{h}, \dot{\alpha}\}^T$:

$$\begin{aligned} \dot{x} &= Ax + Bu \\ y &= Cx + Du \end{aligned} \tag{2.6}$$

The A, B, C, and D matrices are constructed from Eq.2.6 as follows:

$$\bar{A} = \begin{bmatrix} [0]_{2\times 2} & [I]_{2\times 2} \\ -\bar{M}^{-1}(\bar{K} - \bar{F}_1) & -\bar{M}^{-1}(\bar{C} - \bar{F}_2) \end{bmatrix} \tag{2.7}$$

$$B = \begin{bmatrix} [0]_{2\times 1} \\ \bar{M}^{-1}\bar{B} \end{bmatrix} \tag{2.8}$$

$$C = \begin{bmatrix} 1 & 0 & 0 & 0 \\ 0 & 1 & 0 & 0 \\ 0 & 0 & 1 & 0 \\ 0 & 0 & 0 & 1 \end{bmatrix} \tag{2.9}$$

$$D = \begin{bmatrix} 0 \\ 0 \\ 0 \\ 0 \end{bmatrix} \tag{2.10}$$

The numerical values of the A and B matrices are provided in Appendix A for the U = 6 m/s and U = 12.5 m/s cases.

In order to model the nonlinear aeroelastic system, a fictitious control input is created to incorporate the effect of the nonlinear spring stiffness. This requires augmenting the B, C, and D matrices in the state-space model to accommodate the second input.

The simulation environment presented in Figure 2.2 was developed to run open-loop simulations of the nonlinear aeroelastic system. In the MPC implementation, optimal control inputs are computed using the MATLAB *fmincon* function. These control commands are then used to simulate the close-loop system response.

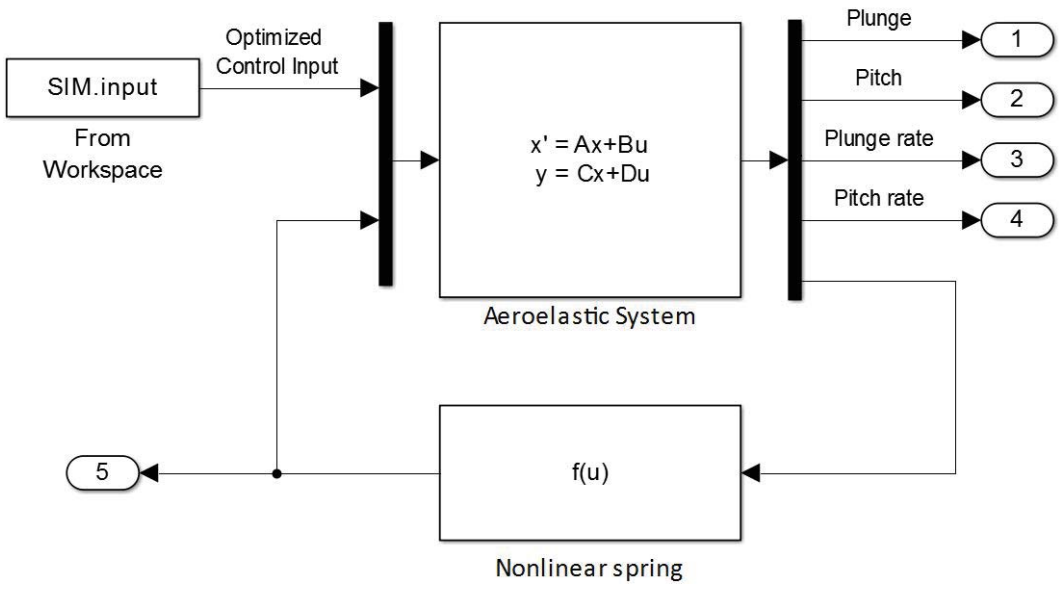


Figure 2.2. Aeroelastic system simulation setup in Simulink.

## 2.2 Open-Loop Response of the Aeroelastic System

Open-loop plunge and pitch responses for both the linear and nonlinear aeroelastic systems were simulated at free-stream velocities of U = 6 m/s and U = 12.5 m/s. The results provided a qualitative assessment of the stability of the linear and nonlinear aeroelastic systems at different flight conditions. In addition, they provide a baseline pitch response for comparison with the pitch responses obtained using the linear and nonlinear MPC controllers, which are designed in later chapters.

The stability of the linear systems is quantified in terms of the eigenvalues of the A matrix. The eigenvalues for the linear system at U = 6 m/s and U = 12.5 m/s are given in Table 2.2.

Table 2.2. Eigenvalues for the linear aeroelastic system.

| **Poles** ($\lambda$) | **Frequency** ($\omega$) | **Damping Ratio** ($\zeta$) | **Time to Settle** ($t_s$) |
|---|---|---|---|
| ***U = 6 m/s*** | | | |
| $-2.063 \pm 16.368\hat{\imath}$ | 16.5 rad/s | 0.125 | 1.45 s |
| $-2.965 \pm 6.777\hat{\imath}$ | 7.40 rad/s | 0.401 | 1.01 s |
| ***U = 12.5 m/s*** | | | |
| $0.0876 \pm 13.898\hat{\imath}$ | 13.9 rad/s | -6.30$\times 10^{-3}$ | 34.2 $s$ (Time to Double) |
| $-5.238 \pm 9.421\hat{\imath}$ | 10.8 rad/s | 0.486 | 0.573 s |

A quantitative analysis of the closed-loop control results is provided by calculating the Root-Mean-Square Error (RMSE) of the pitch response and the Control Effort (CE) using the following equations:

$$RMSE = \sqrt{\frac{1}{n}\sum_{i=1}^{n}(y_i - \hat{y}_i)^2} \tag{2.11}$$

$$CE = \sqrt{\frac{1}{n}\sum_{i=1}^{n}(\beta_i)^2} \tag{2.12}$$

The RMSE defines how much the response deviates from the reference value ($\hat{y}_i$). The concept is similar to standard deviation in statistics with the only exception that RMSE uses data from an estimator or model, while standard deviation uses data from a population.

Figures 2.3 and 2.4 shown the open-loop responses for plunge and pitch respectively with initial pitch angle set at 5 degrees for the case where U = 6 m/s. The oscillation in the open-loop plunge response is minimal as the magnitude is $10^{-4}$. The open-loop responses for both plunge and pitch converge to zero with a short settling time of 2.5 seconds. Hence, the aeroelastic system is stable at a free-stream velocity of 6 m/s for both the linear and nonlinear cases.

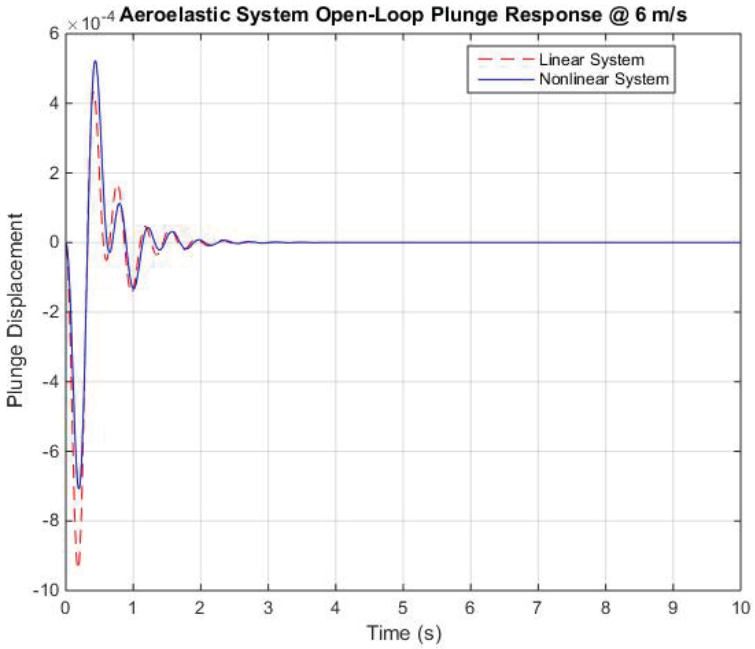


Figure 2.3. Open-loop plunge response for both linear and nonlinear aeroelastic systems at 6 m/s.

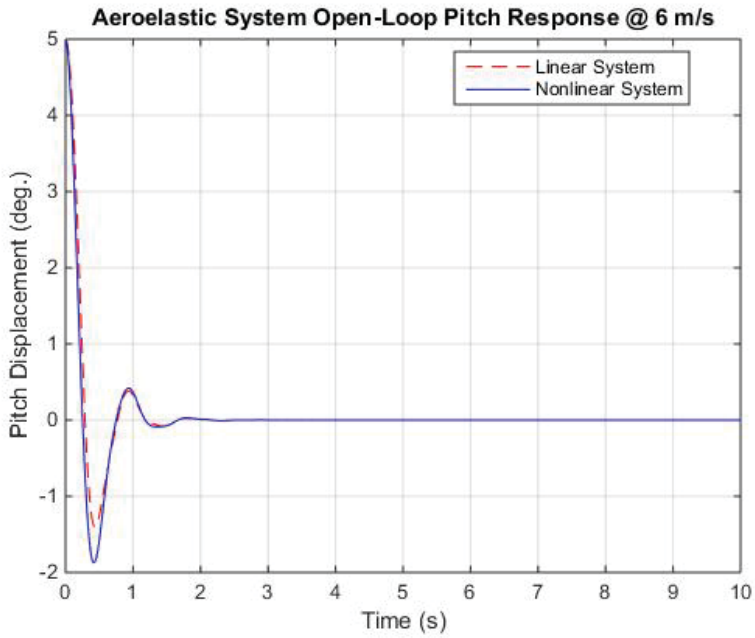


Figure 2.4. Open-loop pitch response for both linear and nonlinear aeroelastic systems at 6 m/s.

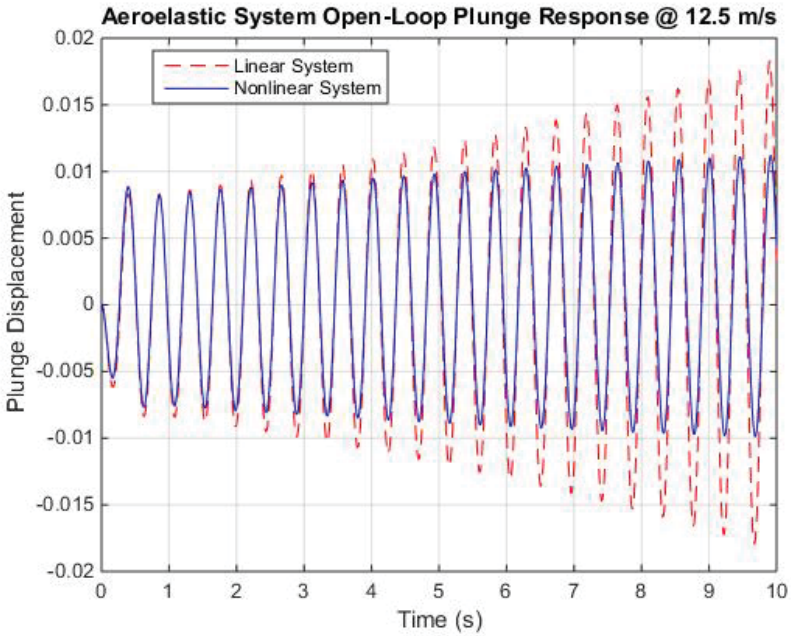


Figure 2.5. Open-loop plunge response for both linear and nonlinear aeroelastic systems at 12.5 m/s.

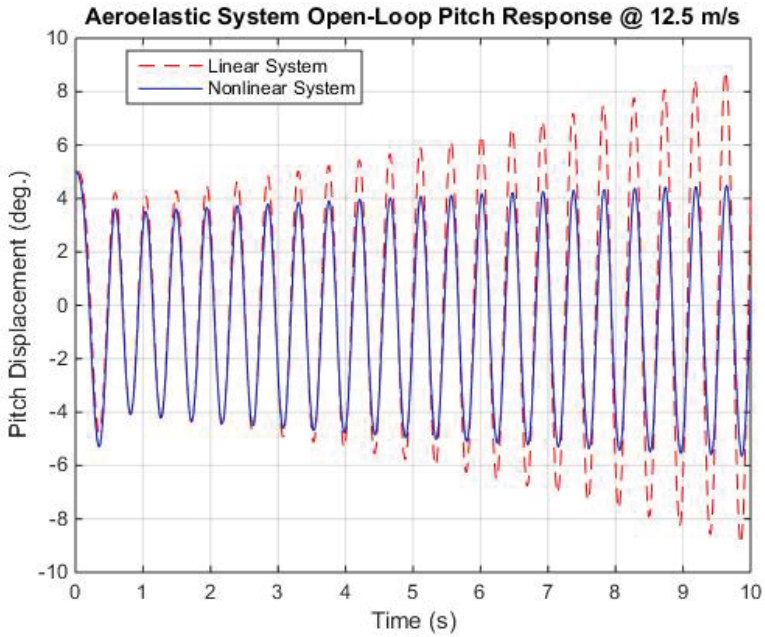


Figure 2.6. Open-loop pitch response for both linear and nonlinear aeroelastic systems at 12.5 m/s.

The free-stream velocity U = 12.5 m/s corresponds to the flutter speed of the linear aeroelastic system. Thus, it is important to investigate the limitation of the MPC controller and whether or not it will successfully stable the aeroelastic system at this flight condition. The plunge and pitch open-loop responses at this flight condition are unstable as both responses exhibit oscillations with increasing amplitude, as shown in Figures 2.5 and 2.6 respectively. The response of the nonlinear aeroelastic system converges to oscillations with constant amplitude, corresponding to a limit cycle oscillation.

## 2.3 Classical Linear Quadratic Regulator (LQR) Control

A classical Linear Quadratic Regulator (LQR) was developed as a baseline controller for comparison with the Volterra-based MPC results. The LQR is a linear controller that regulates the states of a linear system to zero while minimizing a quadratic cost function.

For an infinite horizon continuous time LQR, the cost function is defined as follows:

$$J = \frac{1}{2}\int_0^\infty (x^T Q x + u^T R u) dt \tag{2.13}$$

where $Q \in \mathbb{R}^{n\times n}$ and $R \in \mathbb{R}^{m\times m}$ are symmetric positive-semidefinite and positive-definite matrices representing the weighting of the states and control effort respectively. The state $\underline{x} \in \mathbb{R}^n$, with initial condition $\underline{x}(0) = \underline{x}_0$ evolves according to the linear dynamic model:

$$\dot{\underline{x}} = A\underline{x} + B\underline{u}$$

where $\underline{u} \in \mathbb{R}^m$ is the control input. The $Q$ and $R$ matrices are tuning parameters in the controller and ultimately determine the closed-loop response of the system. For the aeroelastic system presented in this thesis, the $R$ matrix is a scalar constant as the trailing edge flap is the only control input. The matrix $Q$ is chosen to be diagonal with each element representing a direct weighting of the corresponding state. A common method to select the diagonal entries in $Q$ is to set a maximum allowable value for each of the states (i.e. $Q^h_{max}$, $Q^\alpha_{max}$, $Q^{\dot{h}}_{max}$ & $Q^{\dot{\alpha}}_{max}$), and define the $Q$ matrix as

$$Q = \begin{bmatrix} \frac{1}{(Q^h_{max})^2} & 0 & 0 & 0 \\ 0 & \frac{1}{(Q^\alpha_{max})^2} & 0 & 0 \\ 0 & 0 & \frac{1}{(Q^{\dot{h}}_{max})^2} & 0 \\ 0 & 0 & 0 & \frac{1}{(Q^{\dot{\alpha}}_{max})^2} \end{bmatrix} \tag{2.14}$$

A second choice of $Q$ is designed to reproduce the weighting in the MPC cost function to be developed later. In the Volterra-based MPC algorithm, the plunge and pitch outputs are treated separately with their own cost functions that correspond to quadratic weighting of the pitch and plunge states respectively. To employ an equivalent strategy to control pitch on the 4-states linear system, the maximum value of pitch, $Q^\alpha_{max}$, is selected and $Q$ is then defined as a positive semi-definite matrix instead of a positive-definite matrix:

$$Q = \begin{bmatrix} 0 & 0 & 0 & 0 \\ 0 & \frac{1}{(Q^\alpha_{max})^2} & 0 & 0 \\ 0 & 0 & 0 & 0 \\ 0 & 0 & 0 & 0 \end{bmatrix} \tag{2.15}$$

A similar approach can be taken to control the plunge state. To determine the control input that minimizes the quadratic cost function given in Eq.(2.13), the following feedback control law is used:

$$u = -Kx \tag{2.16}$$

where $K$ is given as

$$K = R^{-1}B^{T}P \tag{2.17}$$

and $P$ is computed by solving the following continuous time Riccati differential equation (Ogata & Yang, 1970):

$$A^{T}P + PA - PBR^{-1}B^{T}P + Q = 0 \tag{2.18}$$

For specific choices of $Q$ and $R$, the LQR optimal feedback gain ($K_{LQR}$) can be found using the LQR function within MATLAB. The LQR controller was implemented on the simulated aeroelastic system in Simulink, which is shown in Figures 2.7 and 2.8 for the linear and nonlinear aeroelastic system respectively.

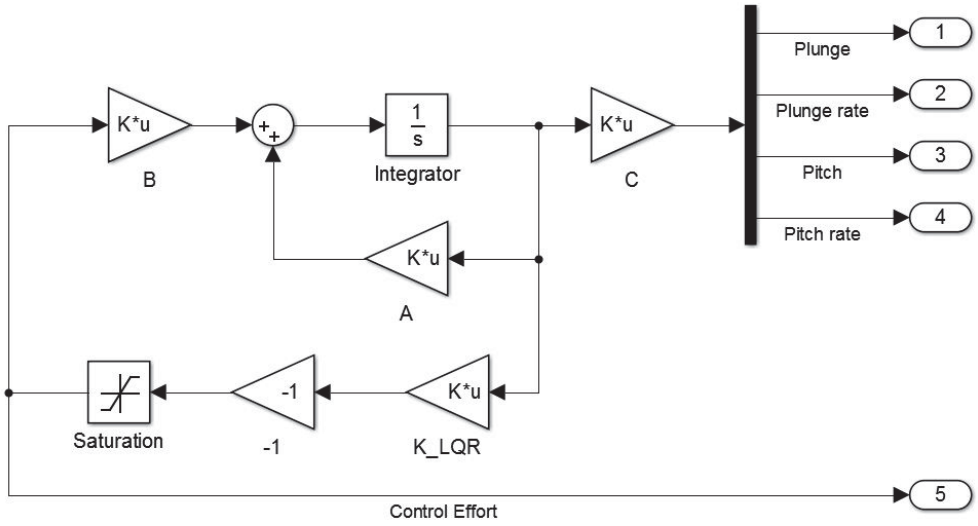


Figure 2.7. Linear aeroelastic system with LQR controller in Simulink.

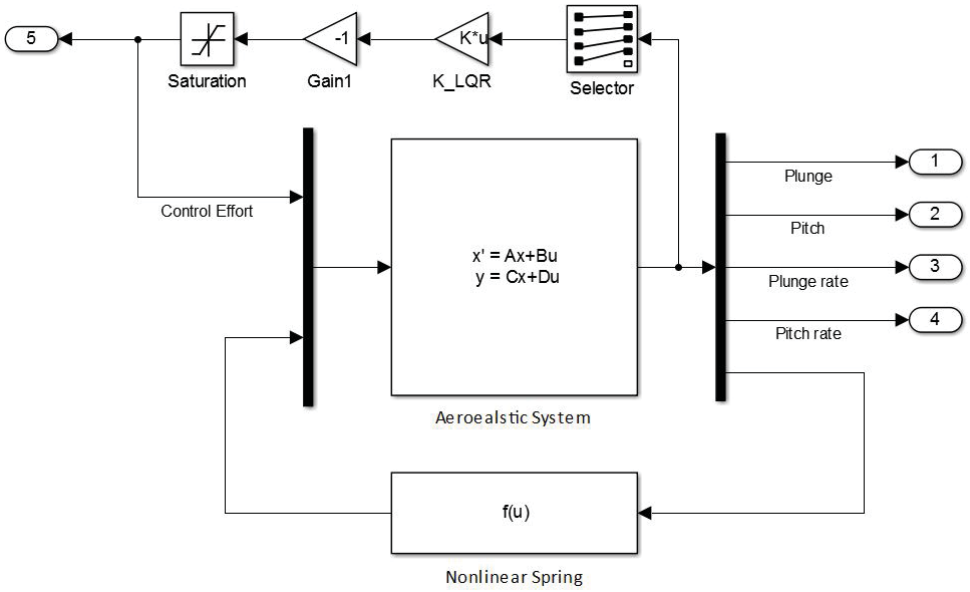


Figure 2.8. Nonlinear aeroelastic system with LQR controller in Simulink.

# 3. Volterra Modeling & MPC Algorithm

## 3.1 Volterra Series Representations

Mathematically, a system can be defined as a mapping of an output signal $y(t)$ to an input signal $u(t)$. A system operator $H$ is used to map the input to the output function space (Franz & Schölkopf, 2006).

$$y(t) = Hu(t) \tag{3.1}$$

Under general conditions, the Volterra theory states that the output $y(t)$ of a single output nonlinear dynamical system can be expressed in terms of an infinite series of integral operators (Schetzen, 1980).

$$y(t) = y_1(t) + y_2(t) + \cdots + y_\infty(t) = \sum_{n=1}^{\infty} y_n(t) \tag{3.2}$$

where $y_n(t)$ denotes the n-th order Volterra operator of the system output. The Volterra series must be truncated in practice. This work will consider Volterra models that are truncated to include terms no higher then the third-order operators, which is suitable for modeling weakly nonlinear systems. For casual, time-invariant SISO systems, the first-, second- and third-order Volterra operators take the following form:

$$y_1(t) = \int_0^t V_1(\alpha)u(t-\alpha)d\alpha \tag{3.3}$$

$$y_2(t) = \int_0^t \int_0^t V_2(\alpha,\beta)u(t-\alpha)u(t-\beta)d\alpha d\beta \tag{3.4}$$

$$y_3(t) = \int_0^t \int_0^t \int_0^t V_3(\alpha, \beta, \gamma) u(t-\alpha) u(t-\beta) u(t-\gamma) d\alpha d\beta d\gamma \tag{3.5}$$

where $u$ is the system input and $V_1$, $V_2$ and $V_3$ represent the first-, second- and third-order Volterra kernels. Once the kernels are identified, the response to any input can be determined. The first-order kernel represents the linear dynamics of the system, while the second- and third-order kernels represent the nonlinear dynamics. For a linear system, the first-order kernel is equivalent to the impulse response of the system (Schetzen, 1980).

The kernels defined in these representations are defined on domains of increasing dimension (i.e., the third-order kernel is supported on a three-dimensional domain); therefore, it is desired to obtain reduced-order kernel representations. The Volterra series is used to model systems with fading memory. The memory length of the first-, second- and third-order kernels are defined as $T_1$, $T_2$ and $T_3$, respectively. Kernels expressed in symmetric form are unique for a given system, thus the second-order kernel can be assumed to be symmetric on the $[0, T_2] \times [0, T_2]$ square domain, while the third-order kernel is symmetric over a $[0, T_3] \times [0, T_3] \times [0, T_3]$ cubic domain (Schetzen, 1980).

## 3.2 Volterra Kernel Identification

A critical challenge in using the Volterra series is identifying the Volterra kernels that characterize the system. Kernel identification is an ill-posed problem as the objective is to determine the structure of the system using only input and output

measurements. In practice, input and output measurements are frequently corrupted by sensor noise. Furthermore, the Volterra series is not orthogonal; thus the Volterra kernels must be identified simultaneously (Schetzen, 1980). To address this problem, Norbert Wiener, an American mathematician, developed a variation of the Volterra series that is orthogonal provided that the input signal is Gaussian white noise, which is known as the Wiener series (Wiener, 1966).

There are many approaches used to determine the Volterra kernels in both the time and frequency domain. Statistical methods such as the cross-correlation technique were developed to determine the Wiener kernels (Lee & Schetzen, 1965). Neural networks have also been used to estimate Volterra kernels (Wray & Green, 1994). Another common approach is to express the kernels in terms of a set of basis functions. For instance, discrete Laguerre functions have been used to estimate the kernels of a biological system (Marmarelis, 1993), while first- and second-order kernels of an aeroelastic system have been expressed in terms of decaying exponential functions (Reisenthel, 1999).

Volterra kernels have also been represented in terms of wavelet bases with the objective of obtaining reduced-order representations. Beylkin et al. have shown that wavelets are effective for compressing various integral operators (Beylkin, Coifman, & Rokhlin, 1991). With this advantage in mind, bi-orthogonal wavelets were used to compress first- and second-order Volterra kernels (Nikolaou & Mantha, 1998). Prazenica et al. have constructed wavelets over the domain of support of the triangular form of the second-order kernel (Prazenica & Kurdila, 2004). These piecewise-

constant triangular wavelets fit the domain of the second-order kernel and exist in closed form. The drawbacks include the fact that these wavelets do not yield smooth kernel estimates and it is not a straightforward process to extend the approach for higher order kernels.

Prazenica and Kurdila constructed piecewise-polynomial multiwavelets, which are generated using the technique of intertwining (Donovan, Geronimo, & Hardin, 1996), to represent Volterra kernels. These multiwavelets are orthonormal, compactly-supported, and symmetric or antisymmetric. This class of piecewise-polynomial multiwavelets combines many desirable properties of the bi-orthogonal and triangular wavelets without many of the disadvantages. The multiwavelet-based kernel identification algorithm shows a significant improvement over other wavelet-based approaches from the perspective of speed, accuracy, generality and implementation (Prazenica & Kurdila, 2006).

Multiwavelets are composed of a set of wavelet functions $\{\psi^1, \cdots, \psi^n\}$ that are formed or generated by a set of n scaling functions $\{\phi^1, \cdots, \phi^n\}$. The multiwavelet basis is composed of the scaled translates and dilates of the original set $\{\psi^1, \cdots, \psi^n\}$, resulting in basis functions with localized time and varying frequency. The kernels are expressed in terms of the orthonormal multiwavelet basis functions as follows:

$$V_1(\xi) = \sum_{j=1}^{N_1} c_{1,j} f_{1,j}(\xi) \tag{3.6}$$

$$V_2(\xi, \eta) = \sum_{j=1}^{N_2} c_{2,j} f_{2,j}(\xi, \eta) \tag{3.7}$$

$$V_3(\xi,\eta,\gamma) = \sum_{j=1}^{N_3} c_{3,j} f_{3,j}(\xi,\eta,\gamma) \tag{3.8}$$

There are many other possible choices of the basis functions, $\{f_{1,j}\}_{j=1}^{N_1}$, $\{f_{2,j}\}_{j=1}^{N_2}$ and $\{f_{3,j}\}_{j=1}^{N_3}$. In the multiwavelet case, two and three-dimensional wavelet functions are constructed from the tensor products of the one-dimensional wavelet basis functions. Once the kernels are expressed in terms of a set of basis functions, the kernel identification problem reduces to a linear least-squares problem, which can be solved to obtain the wavelet basis coefficients. Frequently, many wavelet coefficients are close to zero and can be neglected, which can lead to reduced-order representations of the kernels (Prazenica, Reisenthel, Kurdila, & Brenner, 2004).

A drawback of representing aeroelastic systems with Volterra series is that the kernels are parametrically dependent on flight condition. In order to represent the dynamics of an aeroelastic system, a different set of Volterra kernels must be identified at each flight condition. In the following example, Volterra kernels were identified using the multiwavelet-based kernel identification algorithm with simulation data for the case of free-stream velocity of 6 m/s. The aeroelastic system has two outputs, the pitch angle and plunge displacement, and a single input corresponding to the trailing edge flap deflection. Thus, there will be two sets of Volterra kernels, each corresponding to the respective output. The first-order kernels shown in Figure 3.1 are represented in terms of 257 basis functions, while the second-order kernels are generated in terms of 153 unique basis functions (Prazenica, 2014). Figure 3.1 only

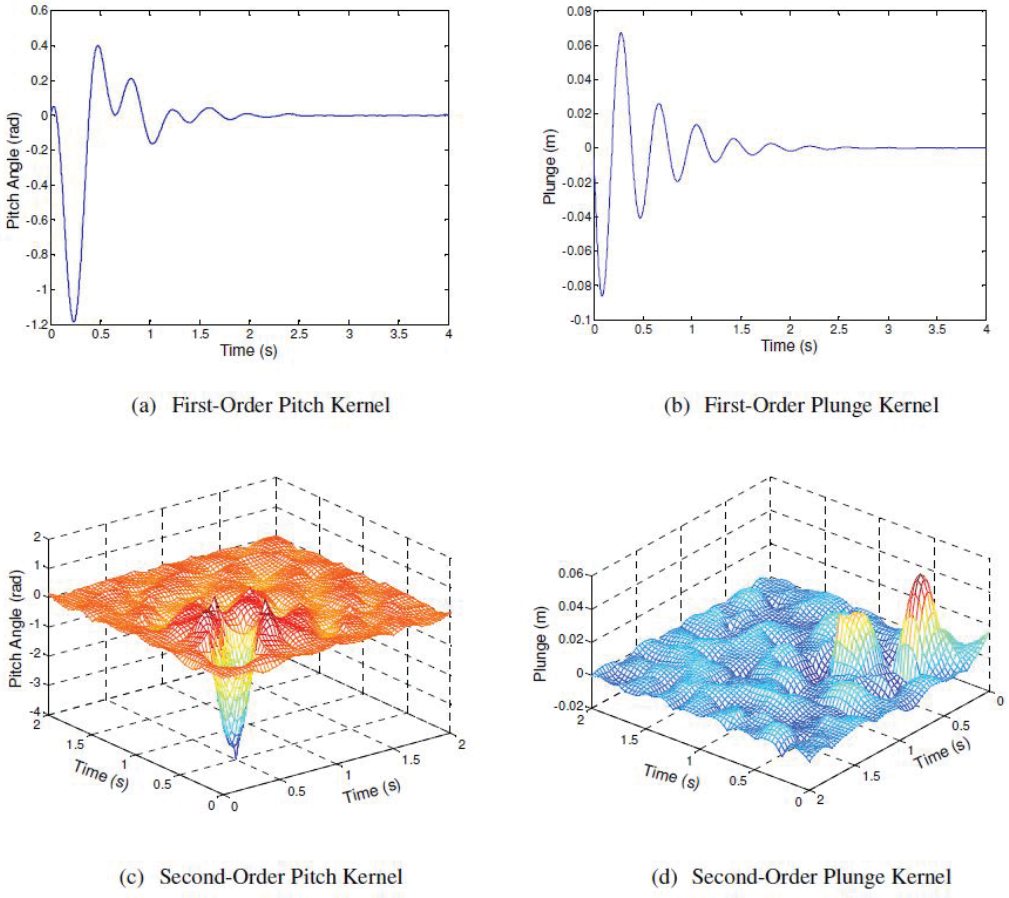


(a) First-Order Pitch Kernel

(b) First-Order Plunge Kernel

(c) Second-Order Pitch Kernel

(d) Second-Order Plunge Kernel

Figure 3.1. Identified first- and second-order pitch and plunge Volterra kernels at $U = 6$ m/s (Prazenica, 2014).

shows the first- and second-order kernels as the third-order kernel is difficult to display as it is supported over a three-dimensional domain.

In order to consider modeling the system output for nonzero initial conditions, it is necessary to add an extra term to the Volterra series, which is referred to as the zero-order Volterra kernel ($V_0$). The zero-order kernel accounts for the portion of the system response in which the output is dependent on the initial condition. On the other hand, first-order and higher-order kernels account for the effects of external

inputs to the system. The zero-order kernel for a given system is generally represented as a function of the initial condition of all states.

$$V_0^h(t) = \alpha_0 h(t)|_{\alpha_0=1} + \dot{\alpha_0} h(t)|_{\dot{\alpha_0}=1} + h_0 h(t)|_{h_0=1} + \dot{h_0} h(t)|_{\dot{h_0}=1} \tag{3.9}$$

$$V_0^\alpha(t) = \alpha_0 \alpha(t)|_{\alpha_0=1} + \dot{\alpha_0} \alpha(t)|_{\dot{\alpha_0}=1} + h_0 \alpha(t)|_{h_0=1} + \dot{h_0} \alpha(t)|_{\dot{h_0}=1} \tag{3.10}$$

The above equations express the zero-order kernel for plunge displacement and pitch angle as functions of the initial conditions for the pitch, pitch rate, plunge displacement and plunge displacement rate $\{\alpha_0, \dot{\alpha_0}, h_0, \dot{h_0}\}$ and the measured plunge and pitch response to a unit initial condition for each state. The inclusion of the zero-order Volterra kernel is important while implementing MPC because the algorithm solves optimization problems over a relative short time horizon with nonzero initial conditions.

### 3.3 Volterra-Based Model Predictive Control Algorithm

The objective of MPC is to minimize a given cost function $J(x, u)$ over a finite time cost horizon, $T_H$. An optimal control sequence is computed by minimizing the cost function by solving a typical nonlinear optimization problem. Then, the control sequence is applied to the system over a control time horizon, $T_C$, where $T_C \leq T_H$. With the same procedure, the optimal control input is re-calculated and applied over a receding horizon.

The choice of cost function and constraints varies with different systems. Generally, they are expressed in terms of the state $x(t)$ and the input $u(t)$. For the aeroe-

lastic system in this case study, quadratic cost functions are specified as function of the pitch angle, plunge displacement, and control input, resulting in the following expressions:

$$J(\alpha,\beta)=\int_0^{T_H}\{w_\alpha[\alpha(t)-\alpha_{ref}(t)]^2+w_\beta\beta^2(t)\}dt \tag{3.11}$$

$$J(h,\beta)=\int_0^{T_H}\{w_h[h(t)-h_{ref}(t)]^2+w_\beta\beta^2(t)\}dt \tag{3.12}$$

where $w_\alpha$, $w_h$, and $w_\beta$ represents weighting factors and the specified reference/ command pitch angle and plunge displacement are denoted as $\alpha_{ref}(t)$ and $h_{ref}(t)$ respectively. The weighting factors in the cost function allow adjustment on the priority of minimizing the pitch angle or plunge displacement error relative to minimizing the control effort from the trailing edge flap.

A dynamic model is required in the MPC algorithm to predict system response from a given control input history. A Volterra-based model of the aeroelastic system is used, which consists of the zero-order kernel that handles nonzero initial conditions and the identified first-, second- and third-order Volterra kernels. The predicted pitch angle and plunge displacement responses to a given trailing edge control input sequence $\beta(t)$, $0\le t<T_H$, are given by:

$$\begin{aligned}\alpha(t)=V_0^\alpha(t)+\int_0^t V_1^\alpha(\xi)u(t-\xi)d\xi+\int_0^t\int_0^t V_2^\alpha(\xi,\eta)u(t-\xi)u(t-\eta)d\xi d\eta\\+\int_0^t\int_0^t\int_0^t V_3^\alpha(\xi,\eta,\gamma)u(t-\xi)u(t-\eta)u(t-\gamma)d\xi d\eta d\gamma\end{aligned} \tag{3.13}$$

$$\begin{aligned}h(t)=V_0^h(t)+\int_0^t V_1^h(\xi)u(t-\xi)d\xi+\int_0^t\int_0^t V_2^h(\xi,\eta)u(t-\xi)u(t-\eta)d\xi d\eta\\+\int_0^t\int_0^t\int_0^t V_3^h(\xi,\eta,\gamma)u(t-\xi)u(t-\eta)u(t-\gamma)d\xi d\eta d\gamma\end{aligned} \tag{3.14}$$

where $\{V_0^\alpha, V_1^\alpha, V_2^\alpha, V_3^\alpha\}$ and $\{V_0^h, V_1^h, V_2^h, V_3^h\}$ define the pitch and plunge Volterra kernels respectively. Constraints are imposed on the trailing edge flap deflection that bound the deflection angle and rate of change over the cost horizon. These constraints are specified as follow:

$$|\beta(t)| \leq \beta_{max} \qquad |\dot{\beta}(t)| \leq \dot{\beta}_{max} \qquad \forall t \in [0, T_H] \tag{3.15}$$

The Volterra-based model predictive control is implemented in discrete time with time step $\Delta T$. Instead of computing the entire optimal control sequence, the MPC algorithm computes the nodal values of the optimal control sequence and linearly interpolate the nodal values to obtain the full optimal control sequence within the cost horizon period. By calculating the nodal values, the computational time on the optimization problem is significantly reduced. The nodal values of the optimal control sequence is calculated by minimizes Eq.(3.16) over the optimization horizon.

$$J = \sum_{k=0}^{n} \{w_\alpha [\alpha(k) - \alpha_{ref}]^2 + w_\beta \beta^2(k)\} \Delta T \tag{3.16}$$

subject to the control input constraint shown in Eq.(3.15) and the discrete-time Volterra predictive model:

$$\begin{aligned} \alpha(n) = V_0^\alpha(n)\Delta T + \sum_{k=0}^{n} V_1^\alpha(k)\beta(n-k)\Delta T + \sum_{k=0}^{n}\sum_{l=0}^{n} V_2^\alpha(k,l)\beta(n-k)\beta(n-l)\Delta T^2 \\ + \sum_{k=0}^{n}\sum_{l=0}^{n}\sum_{m=0}^{n} V_3^\alpha(k,l,m)\beta(n-k)\beta(n-l)\beta(n-m)\Delta T^3 \end{aligned} \tag{3.17}$$

To implement the MPC algorithm, the *fmincon* function within MATLAB's optimization toolbox is utilized. The function is a nonlinear programming solver that determines the minimum of an objective function subject to constraints that can be specified as

$$\min_x f(x) \ni \begin{cases} c(x) \leq 0 \\ ceq(x) = 0 \\ A \cdot x \leq b \\ Aeq \cdot x = beq \\ lb \leq x \leq ub \end{cases} \tag{3.18}$$

where $c(x)$ and $ceq(x)$ represent nonlinear inequality and equality constraints, $A$ (matrix form) and $b$ (vector form) are linear inequality constraints, $Aeq$ (matrix form) and $beq$ (vector form) are linear equality constraints, and lastly $lb$ and $ub$ represent lower and upper bounds respectively.

In the MPC routine implementation, the *fmincon* function employs an iterative strategy to minimize the cost function defined in Eq.(3.11). Equality and inequality constraints do not exist in this optimization problem, thus the parameters for those constraint fields are left empty. The upper and lower bounds, which are defined as the upper and lower limits of the trailing edge flap deflection, are specified as in Eq.(3.15). With these constraints in place, the optimized control action will not exceed the trailing edge flap's deflection limits. An extra *fmincon* parameter named *option* is added to activate the parallel computing option within MATLAB while

running simulations for controller designs that are being implemented on the nonlinear aeroelastic system. This parallel computing option reduced the computational time for the nonlinear MPC implementation by half or more.

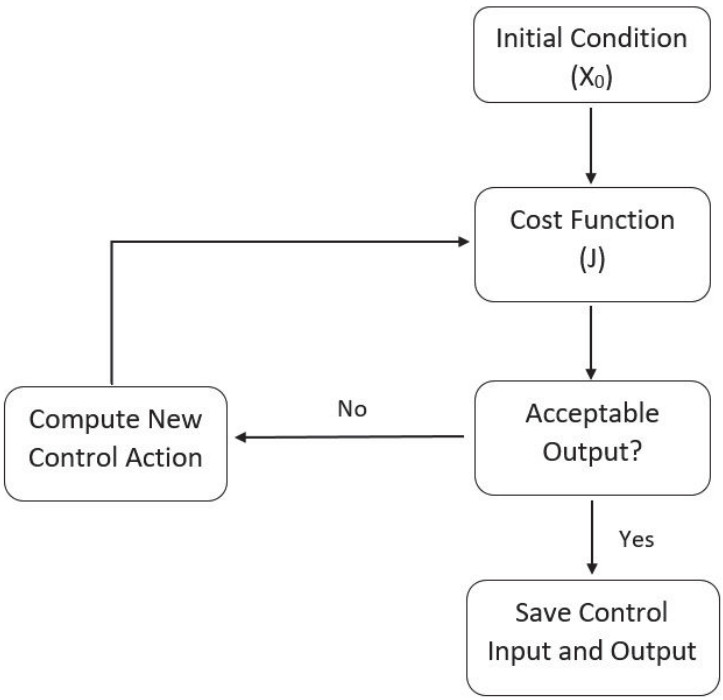


Figure 3.2. Optimization function *fmincon* routine in flowchart form.

With all the input parameters and constraints defined, the solver's optimization routine is depicted in Figure 3.2. The initial conditions of all states and the control are passed into the cost function. If the solution of the cost function is acceptable, then the optimized control input with its corresponding states will be saved as a time history. On the other hand, if the solution is not acceptable, then a new control action will be computed. The optimization process continues until the optimal control input sequence is obtained.

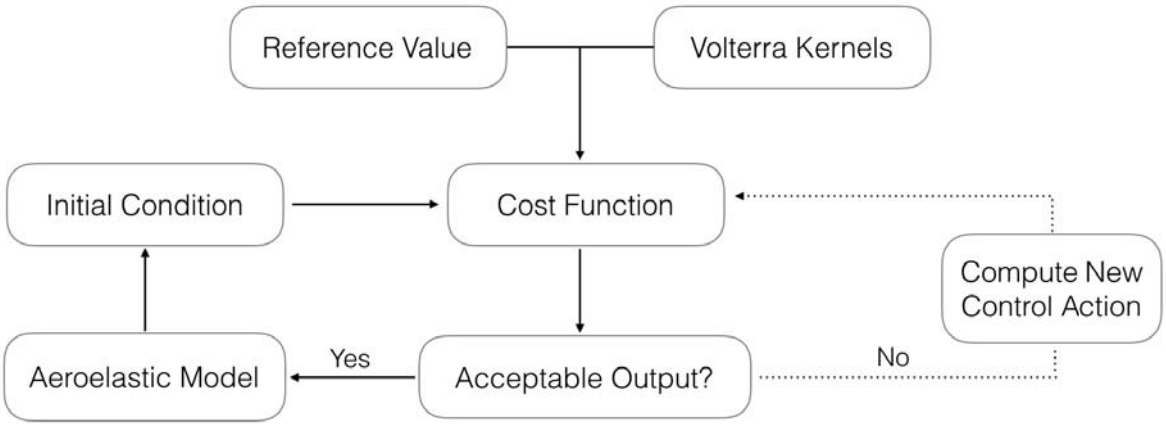


Figure 3.3. MPC routine in flowchart form.

The optimization routine is incorporated into the MPC algorithm as depicted in the flow chart in Figure 3.3. The process begins with the initial condition defined by the user, which is sent to the cost function along with the reference output value and the Volterra kernels. The Volterra kernels are used to form the Volterra-based predictive model that computes the predicted output values. The *fmincon* function is used to minimize the cost function and determine the allowable optimized control action. If the output is acceptable, the optimized control action will be applied to the aeroelastic simulation model created in Simulink. State outputs from the simulation model will define the initial condition for the next optimization interval and the process continues until the simulation reaches the final time.

# 4. Controller Implementation on a Linear Aeroelastic System

In this chapter, different linear controllers were implemented on the linear aeroelastic system. These controllers include the LQR baseline controller in continuous and discrete time using different methods to define the $Q$ matrix , the LQR-based MPC controller and the LMPC controller. Each controller's response and performance are presented and discussed within this chapter. Furthermore, a comparison is performed between all chosen controllers for regulator and tracking cases at U = 6 m/s and U = 12.5 m/s.

## 4.1 Classical LQR Baseline Controller

The LQR controller described in Chapter 2 was applied to the linear aeroelastic system to provide a baseline for evaluating the performance of the MPC strategies. Referring to Chapter 2, two methods were used to define the $Q$ matrix. Tables 4.1 - 4.8 present different combinations of values that were chosen for the $Q$ and $R$ matrices to tune the LQR controller in both continuous and discrete time for the U = 6 m/s and U = 12.5 m/s cases respectively.

Table 4.1. Maximum value for each state in $Q$ using method 1 for the continuous-time LQR controller at 6 m/s.

| **Sets** | $Q^h_{max}$ | $Q^{\dot{h}}_{max}$ | $Q^{\alpha}_{max}$ | $Q^{\dot{\alpha}}_{max}$ | $R_{Pitch}$ |
|---|---|---|---|---|---|
| 1 | 1 | 1 | 10 | 5 | 5 |
| 2 | | | 20 | 5 | 10 |
| 3 | | | 20 | 20 | 1 |
| 4 | | | 20 | 10 | 1 |

Table 4.2. Maximum value for each state in $Q$ using method 1 for the continuous-time LQR controller at 12.5 m/s.

| **Sets** | $Q^h_{max}$ | $Q^{\dot{h}}_{max}$ | $Q^{\alpha}_{max}$ | $Q^{\dot{\alpha}}_{max}$ | $R_{Pitch}$ |
|---|---|---|---|---|---|
| 1 | 1 | 1 | 20 | 5 | 1 |
| 2 | 0.1 | 0.1 | 10 | 1 | 0.5 |
| 3 | | | 1 | | 0.5 |
| 4 | | | 0.5 | | 0.5 |

Table 4.3. Maximum value for each state in $Q$ using method 2 for the continuous-time LQR controller at 6 m/s.

| $Q^h_{max}$ | $Q^{\dot{h}}_{max}$ | $Q^{\alpha}_{max}$ | $Q^{\dot{\alpha}}_{max}$ | $R_{Pitch}$ |
|---|---|---|---|---|
| 0 | 0 | 0.25 | 0 | 5 |
| | | 0.5 | | |
| | | 1 | | |
| | | 10 | | |

Table 4.4. Maximum value for each state in $Q$ using method 2 for the continuous-time LQR controller at 12.5 m/s.

| $Q^h_{max}$ | $Q^{\dot{h}}_{max}$ | $Q^{\alpha}_{max}$ | $Q^{\dot{\alpha}}_{max}$ | $R_{Pitch}$ |
|---|---|---|---|---|
| 0 | 0 | 0.5 | 0 | 1 |
| | | 0.8 | | |
| | | 1 | | |
| | | 0.5 | | 5 |
| | | 1 | | |

Table 4.5. Maximum value for each state in $Q$ using method 1 for the discrete-time LQR controller at 6 m/s.

| **Sets** | $Q^h_{max}$ | $Q^{\dot{h}}_{max}$ | $Q^{\alpha}_{max}$ | $Q^{\dot{\alpha}}_{max}$ | $R_{Pitch}$ |
|---|---|---|---|---|---|
| 1 | 1 | 1 | 5 | 2 | 1 |
| 2 | | | | 5 | |
| 3 | | | | 2 | 5 |
| 4 | | | | 5 | |

Table 4.6. Maximum value for each state in $Q$ using method 1 for the discrete-time LQR controller at 12.5 m/s.

| **Sets** | $Q^h_{max}$ | $Q^{\dot{h}}_{max}$ | $Q^{\alpha}_{max}$ | $Q^{\dot{\alpha}}_{max}$ | $R_{Pitch}$ |
|---|---|---|---|---|---|
| 1 | 1 | 1 | 5 | 2 | 1 |
| 2 | | | | | 5 |
| 3 | | | | 5 | |

Table 4.7. Maximum value for each state in $Q$ using method 2 for the discrete-time LQR controller at 6 m/s.

| $Q^h_{max}$ | $Q^{\dot{h}}_{max}$ | $Q^{\alpha}_{max}$ | $Q^{\dot{\alpha}}_{max}$ | $R_{Pitch}$ |
|---|---|---|---|---|
| 0 | 0 | 1 | 0 | 1 |
| | | | | 5 |
| | | 5 | | 10 |
| | | | | 50 |

Table 4.8. Maximum value for each state in $Q$ using method 2 for the discrete-time LQR controller at 12.5 m/s.

| $Q^h_{max}$ | $Q^{\dot{h}}_{max}$ | $Q^{\alpha}_{max}$ | $Q^{\dot{\alpha}}_{max}$ | $R_{Pitch}$ |
|---|---|---|---|---|
| 0 | 0 | 3 | 0 | 2 |
| | | | | 5 |
| | | 5 | | 2 |
| | | | | 5 |

### 4.1.1 Continuous-Time LQR: Free-stream Velocity at 6 m/s

In general, the pitch response and control effort are more aggressive after the LQR controller is applied to the linear aeroelastic system. Due to the control action, the settling time of the response has reduced compared to the open-loop response.

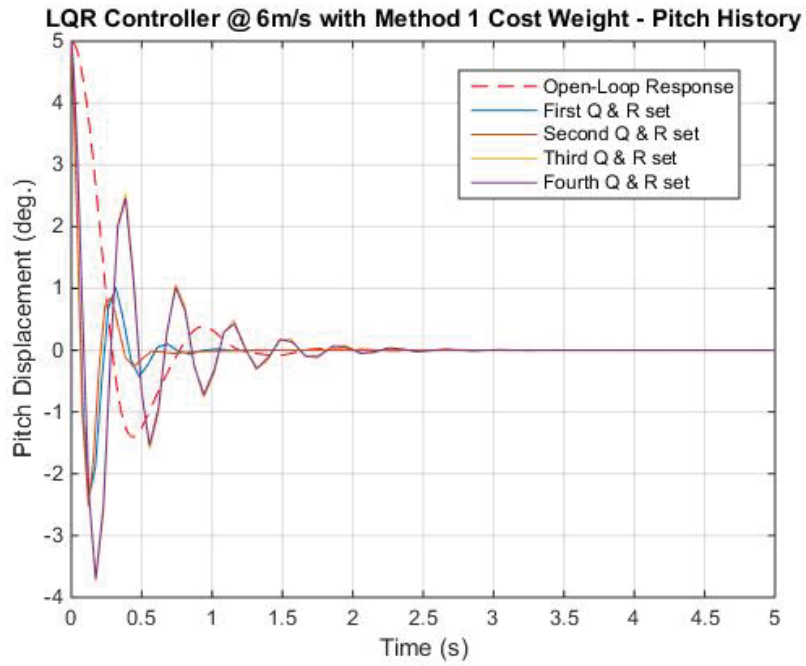


Figure 4.1. Pitch response for LQR baseline controller on the linear aeroelastic system with $Q$ chosen using method 1 at 6 m/s.

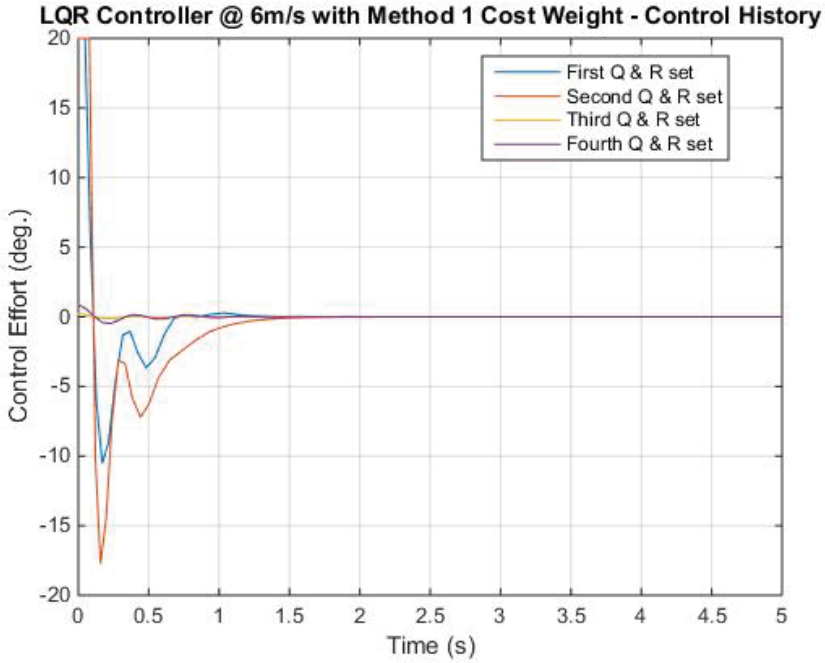


Figure 4.2. Control effort for LQR baseline controller on the linear aeroelastic system with $Q$ chosen using method 1 at 6 m/s.

Table 4.9 shows the performance of the LQR controller through the pitch RMS error and the control effort. As $Q^{\dot{\alpha}}_{max}$ gets larger, the error on pitch increases while the control effort is reduced. This can also be seen in Figure 4.1, where there are more oscillations in the pitch response for both the third and fourth sets of the $Q$ and $R$ matrices. The first set of $Q$ and $R$ (light blue) yields the best qualitative balance of pitch response and control effort out of all the sets. Although the time to settle is slightly greater than the pitch response from the second set of $Q$ and $R$, the qualitative controller performance is reasonable, within limitations and not overly aggressive.

Table 4.9. RMSE and control effort for LQR controller using method 1 to determine the $Q$ matrix at 6 m/s.

| **Sets** | $Q^{h}_{max}$ | $Q^{\dot{h}}_{max}$ | $Q^{\alpha}_{max}$ | $Q^{\dot{\alpha}}_{max}$ | $R_{Pitch}$ | **Pitch RMSE** | **Control Effort** |
|---|---|---|---|---|---|---|---|
| 1 | 1 | 1 | 10 | 5 | 5 | 1.479 | 7.414 |
| 2 | | | 20 | 5 | 10 | 1.461 | 8.362 |
| 3 | | | 20 | 20 | 1 | 1.639 | 0.067 |
| 4 | | | 20 | 10 | 1 | 1.628 | 0.260 |

According to Table 4.10, the value of $Q^{\alpha}_{max}$ has a proportional and inverse relationship with pitch error and control effort respectively. Referring to Figures 4.3 and 4.4, the pitch response oscillates for almost 2 seconds before it settles to zero when $Q^{\alpha}_{max}$ is chosen to be 10. The pitch response and control effort obtained from the LQR controller with $Q^{\alpha}_{max} = 1$ and $R_{Pitch} = 5$ in the cost function (light blue) provides the best qualitative performance out of all combinations of $Q$ and $R$ that were implemented. Although the closed-loop pitch response overshoots more than the open-loop response, the time to settle is shorter and the largest flap deflection required is -5 degrees.

Table 4.10. RMSE and control effort for LQR controller using method 2 to determine the $Q$ matrix at 6 m/s.

| $Q^{h}_{max}$ | $Q^{\dot{h}}_{max}$ | $Q^{\alpha}_{max}$ | $Q^{\dot{\alpha}}_{max}$ | $R_{Pitch}$ | **Pitch RMSE** | **Control Effort** |
|---|---|---|---|---|---|---|
| 0 | 0 | 0.25 | 0 | 5 | 1.441 | 8.339 |
| | | 0.5 | | | 1.487 | 7.220 |
| | | 1 | | | 1.506 | 5.077 |
| | | 10 | | | 1.636 | 0.093 |

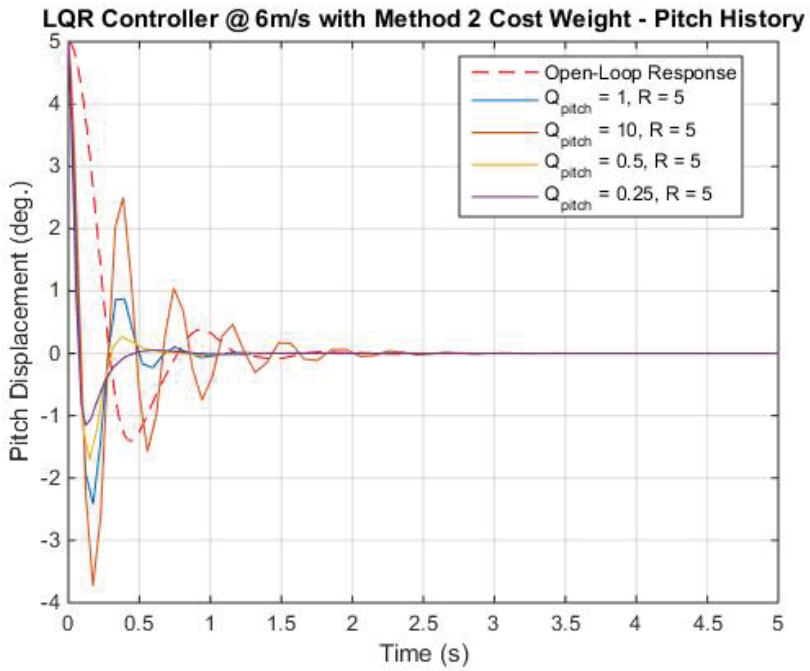


Figure 4.3. Pitch response for LQR baseline controller on the linear aeroelastic system with $Q$ chosen using method two.

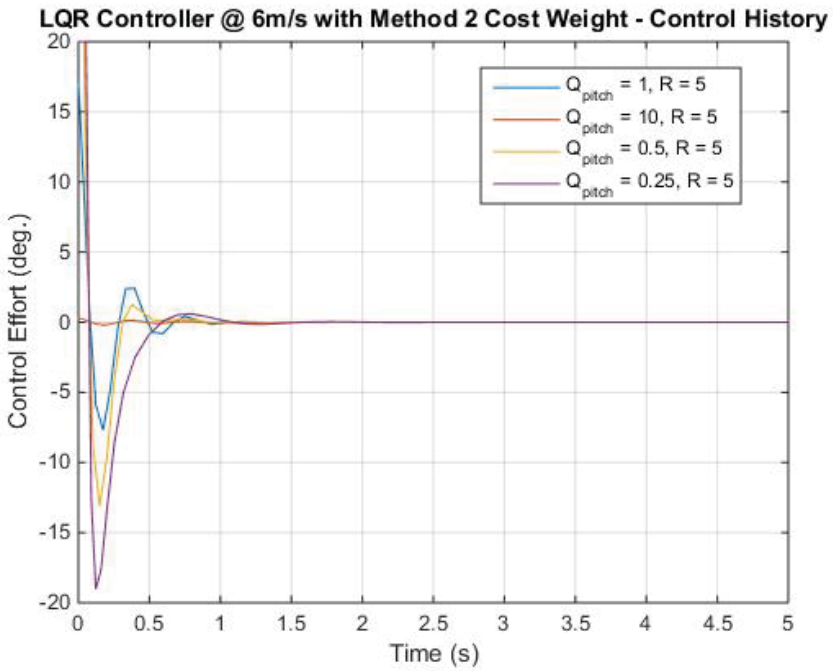


Figure 4.4. Control effort for LQR baseline controller on the linear aeroelastic system with $Q$ chosen using method two.

### 4.1.2 Continuous-Time LQR: Free-stream Velocity at 12.5 m/s

A LQR controller was designed to stabilize the linear aeroelastic system at U = 12.5 m/s and regulate the pitch response to zero. Recall that the open-loop system is unstable at this flight condition. Four different sets of $Q$ and $R$ matrix combinations were used to tune the controller. The RMS error presented in Table 4.11 shows that the second, third and fourth sets yield a better pitch response compared to the first set as the pitch RMS error is less, and the response has more damping with a shorter settling time. While the pitch error and performance of the controller are similar between the second, third and fourth sets, it can be concluded that the controller using the third set of $Q$ and $R$ matrices yields the most reasonable performance.

Table 4.11. RMSE and control effort for LQR controller using method 1 to determine the $Q$ matrix at 12.5 m/s.

| **Sets** | $Q^h_{max}$ | $Q^{\dot{h}}_{max}$ | $Q^{\alpha}_{max}$ | $Q^{\dot{\alpha}}_{max}$ | $R_{Pitch}$ | **Pitch RMSE** | **Control Effort** |
|---|---|---|---|---|---|---|---|
| 1 | 1 | 1 | 20 | 5 | 1 | 1.490 | 2.719 |
| 2 | 0.1 | 0.1 | 10 | 1 | 0.5 | 1.416 | 5.162 |
| 3 | | | 1 | | | 1.415 | 5.216 |
| 4 | | | 0.5 | | | 1.412 | 5.379 |

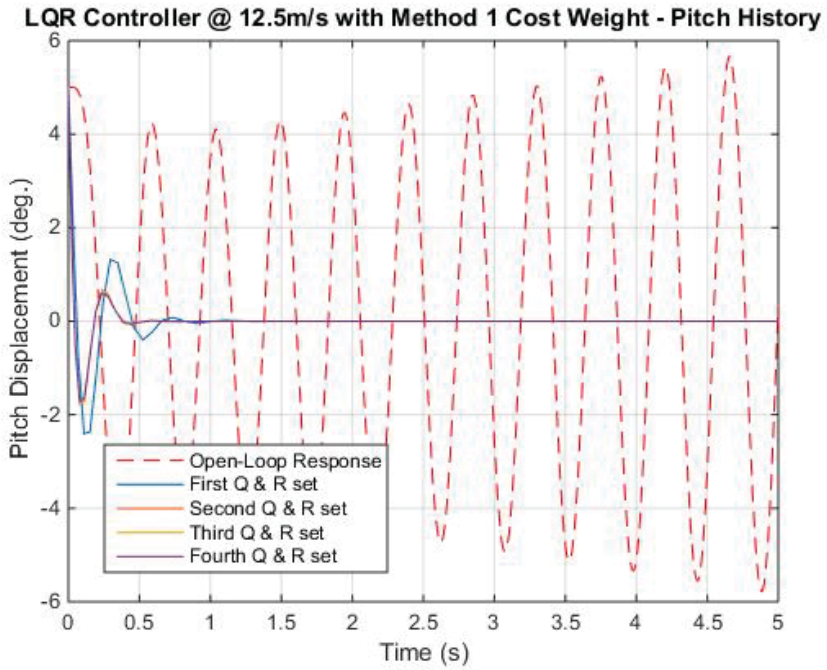


Figure 4.5. Pitch response for LQR baseline controller on the linear aeroelastic system at U = 12.5 m/s with $Q$ chosen using method one.

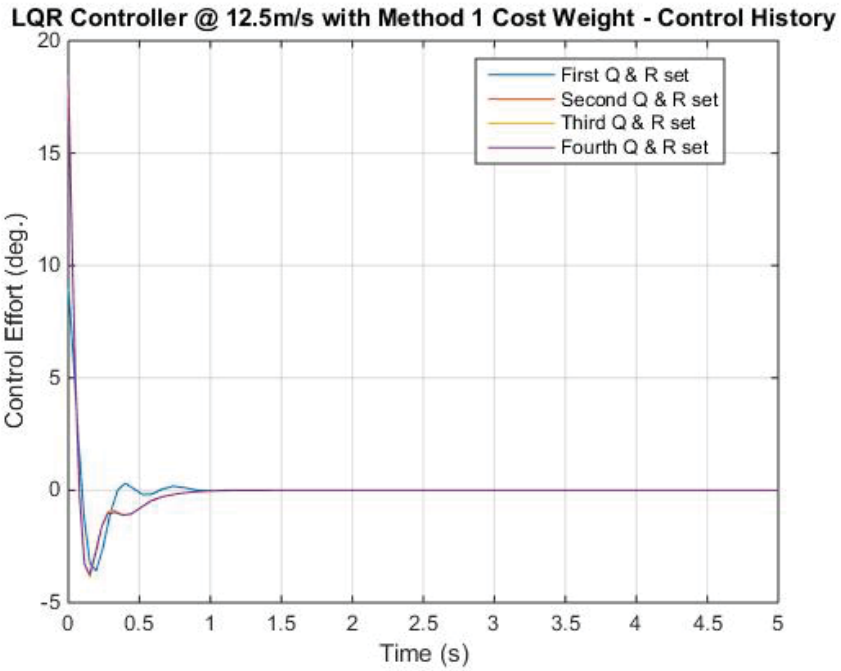


Figure 4.6. Control effort for LQR baseline controller on the linear aeroelastic system at U = 12.5 m/s with $Q$ chosen using method one.

According to the results in Table 4.12, using the second method to determine the $Q$ matrix sufficiently reduced the control effort compared to the first method summarized in Table 4.11. By allowing more control deflection on the trailing edge flap, the pitch error is minimized. Within these designs, the controller with $Q^{\alpha}_{max} = 0.5$ and $R_{Pitch} = 5$, depicted as a purple line in Figures 4.7 and 4.8, provides a response with the least pitch RMS error with acceptable control effort. From Figure 4.8, the controller yielded a pitch response with the shortest settling time and a smooth control action with the largest deflection no more than -5 degrees.

Table 4.12. RMSE and control effort for LQR controller using method 2 to determine the $Q$ matrix at 12.5 m/s.

| $Q^{h}_{max}$ | $Q^{\dot{h}}_{max}$ | $Q^{\alpha}_{max}$ | $Q^{\dot{\alpha}}_{max}$ | $R_{Pitch}$ | **Pitch RMSE** | **Control Effort** |
|---|---|---|---|---|---|---|
| 0 | 0 | 0.5 | 0 | 1 | 1.466 | 3.378 |
| | | 0.8 | | | 1.522 | 2.266 |
| | | 1 | | | 1.562 | 1.889 |
| | | 0.5 | | 5 | 1.024 | 5.004 |
| | | 1 | | | 1.569 | 7.208 |

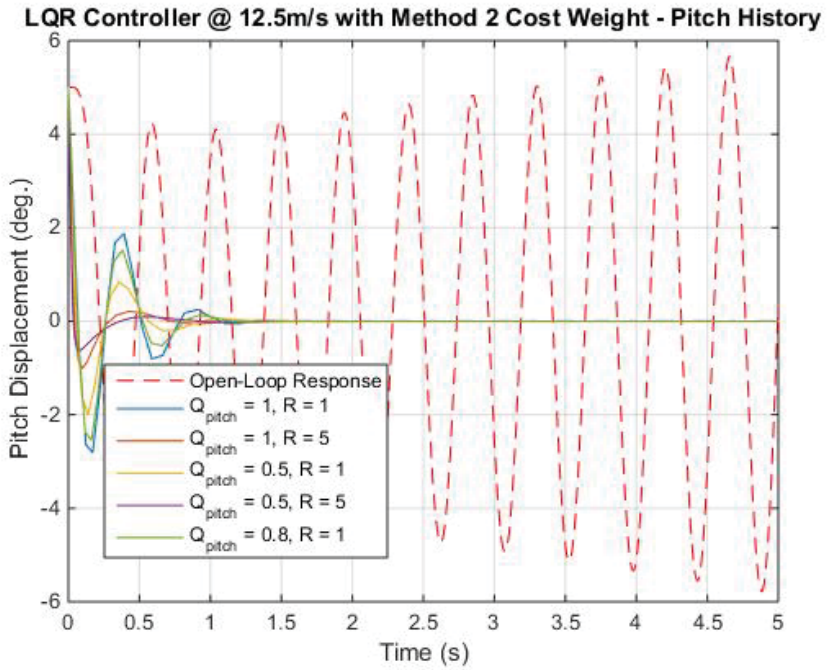


Figure 4.7. Pitch response for LQR baseline controller on the linear aeroelastic system at U = 12.5 m/s with $Q$ chosen using method two.

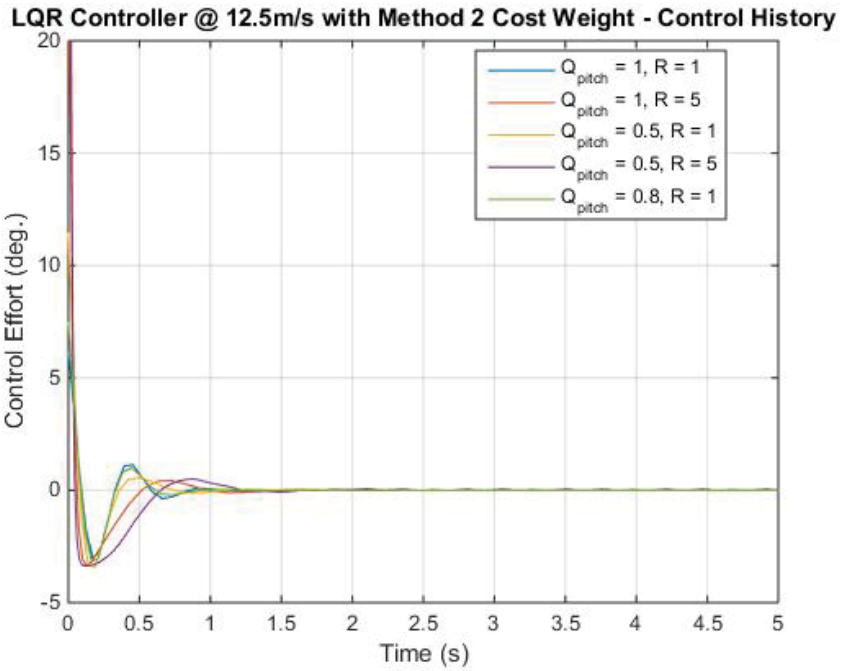


Figure 4.8. Control effort for LQR baseline controller on the linear aeroelastic system at U = 12.5 m/s with $Q$ chosen using method two.

### 4.1.3 Discrete-Time LQR: Free-stream Velocity at 6 m/s

The LQR baseline controller was implemented in discrete-time to yield responses that are comparable with the LMPC controller. New sets of $Q$ and $R$ matrices were defined in Tables 4.5-4.8 for the LQR controller in discrete-time.

Table 4.13. RMSE and control effort for discrete-time LQR controller using method 1 to determine the $Q$ matrix at 6 m/s.

| **Sets** | $Q^h_{max}$ | $Q^{\dot{h}}_{max}$ | $Q^{\alpha}_{max}$ | $Q^{\dot{\alpha}}_{max}$ | $R_{Pitch}$ | **Pitch RMSE** | **Control Effort** |
|---|---|---|---|---|---|---|---|
| 1 | 1 | 1 | 5 | 2 | 1 | 1.548 | 2.662 |
| 2 | | | | 5 | | 1.615 | 0.644 |
| 3 | | | | 2 | 5 | 1.631 | 8.349 |
| 4 | | | | 5 | | 1.495 | 5.441 |

Table 4.13 shows the performance of the discrete-time LQR controller through the pitch RMS error and the control effort. As $Q^{\dot{\alpha}}_{max}$ gets larger, the error on pitch increases while the control effort is reduced. This can also be seen in Figure 4.9, where the second set has the least overshoot in the pitch response, and results in having a large control action which is close to the control surface's limitation. The first set of $Q$ and $R$ (purple) yields the best qualitative balance of pitch response and control effort out of all the sets. Although the time to settle is slightly greater than the pitch response from the fourth set of $Q$ and $R$, the qualitative controller performance is reasonable, within limitations and not overly aggressive.

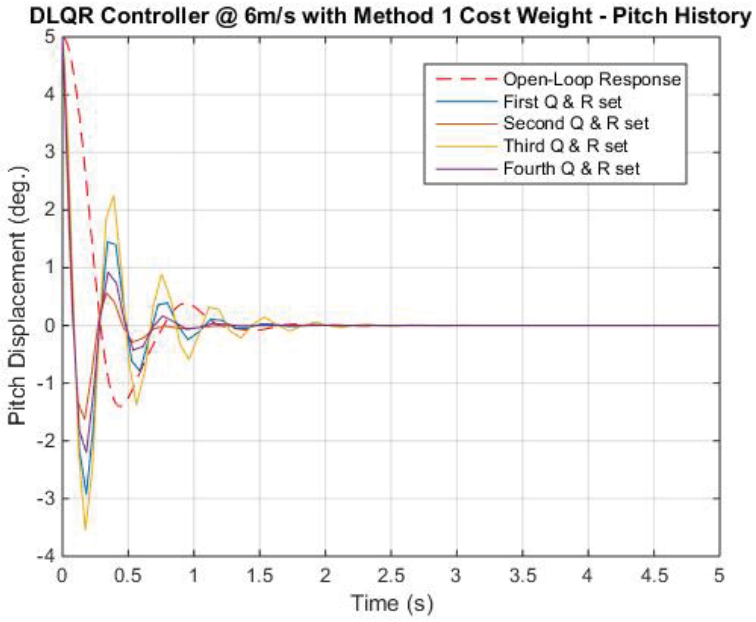


Figure 4.9. Pitch response for discrete-time LQR baseline controller on the linear aeroelastic system with $Q$ chosen using method 1 at 6 m/s.

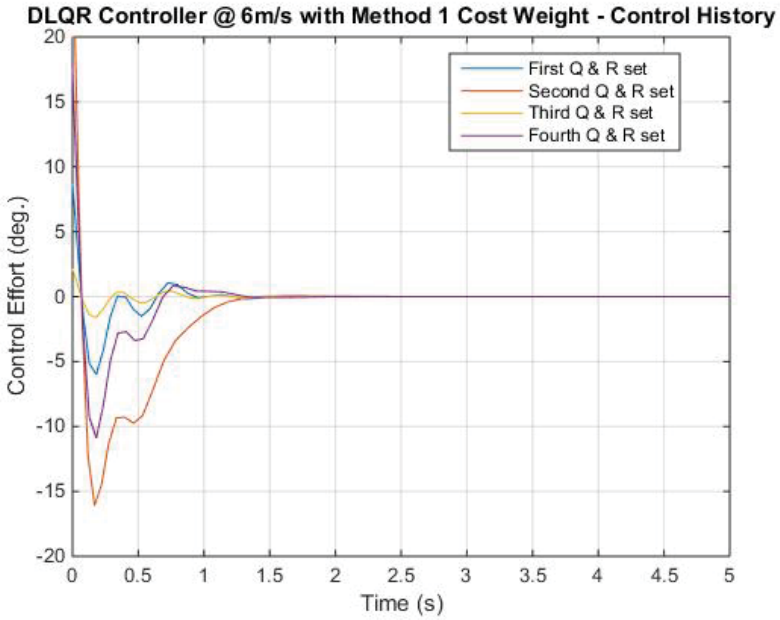


Figure 4.10. Control effort for discrete-time LQR baseline controller on the linear aeroelastic system with $Q$ chosen using method 1 at 6 m/s.

According to Table 4.14, more control effort is being used as the value of $R_{Pitch}$ gets larger with the $Q^{\alpha}_{max}$ value remaining unchanged. Referring to Figure 4.12, all sets of $Q$ and $R$ matrices yield control effort within the limitation. The pitch response and control effort obtained from the discrete-time LQR controller with $Q^{\alpha}_{max} = 5$ and $R_{Pitch} = 50$ in the cost function (purple) provides the best qualitative performance, which is shown in Figure 4.9. Although it used the most control effort out of all combinations of $Q$ and $R$ matrices, the closed-loop pitch response has the least overshoot and the shortest settling time.

Table 4.14. RMSE and control effort for discrete-time LQR controller using method 2 to determine the $Q$ matrix at 6 m/s.

| $Q^{h}_{max}$ | $Q^{\dot{h}}_{max}$ | $Q^{\alpha}_{max}$ | $Q^{\dot{\alpha}}_{max}$ | $R_{Pitch}$ | **Pitch RMSE** | **Control Effort** |
|---|---|---|---|---|---|---|
| 0 | 0 | 1 | 0 | 1 | 1.629 | 0.212 |
| | | | | 5 | 1.566 | 2.597 |
| | | 5 | | 10 | 1.611 | 0.731 |
| | | | | 50 | 1.538 | 4.774 |

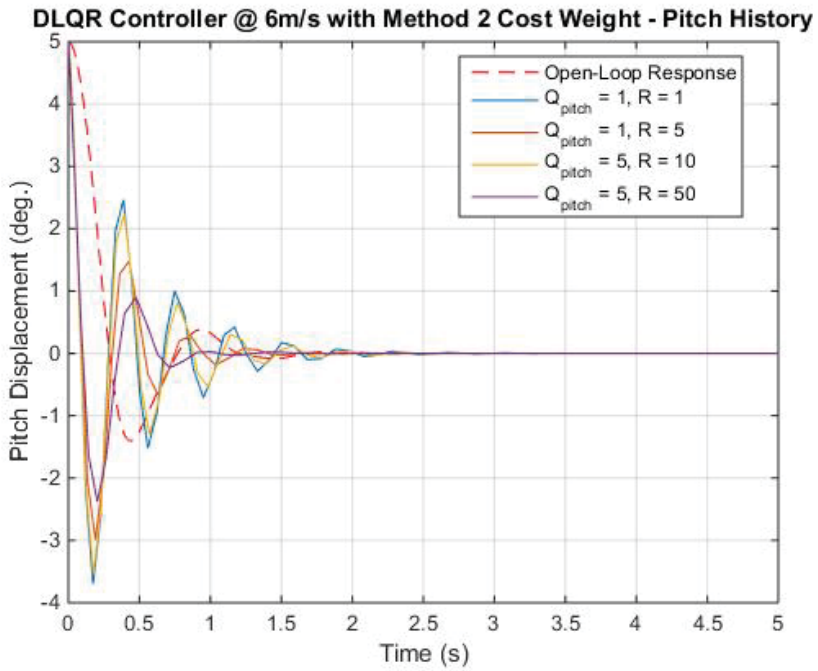


Figure 4.11. Pitch response for discrete-time LQR baseline controller on the linear aeroelastic system with $Q$ chosen using method two.

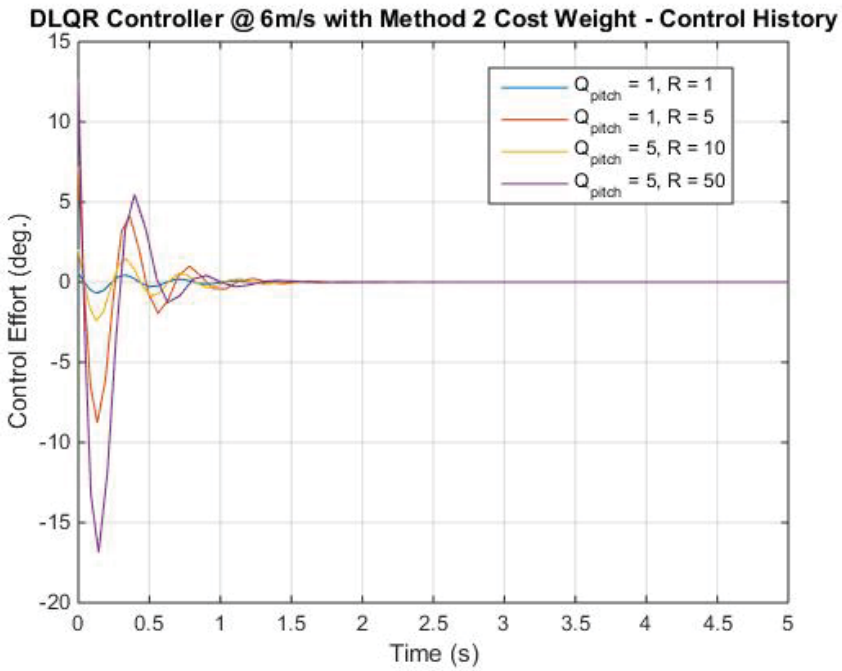


Figure 4.12. Control effort for discrete-time LQR baseline controller on the linear aeroelastic system with $Q$ chosen using method two.

### 4.1.4 Discrete-Time LQR: Free-stream Velocity at 12.5 m/s

A discrete-time LQR controller was designed to stabilize the linear aeroelastic system at U = 12.5 m/s and regulate the pitch response to zero. Recall that the open-loop system is unstable at this flight condition. Three different sets of $Q$ and $R$ matrix combinations were used to tune the controller. The RMS error presented in Table 4.15 shows that the third set yields a good balance between the pitch RMS error and control effort quantitatively. This conclusion can also be drawn qualitatively by analyzing the pitch response and control effort plots of the discrete-time LQR controller through Figures 4.13 and 4.14.

Table 4.15. RMSE and control effort for discrete-time LQR controller using method 1 to determine the $Q$ matrix at 12.5 m/s.

| **Sets** | $Q^h_{max}$ | $Q^{\dot{h}}_{max}$ | $Q^{\alpha}_{max}$ | $Q^{\dot{\alpha}}_{max}$ | $R_{Pitch}$ | **Pitch RMSE** | **Control Effort** |
|---|---|---|---|---|---|---|---|
| 1 | 1 | 1 | 5 | 2 | 1 | 1.485 | 2.448 |
| 2 | | | | | 5 | 1.458 | 3.801 |
| 3 | | | | 5 | | 1.467 | 2.997 |

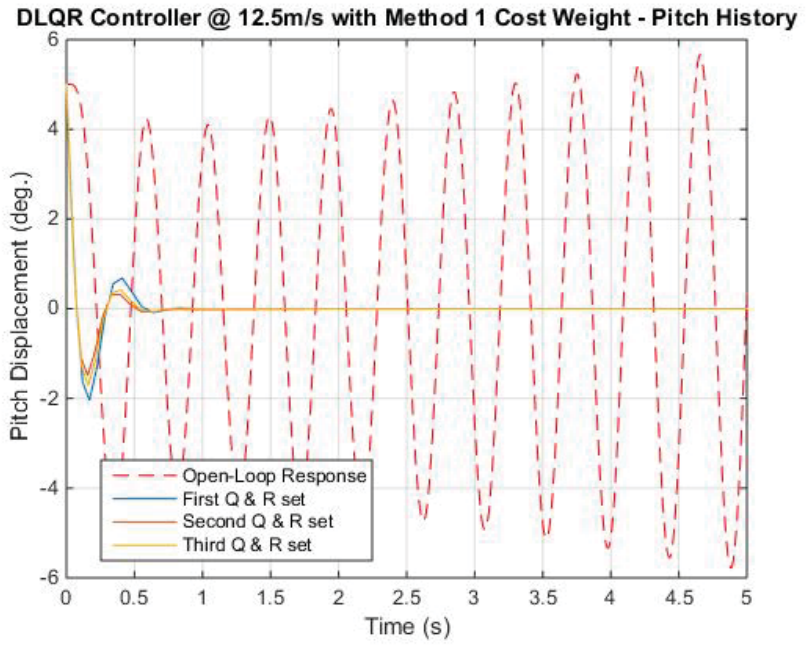


Figure 4.13. Pitch response for discrete-time LQR baseline controller on the linear aeroelastic system at U = 12.5 m/s with $Q$ chosen using method one.

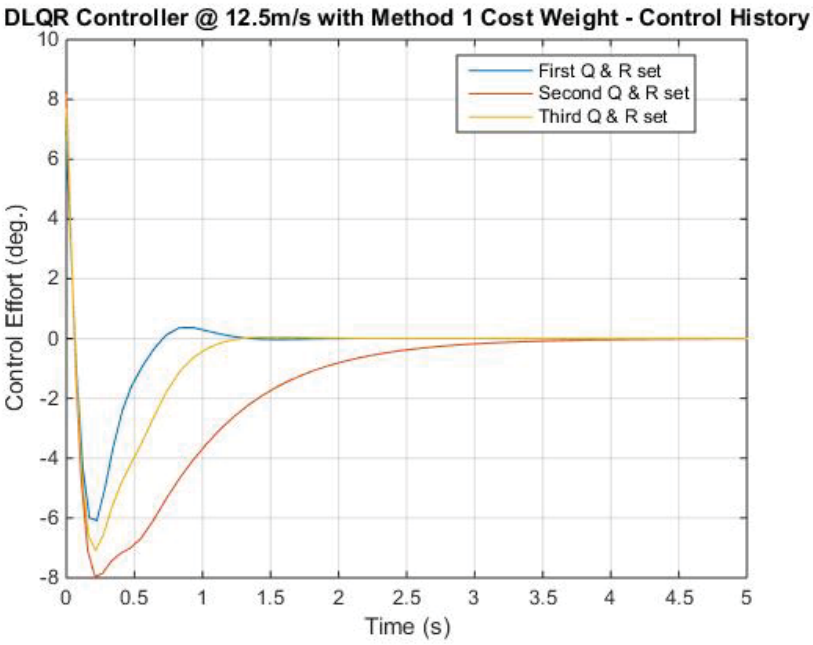


Figure 4.14. Control effort for discrete-time LQR baseline controller on the linear aeroelastic system at U = 12.5 m/s with $Q$ chosen using method one.

According to the results in Table 4.16, using the second method to determine the $Q$ matrix sufficiently reduced the control effort compared to the first method summarized in Table 4.15. Within these designs, the controller with $Q^{\alpha}_{max} = 3$ and $R_{Pitch} = 5$, depicted as an orange line in Figures 4.15 and 4.16, provides a response with the least pitch RMS error with acceptable control effort. From Figure 4.15, the controller yielded a pitch response with the shortest settling time and minimal overshoot.

Table 4.16. RMSE and control effort for discrete-time LQR controller using method 2 to determine the $Q$ matrix at 12.5 m/s.

| $Q^{h}_{max}$ | $Q^{\dot{h}}_{max}$ | $Q^{\alpha}_{max}$ | $Q^{\dot{\alpha}}_{max}$ | $R_{Pitch}$ | **Pitch RMSE** | **Control Effort** |
|---|---|---|---|---|---|---|
| 0 | 0 | 3 | 0 | 2 | 1.783 | 0.985 |
| | | | | 5 | 1.617 | 1.633 |
| | | 5 | | 2 | 1.968 | 1.734 |
| | | | | 5 | 1.683 | 1.237 |

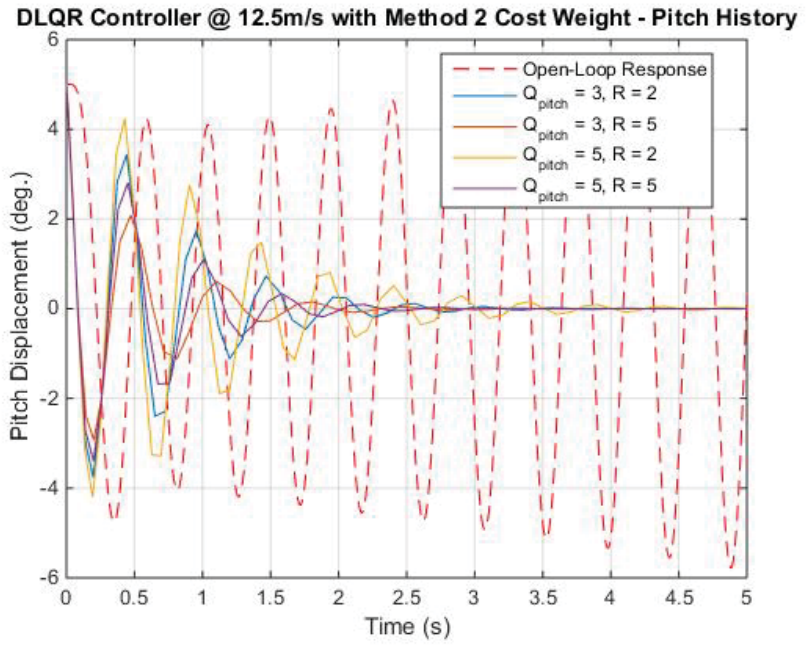


Figure 4.15. Pitch response for discrete-time LQR baseline controller on the linear aeroelastic system at U = 12.5 m/s with $Q$ chosen using method two.

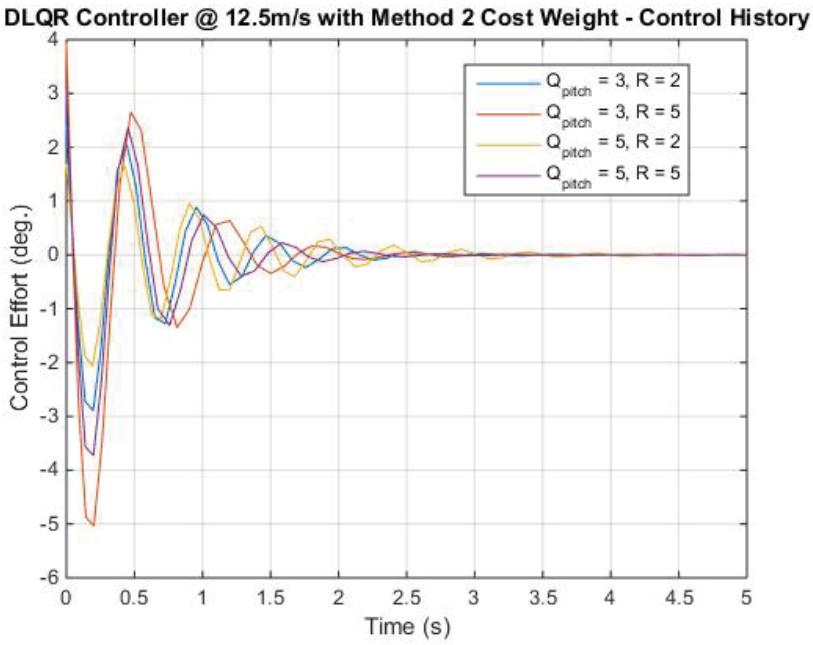


Figure 4.16. Control effort for discrete-time LQR baseline controller on the linear aeroelastic system at U = 12.5 m/s with $Q$ chosen using method two.

## 4.2 LMPC Stability

It is well known that linear controllers with quadratic cost function with infinite horizon have powerful stability properties. Hence, LQR controllers are used to stabilize linear system in various industrial applications world-wide. With MPC getting popular in the 1970s, extensive research has been done on investigating the closed-loop stability properties of a LMPC controller. Two papers, namely *A Modified Quadratic Cost Problem and Feedback Stabilization of a Linear System* and *Stabilizing state-feedback design via the Moving Horizon Method* written by Kwon and his colleagues set the stage for LMPC closed-loop stability. The first paper showed asymptotic stability is achieved with a modified control law using the receding horizon concept with fixed terminal constraints on the state. The methods for stabilizing a linear time-invariant system and linear time-varying system were discussed. The second paper considered a modification in the cost function by including a terminal cost term over a fixed depth horizon, which yields a stable closed-loop system. The details for each paper are discussed in the following sections.

### 4.2.1 Method 1: Terminal Constraint

Consider a linear time-invariant system with constant $A$, $B$ and $C$ matrices:

$$\begin{aligned} \dot{x}(t) &= Ax(t) + Bu(t) \\ y(t) &= Cx(t) \end{aligned} \tag{4.1}$$

Kwon and Pearson utilized the following cost function (Kwon & Pearson, 1977):

$$J(u) = \int_{t_0}^{t_f} [x^T(t)Qx(t) + u^T(t)Ru(t)]dt \tag{4.2}$$

where $Q$ and $R$ are symmetric positive semi-definite and positive definite matrices respectively with boundary conditions of

$$x(t_0) = x_0$$

$$x(t_f) = 0$$

If $\{A, B\}$ is completely controllable, the minimization of Eq.(4.2) subject to the terminal constraint results in the following optimal feedback control law:

$$u(t) = -R^{-1}B^T P^{-1}(t)x(t) \tag{4.3}$$

where $P(t)$ is obtained by solving the following matrix Riccati equation:

$$\frac{\mathrm{d}P(t)}{\mathrm{d}t} = -AP(t) - P(t)A^T - P(t)C^T QCP(t) + BR^{-1}B^T \tag{4.4}$$

The above procedure for computing the optimal input forms Theorem 3.1 (Kwon & Pearson, 1977), which states that if the $A$ and $B$ matrices of the LTI system is controllable, then the system with the fixed optimal feedback gain is asymptotically stable.

On the other hand, a similar approach is used to determine the optimal feedback control that leads a linear time-varying system to achieve asymptotic stability. Consider the following LTV system:

$$\begin{aligned} \dot{x}(t) &= A(t)x(t) + B(t)u(t) \\ y(t) &= C(t)x(t) \end{aligned} \tag{4.5}$$

where $A(t)$, $B(t)$ and $C(t)$ are piecewise continuous matrices and consider a cost function in the following form:

$$J(u) = \int_{t_0}^{t_f} [x^T(t)Q(t)x(t) + u^T(t)R(t)u(t)]dt \tag{4.6}$$

where $Q(t)$ and $R(t)$ are piecewise continuous symmetric positive definite matrices with the same initial and terminal boundary conditions as the LTI system. A two dimension Hamiltonian system is introduced to obtain the optimal solution:

$$\begin{bmatrix} \dot{x}(t) \\ \dot{p}(t) \end{bmatrix} = \begin{bmatrix} A(t) & -B(t)R^{-1}(t)B^T(t) \\ -c^T(t)Q(t)C(t) & -A^T(t) \end{bmatrix} \begin{bmatrix} x(t) \\ p(t) \end{bmatrix} \tag{4.7}$$

The state transition matrix of the Hamiltonian system is denoted by $S(t, t_0)$ and defined as the following 2 by 2 matrix:

$$S(t, t_0) = \begin{bmatrix} \psi(t, t_0) & \omega(t, t_0) \\ \chi(t, t_0) & \Lambda(t, t_0) \end{bmatrix} \tag{4.8}$$

If the LTV system is completely controllable within the interval of $[t, tf]$, then the optimal closed-loop feedback control is found to be

$$u(t) = -R^{-1}(t)B^T(t)P^{-1}(t, t_f)x(t) \tag{4.9}$$

where $P(t, t_f)$ can be obtained by integrating the Riccati equation with respect to $\tau$ over the interval $[t, t_f]$:

$$-\frac{\mathrm{d}P(\tau)}{\mathrm{d}t} = -A(\tau)P(\tau) - P(\tau)A^T(\tau) - P(\tau)C^T(\tau)Q(\tau)C(\tau)P(\tau) + B(\tau)R^{-1}(\tau)B^T(\tau) \tag{4.10}$$

Another method to obtain $P(t, t_f)$ is through the use of the Hamiltonian system and the state transition matrix, which result in $P(t, t_f) = -\psi^{-1}(t, t_f)\Omega(t, t_f)$. For the LTV system, Kwon and Pearson concluded that if $\{A(t), B(t)\}$ and $\{A(t), C(t)\}$ are uniformly controllable and observable respectively, with the $Q$ and $R$ matrices fulfilling the following assumptions:

$$\alpha_1 I \leq Q(t) \leq \alpha_2 I$$

$$\alpha_3 I \leq R(t) \leq \alpha_4 I$$

where $\alpha_1$, $\alpha_2$, $\alpha_3$ and $\alpha_4$ are positive constants, then the LTV system with the optimal feedback control law presented in Eq.(4.9) is uniformly asymptotically stable.

### 4.2.2 Method 2: Terminal Cost Term

The second method to guarantee closed-loop stability for the moving horizon method is to amend the cost function by adding a terminal cost term as shown below (Kwon, Bruckstein, & Kailath, 1983):

$$J(u) = \int_{t_0}^{t_f} [x^T(t)Q(t)x(t) + u^T(t)R(t)u(t)]dt + x^T(t_f)F(t_f)x(t_f) \tag{4.11}$$

Here $Q(t)$, $R(t)$ and $F(t)$ are known time-varying symmetric positive definite weighting matrices for the LTV system. These matrices are essentially design parameters and play a crucial role in determining the properties of the controller. Kwon et al. discussed three choices for $F(t)$ within the paper:

$$\text{Choice } 1 : F(t) = 0$$

$$\text{Choice 2} : F(t) = \infty$$

$$\text{Choice 3} : \frac{\mathrm{d}}{\mathrm{d}t}F(t) + A^T(t)F(T) + F(t)A(t) - F(t)B(t)R^{-1}(t)B^T(t)F(t) + Q(t) \leq 0$$

When $F(t) = 0$, the cost function becomes the normal cost function presented in Eq.(4.2). The theorem mentioned if the pair $\{A, B\}$ is controllable with $Q$ and $R$ being symmetric positive-definite matrices, then there exists a finite horizon $(T)$, such that by minimizing the cost function expressed in Eq.(4.2) the optimal feedback control law is:

$$u(t) = -R^{-1}B^T K(T)x(t) \tag{4.12}$$

For a LTI system with constant $Q$, $R$ and $F$ matrices, the constant optimal gain $K(T)$ is computed through the backwards Riccati equation:

$$-\frac{\mathrm{d}K(T)}{\mathrm{d}T} = K(T)A + A^T K(T) - K(T)BR^{-1}B(T)K(T) + Q \tag{4.13}$$

with an initial condition of $K_0 = F$. The optimal control law presented in Eq.(4.12) stabilizes a LTI system without terminal constraints. The same procedure and control law with time-varying matrices will also stabilize a LTV system.

In general, $F(t) = \infty$ turn outs to be important in providing a stabilizing optimal control law for a LTV system and it depends on to the systems controllability properties. An infinite weight assigned to the final state implies that the optimal control obtained from minimizing a quadratic cost over the given time interval is required to drive the final state to zero at the end of the time horizon. For some $\varepsilon > 0$ the

following inequality holds for all time if the pair $\{A(t), B(t)\}$ is uniformly completely controllable:

$$\alpha_1 I \leq W(t, t+\varepsilon) \leq \alpha_2 I$$

$$\|\varphi(t_1, t_2)\| \leq \gamma |t_1 - t_2|$$

In the above inequality, $\alpha$ is a positive constant, $\varphi$ represents the state transition matrix of $A(t)$, $\gamma$ is an operator to map the information between two spaces within the bounded intervals and $W(t, t+\varepsilon)$ is the controllability matrix defined as

$$W(t, t+\varepsilon) = \int_{t_1}^{t_2} \varphi(t_1, \varepsilon) B_\varepsilon B_\varepsilon^T \varphi^T(t_1, \varepsilon) d\varepsilon \tag{4.14}$$

With the above definition, Kwon et al. concluded that when the pair $\{A(t), B(t)\}$ is uniformly completely controllable and satisfies $0 \leq Q_t \leq \alpha_4 I$ and $\alpha_5 I \leq R_t \leq \alpha_6 I$, then for any $T > \varepsilon$, the following optimal feedback control law will stabilize the system:

$$u(t) = -R^{-1}(t) B^T(t) P^{-1}(t, t+T) x(t) \tag{4.15}$$

where $P(t, t+T)$ is obtained from the following Riccati equation with respect to $\tau$ over the interval $[t, t_f]$:

$$-\frac{\mathrm{d}P(\tau)}{\mathrm{d}t} = -P(\tau)A^T(\tau) - A(\tau)P(\tau) - P(\tau)Q(\tau)P(\tau) + B(\tau)R^{-1}(\tau)B(\tau) \tag{4.16}$$

The last case is when F(t) is defined as the third choice, then $K(t, \varepsilon)$ is obtained via the solution of the backward Riccati equation:

$$-\frac{\mathrm{d}K(t,\varepsilon)}{\mathrm{d}t} = K(t,\varepsilon)A(t) + A^T(t)K(t,\varepsilon) - K(t,\varepsilon)B(t)R^{-1}(t)B^T(t)K(t,\varepsilon) + Q \tag{4.17}$$

satisfying the following inequality for $t \leq \varepsilon_1 \leq \varepsilon_2$:

$$K(t, \varepsilon_1 : F_{\varepsilon_1}) \geq K(t, \varepsilon_2 : F_{\varepsilon_2})$$

Moreover, if the $\{A(t), B(t)\}$ pair is uniformly completely controllable and for all time, $\alpha_3 I \leq Q_t \leq \alpha_4 I$ and $\alpha_5 I \leq R_t \leq \alpha_6 I$, then for any $T$ such that $\delta \leq T \leq \infty$ there exist the following bounds on the optimal control gain:

$$\alpha_7 I \leq K(t, t+T) \leq \alpha_8 I$$

The above requirements are presented in Lemma 4.1 of the paper (Kwon et al., 1983). By satisfying the above condition, the optimal feedback control

$$u(t) = -R^{-1}(t)B^T(t)K(t, t+T)x(t) \tag{4.18}$$

yields a closed-loop system that is uniformly asymptotically stable.

### 4.3 LQR Fixed Horizon Controller

The classical LQR controller implemented in the above section utilized a cost function with infinite horizon and has well understood stability properties. The question regarding guaranteed closed-loop stability for a linear system within a fixed horizon is raised. As discussed in Section 4.2.1, if the pair $\{A, B\}$ is completely controllable with $Q \geq 0$ and $R \geq 0$, then the linear time-invariant system is asymptotically stable for any $t > 0$ with the optimal fixed gain control law defined by Eq.(4.3). Before implementing the LQR fixed horizon controller, the controllability of the aeroelas-

tic system is evaluated by determining the rank of the controllability matrix. The controllability matrix is defined by (Hespanha, 2009):

$$\mathrm{C} := \begin{bmatrix} B & AB & A^2B & \cdots & A^{n-1}B \end{bmatrix}_{n\times(kn)}$$

The controllability matrix of the aeroelastic system is full rank; thus the system is completely controllable.

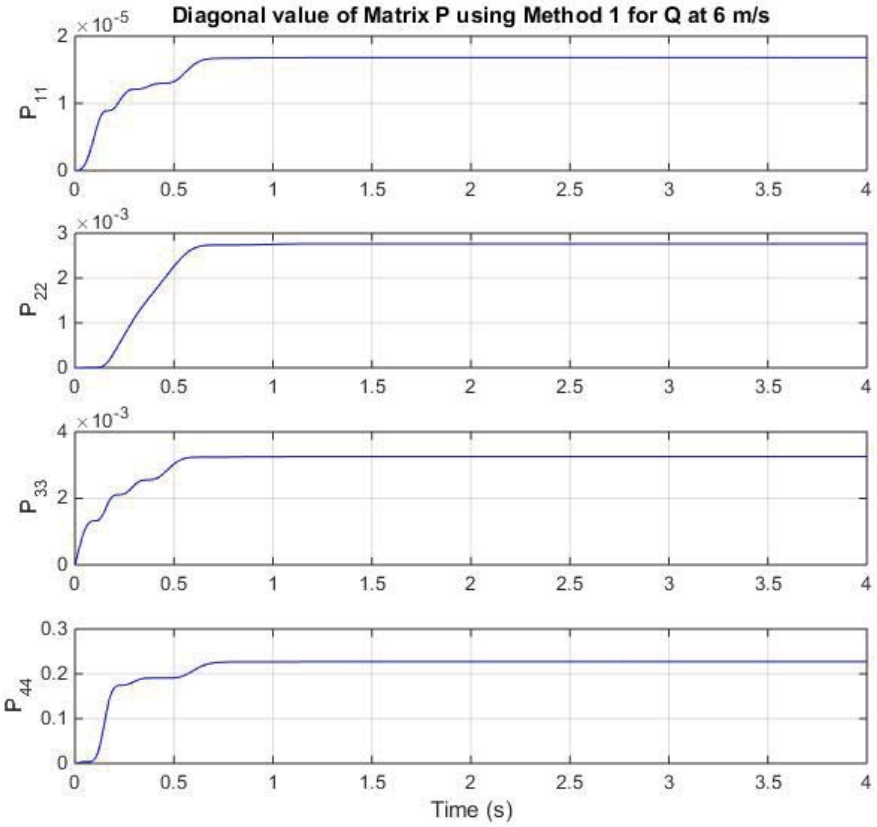


Figure 4.17. Diagonal value of $P$ within the fixed horizon at 6 m/s with Q matrix defined using method 1.

By solving the matrix Ricatti equation defined in Eq.(4.4), the values of $P(t)$ are computed throughout the fixed horizon. As Eq.(4.4) is integrated, the $P$ matrix is

computed at each time step. Figure 4.17 depicts the change of the diagonal of $P$ matrix within the fixed horizon. As the values of $P_{11}$, $P_{22}$, $P_{33}$ and $P_{44}$ converge to constant values within the first second, the optimal control gain also converges to a constant fixed gain. Then, $P(t)$ at the end of the fixed horizon is used to calculate the optimal fixed gain, $K_{LQR_{FH}} = R^{-1}B^{T}P^{-1}(T)$. The following response of the aeroelastic system is obtained by implementing the optimal fixed feedback gain and setting the finite horizon to 4 seconds.

In Section 4.1, the best combination of $Q$ and $R$ matrices is determined at each free-stream velocity. Figures 4.18-4.21 depict the comparison between pitch response and control effort for a LQR controller with these weight matrices combinations using an infinite cost function (blue line) and a finite cost function (dashed red line) at different free-stream velocity with different methods to define the $Q$ matrix. One common factor between all the figures is the LQR controller using a finite horizon cost function performs the same as the classical LQR controller. This observation suggests that the 4 seconds fixed horizon defined in the finite horizon LQR controller is a large horizon compare to the settling time of the aeroelastic system. Hence, the LQR controller with finite horizon set at 4 seconds has the same stability properties that a classical LQR controller possess.

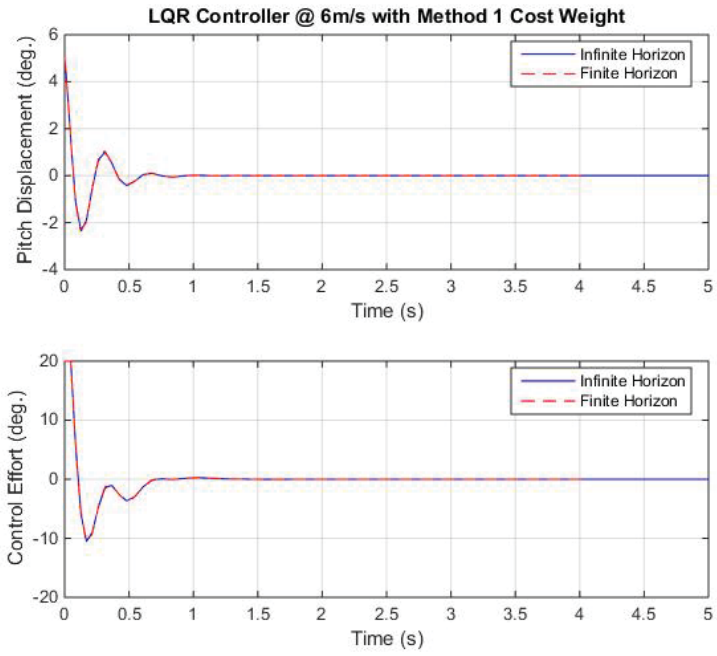


Figure 4.18. Comparison between infinite and fixed horizon LQR controller at 6 m/s with Q matrix defined using method 1.

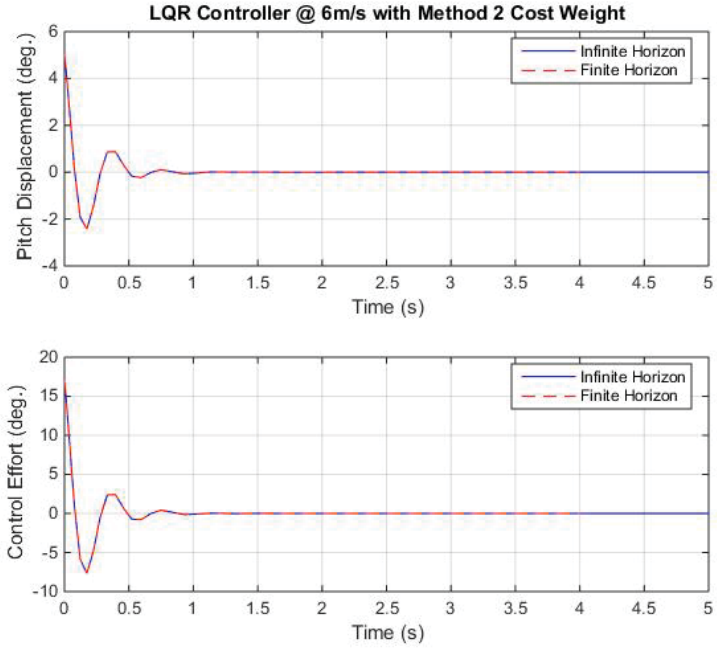


Figure 4.19. Comparison between infinite and fixed horizon LQR controller at 6 m/s with Q matrix defined using method 2.

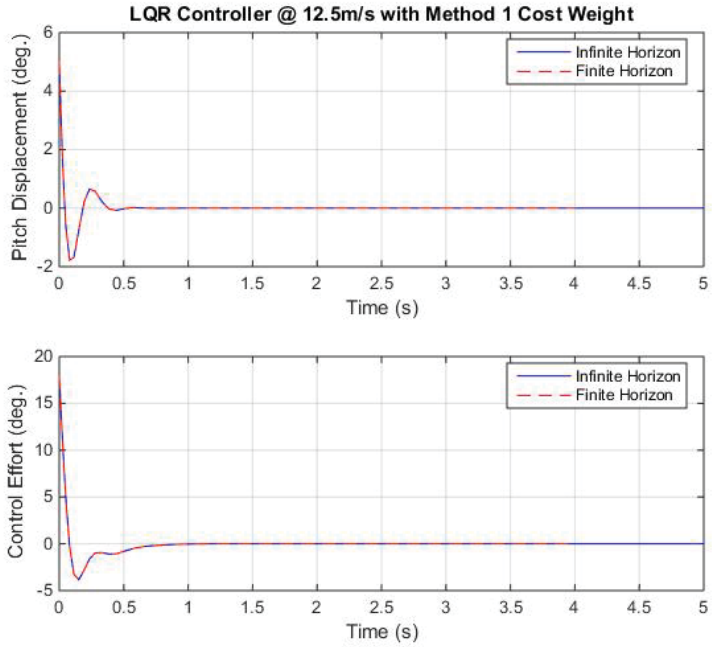


Figure 4.20. Comparison between infinite and fixed horizon LQR controller at 12.5 m/s with Q matrix defined using method 1.

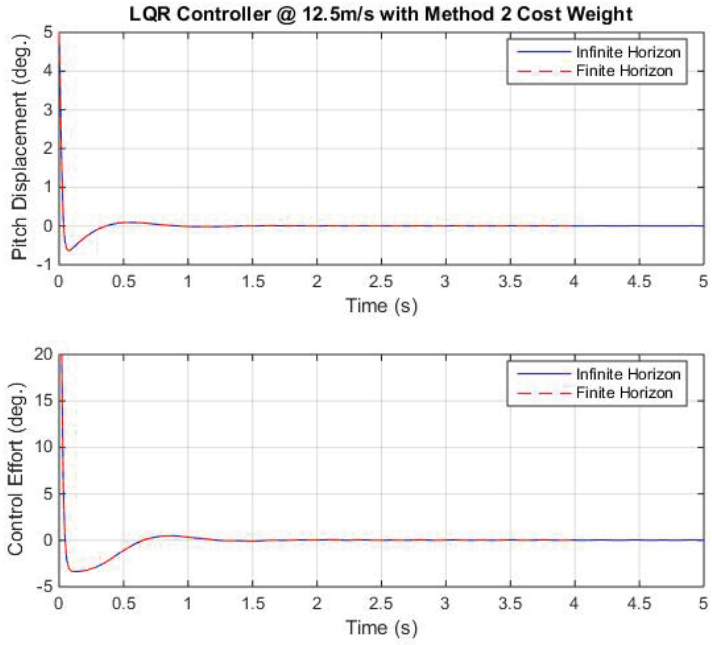


Figure 4.21. Comparison between infinite and fixed horizon LQR controller at 12.5 m/s with Q matrix defined using method 2.

## 4.4 Linear Volterra-Based MPC

The linear Volterra-based MPC was implemented on the linear aeroelastic system for both the U = 6 m/s and U = 12.5 m/s cases. For the linear MPC implementation, only the zero- and first- order Volterra kernels (i.e. $V_0 + V_1$) are used in the predictive model.

### 4.4.1 LMPC: Free-stream Velocity at 6 m/s

Figures 4.22 and 4.23 depict the pitch response and control action of the LMPC with a cost horizon of $T_H = 4$ *sec* and a control horizon of $T_C = 2$ *sec* regulating the pitch to zero at a flight condition of U = 6 m/s. As the control discretization value is reduced, the control effort increases, as shown in Table 4.17. This results in high frequency oscillation of the trailing edge flap as presented in Figure 4.23. Although the pitch response with a 0.25 second control discretization (orange) has slight oscillation between 0.5 and 1.25 seconds with an amplitude of 0.1 degree, which is depicted in Figure 4.22, it is well damped compared to the other responses and has a similar time to settle as the open-loop response.

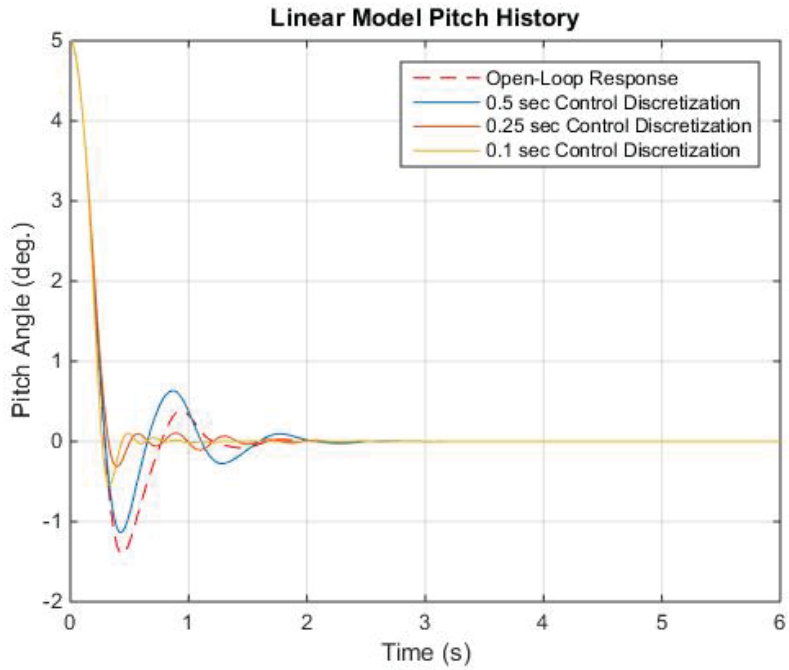


Figure 4.22. Regulator case pitch response for LMPC on the linear aeroelastic system at 6 m/s.

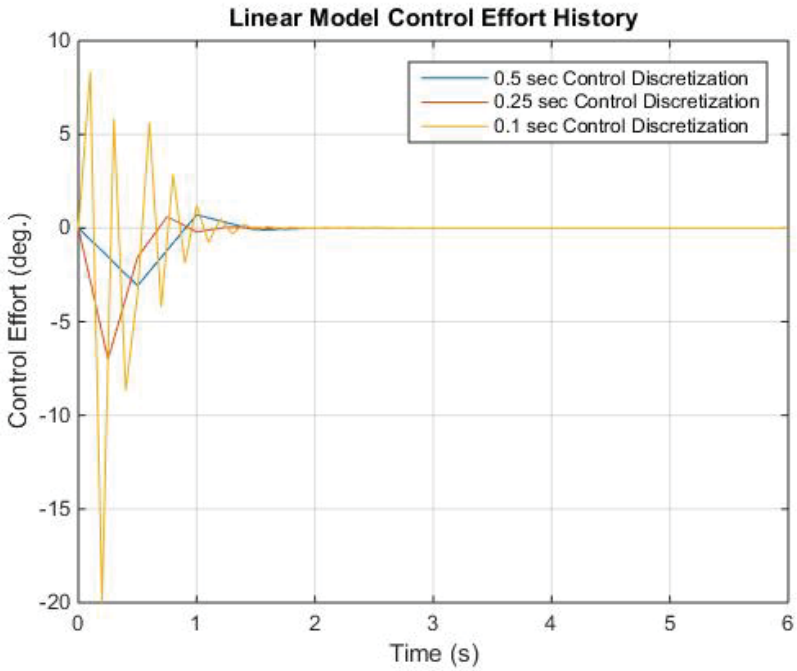


Figure 4.23. Regulator case control effort for LMPC on the linear aeroelastic system at 6 m/s.

Table 4.17. RMSE and control effort for LMPC regulator case on the linear aeroelastic system at 6 m/s.

| **Cost Horizon** ($T_H$) | **Control Horizon** ($T_C$) | **Control Discretization** ($\Delta T_D$) | **Pitch RMSE** | **Control Effort** |
|---|---|---|---|---|
| Open-Loop Response | | | | |
| N/A | | | 0.606 | N/A |
| Linear MPC Controller - ($V_0$ + $V_1$) | | | | |
| 4 | 2 | 0.5 | 0.797 | 0.701 |
| | | 0.25 | 0.768 | 1.258 |
| | | 0.1 | 0.755 | 2.297 |

The discrete-time LQR and LMPC designs that showed the best performance were implemented and compared for the linear regulator case. Figures 4.24 and 4.25 depict the pitch responses and control effort for each controller design. Regardless of the value of the $Q$ matrix, the discrete-time LQR controller resulted in the most overshoot compared to the LMPC and the open-loop response. The LMPC pitch response was well damped with slight oscillation before it regulated to 0 degrees at 1 second with minimal control action from the trailing edge flap. In conclusion, as shown in Table 4.18, the LMPC qualitatively and quantitatively outperformed the baseline discrete-time LQR controller at this flight condition.

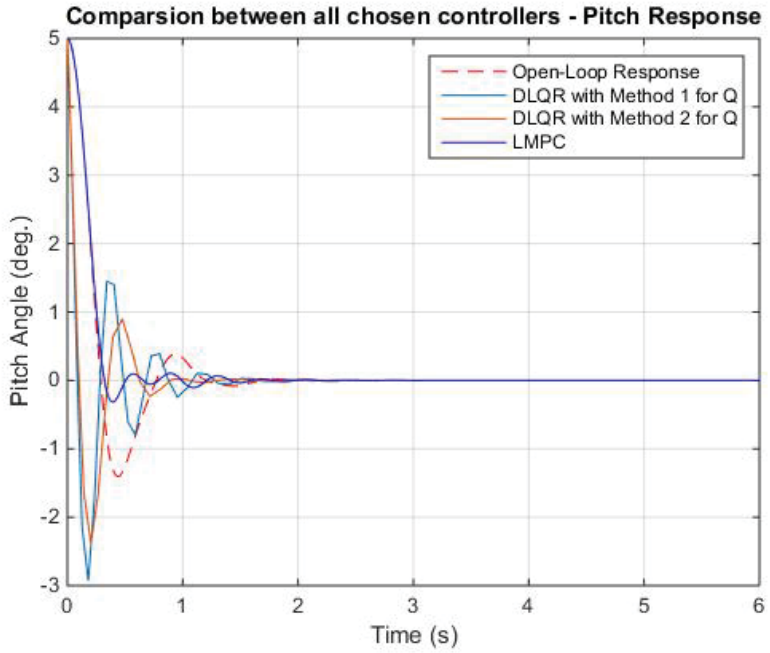


Figure 4.24. Pitch response comparison between open-loop, discrete-time LQR and LMPC on the linear system at free-stream velocity of 6 m/s.

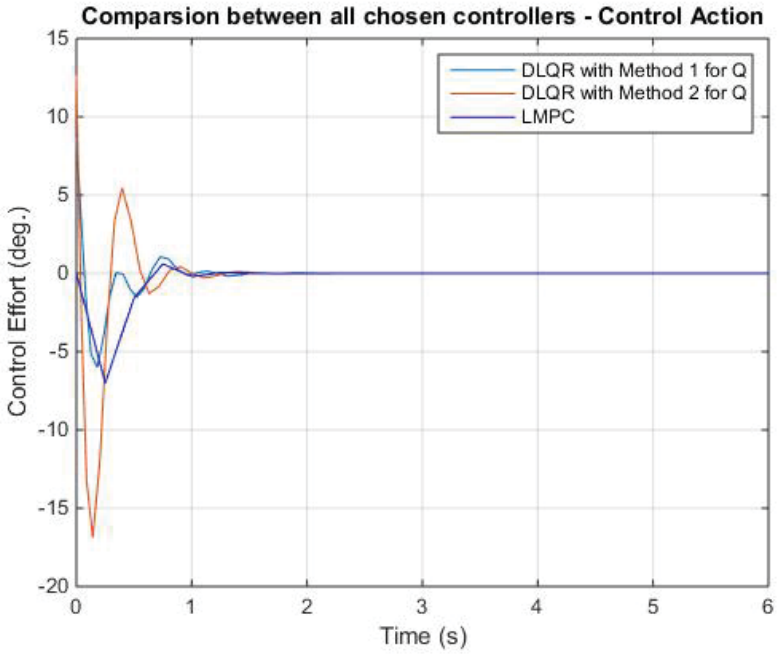


Figure 4.25. Control effort comparison between the discrete-time LQR and LMPC on the linear system at free-stream velocity of 6 m/s.

Table 4.18. RMSE and control effort comparison between chosen controllers at U = 6 m/s.

| **Controller** | **Pitch RMSE** | **Control Effort** |
|---|---|---|
| LMPC | 0.768 | 1.258 |
| DLQR (Q defined using Method 1) | 1.548 | 2.662 |
| DLQR (Q defined using Method 2) | 1.538 | 4.774 |

The LMPC was then implemented for a tracking case in which the goal was to drive the pitch angle from zero to a constant value of 1 degree. Figures 4.26 and 4.27 depict the pitch response and control effort for this case with results obtained by varying the control discretization from 0.1 second to 1 second. The pitch response with control discretization of 0.1 second does not track the reference pitch angle well as it oscillates every 2 seconds after it first approaches the reference value. This deviation happened every 2 seconds causing the control action to oscillate aggressively in an effort to drive the pitch response back to the reference value. The LMPC with $\Delta T_D = 0.5$ seconds yields the best performance with a RMSE of 0.242 degrees for pitch and control effort of 6.351, as presented in Table 4.19.

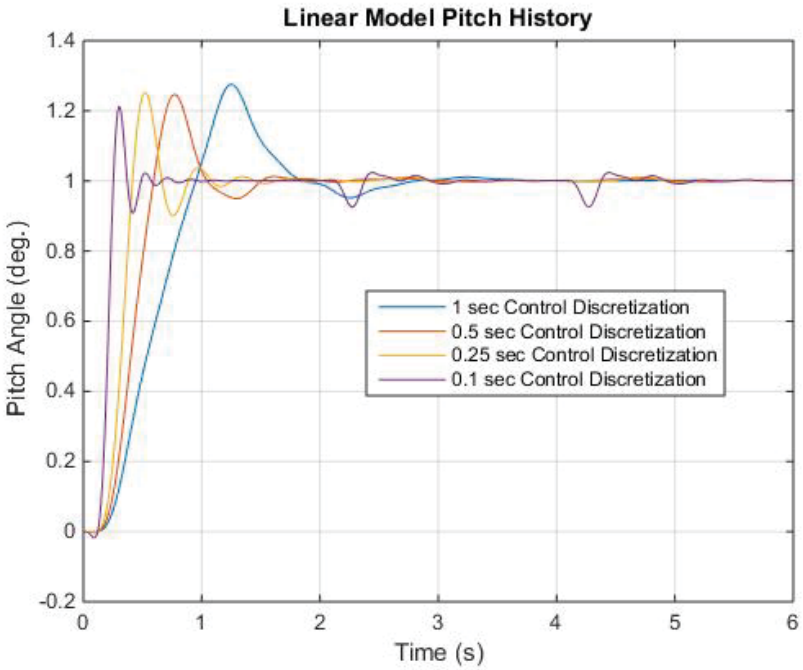


Figure 4.26. Tracking case pitch response using LMPC on the linear aeroelastic system at 6 m/s.

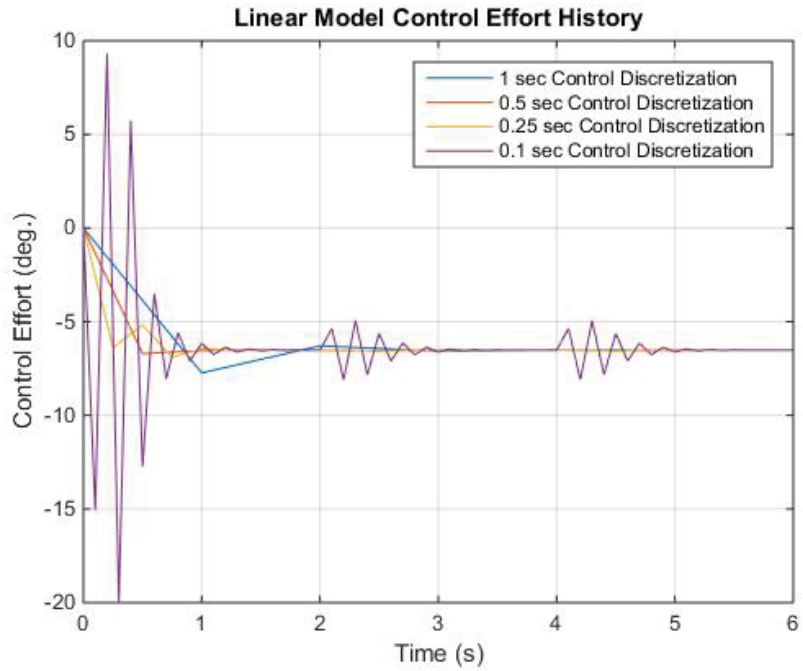


Figure 4.27. Tracking case control effort using LMPC on the linear aeroelastic system at 6 m/s.

Table 4.19. RMSE and control effort for tracking case using LMPC on the linear aeroelastic system at 6 m/s.

| **Cost Horizon** ($T_H$) | **Control Horizon** ($T_C$) | **Control Discretization** ($\Delta T_D$) | **Pitch RMSE** | **Control Effort** |
|---|---|---|---|---|
| 4 | 2 | 1 | 0.277 | 6.301 |
| | | 0.5 | 0.242 | 6.351 |
| | | 0.25 | 0.219 | 6.384 |
| | | 0.1 | 0.179 | 6.762 |

### 4.4.2 LMPC: Free-stream Velocity at 12.5 m/s

The aeroelastic system is unstable at U = 12.5 m/s, which corresponds to the linear flutter speed; thus the primary control objective is to stabilize the system and regulate the pitch response to zero. As shown in Figure 4.28, both LMPC controllers with 0.25 and 0.1 second control discretizations stabilize the system with the pitch response settling at 4 and 2 seconds respectively. Referring to Table 4.20, the LMPC controller with 0.1 second control discretization yields the least pitch RMS error with the drawback of having a higher frequency oscillation in the control action during the first few seconds, which is depicted in Figure 4.29. Hence, the controller with 0.25 second control discretization produced the best performance to stabilize and regulate the linear aeroelastic system's response at the unstable flight condition.

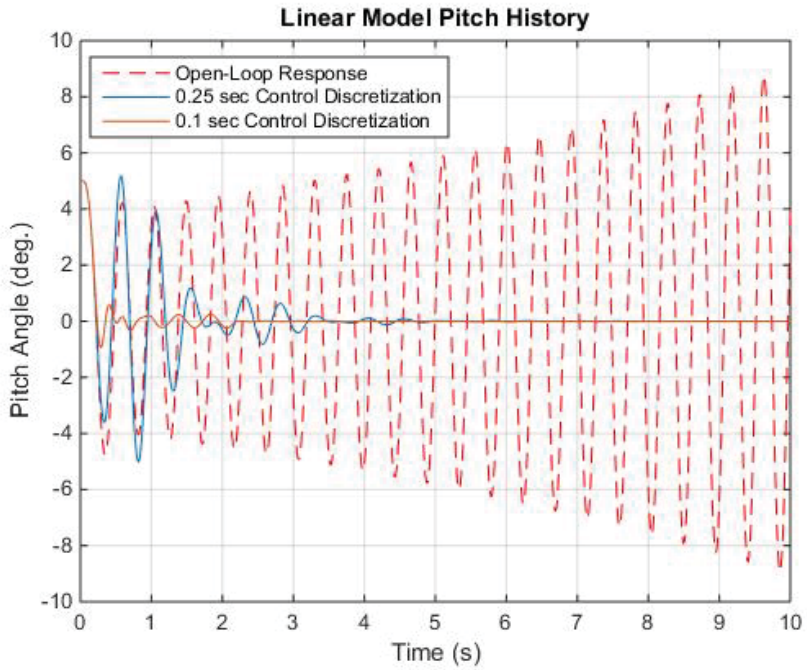


Figure 4.28. Regulator case pitch response using LMPC on the linear aeroelastic system at 12.5 m/s.

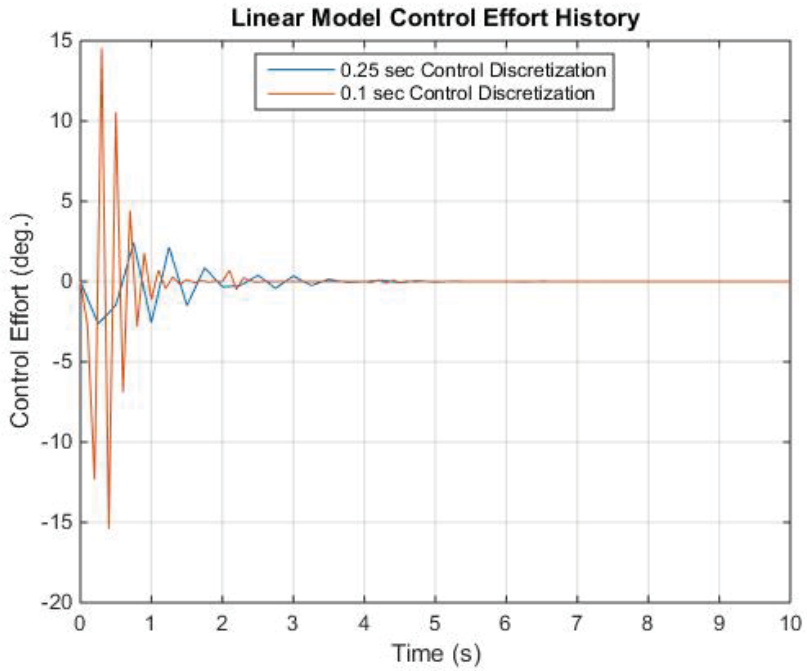


Figure 4.29. Regulator case control effort using LMPC on the linear aeroelastic system at 12.5 m/s.

Table 4.20. RMSE and control effort for regulator case using LMPC on the linear aeroelastic system at 12.5 m/s.

| **Cost Horizon** ($T_H$) | **Control Horizon** ($T_C$) | **Control Discretization** ($\Delta T_D$) | **Pitch RMSE** | **Control Effort** |
|---|---|---|---|---|
| **Open-Loop Response** | | | | |
| N/A | | | 4.421 | N/A |
| **Linear MPC Controller - ($V_0$ + $V_1$)** | | | | |
| 4 | 2 | 0.25 | 0.188 | 2.252 |
| | | 0.1 | 0.157 | 2.324 |

Figures 4.30 and 4.31 portray the pitch responses and control effort for the discrete-time LQR and LMPC controller designs at free-stream velocity of 12.5 m/s. All controllers successfully stabilize the system and regulate the pitch response to zero with different settling times. Although the LMPC has the longest settling time of 5 seconds, its requires the least control action. Both the discrete-time LQR and LMPC controllers have their relative advantages and disadvantages, and further tuning of the parameters and weights could potentially yield improved performance. However, the quantitative analysis of RMS error presented in Table 4.21 concludes that the LMPC controller has better performance than the other chosen controllers.

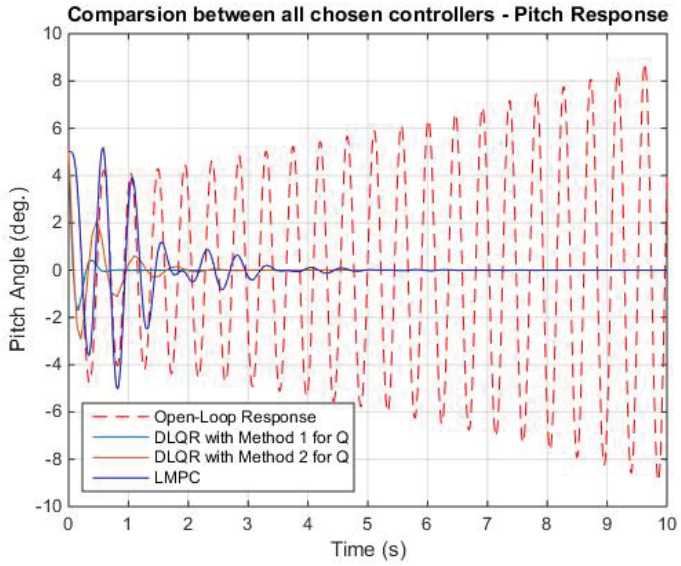


Figure 4.30. Pitch response comparison between open-loop, discrete-time LQR and LMPC for the linear system at U = 12.5 m/s.

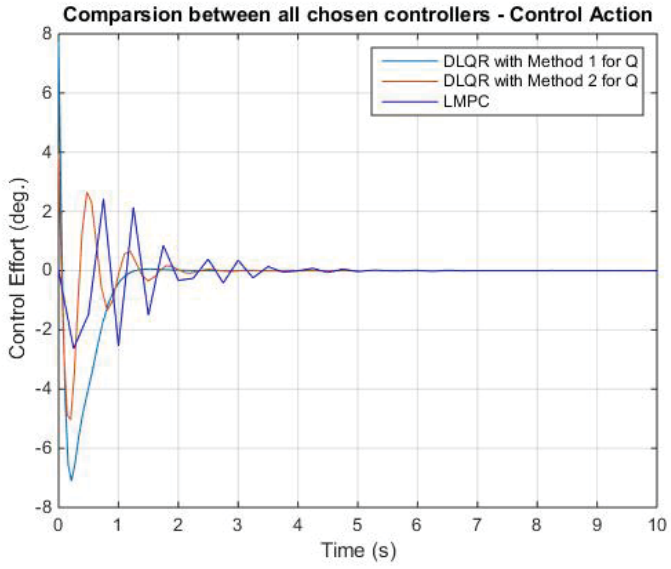


Figure 4.31. Control effort comparison between the discrete-time LQR and LMPC controllers on the linear system at U = 12.5 m/s.

Table 4.21. RMSE and control effort comparison between chosen controllers at U = 12.5 m/s.

| **Controller** | **Pitch RMSE** | **Control Effort** |
|---|---|---|
| LMPC | 0.188 | 2.252 |
| DLQR (Q defined using Method 1) | 1.467 | 2.997 |
| DLQR (Q defined using Method 2) | 1.617 | 1.633 |

Although the LMPC controller successfully stabilizes the system and regulates the pitch response to zero, the LMPC was not effective for the tracking case. The controller did stabilize the pitch response; however it oscillated around the reference value of 1 degree with an amplitude of 0.2 degree without converging to a constant pitch angle. These observations are evident from the responses depicted in Figures 4.32 and 4.33. In this case, the RMSE results presented in Table 4.22 are inconclusive.

Table 4.22. RMSE and control effort for tracking case using LMPC on the linear aeroelastic system at 12.5 m/s.

| **Cost Horizon** ($T_H$) | **Control Horizon** ($T_C$) | **Control Discretization** ($\Delta T_D$) | **Pitch RMSE** | **Control Effort** |
|---|---|---|---|---|
| 4 | 2 | 0.25 | 0.219 | 6.384 |
| | | 0.1 | 0.179 | 6.762 |
| | | 0.05 | 0.165 | 6.959 |

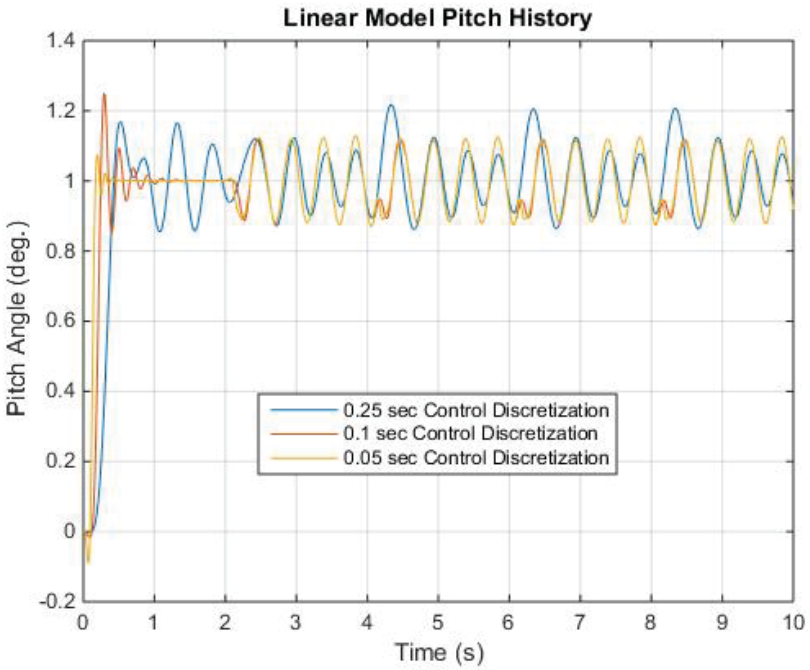


Figure 4.32. Tracking case pitch response using LMPC on the linear aeroelastic system at 12.5 m/s.

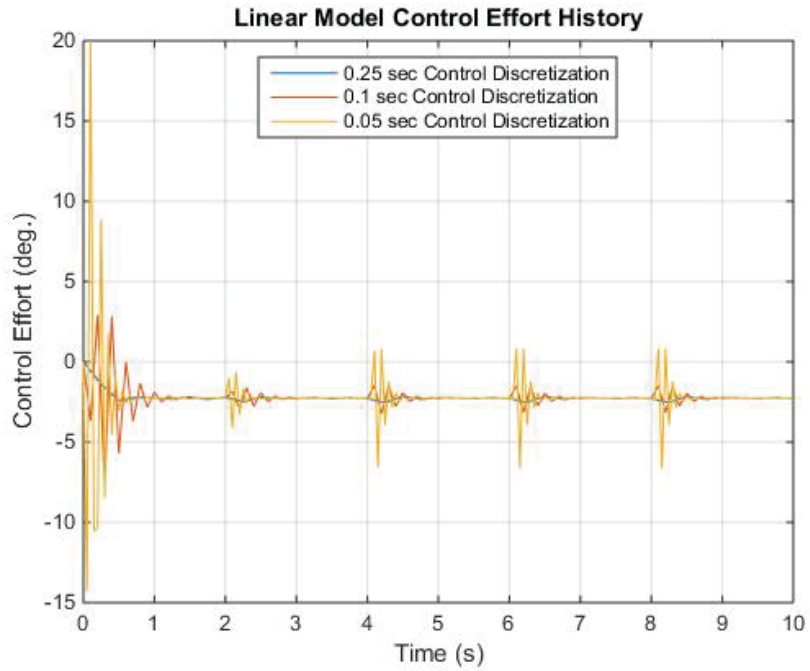


Figure 4.33. Tracking case control effort using LMPC on the linear aeroelastic system at 12.5 m/s.

# 5. Controller Implementation on a Nonlinear Aeroelastic System

In this chapter, different controllers are implemented on the nonlinear aeroelastic system. These controllers include the LQR baseline controller in discrete time using different methods to define the $Q$ matrix and the NMPC controller using a second- and third-order Volterra model. The response and performance of each controller are presented and discussed within this chapter. A performance comparison is provided for all implemented controllers for the regulator case at U = 6 m/s and U = 12.5 m/s.

## 5.1 Classical LQR Baseline Controller

Using the LQR controller design process discussed in Chapter 2, the linear feedback gain is computed and implemented on the nonlinear aeroelastic system. Although applying a linear controller on a nonlinear system will typically not be optimal, this strategy provides a baseline with which to evaluate the performance of the NMPC controller. The following sections present the pitch response and control effort for each controller design at different free-stream velocities. Referring to Chapter 2, there are two methods used to define the $Q$ matrix. Tables 5.1-5.4 present different maximum value combinations that are chosen for the $Q$ matrix to tune the controller.

Table 5.1. Maximum value for each state in $Q$ using method 1 for tuning the LQR controller at 6 m/s.

| **Sets** | $Q^h_{max}$ | $Q^{\dot{h}}_{max}$ | $Q^{\alpha}_{max}$ | $Q^{\dot{\alpha}}_{max}$ | $R_{Pitch}$ |
|---|---|---|---|---|---|
| 1 | 1 | 1 | 1 | 1 | 1 |
| 2 | | | 10 | | 10 |
| 3 | | | 10 | | 0.5 |

Table 5.2. Maximum value for each state in $Q$ using method 1 for tuning the LQR controller at 12.5 m/s.

| **Sets** | $Q^h_{max}$ | $Q^{\dot{h}}_{max}$ | $Q^{\alpha}_{max}$ | $Q^{\dot{\alpha}}_{max}$ | $R_{Pitch}$ |
|---|---|---|---|---|---|
| 1 | 1 | 1 | 1 | 1 | 0.1 |
| 2 | | | | | 0.05 |
| 3 | | | 5 | | 0.1 |
| 4 | | | | | 0.05 |

Table 5.3. Maximum value for each state in $Q$ using method 2 for tuning the LQR controller at 6 m/s.

| $Q^h_{max}$ | $Q^{\dot{h}}_{max}$ | $Q^{\alpha}_{max}$ | $Q^{\dot{\alpha}}_{max}$ | $R_{Pitch}$ |
|---|---|---|---|---|
| 0 | 0 | 1 | 0 | 50 |
| | | | | 100 |
| | | 5 | | 50 |
| | | | | 100 |
| | | 0.5 | | 100 |

Table 5.4. Maximum value for each state in $Q$ using method 2 for tuning the LQR controller at 12.5 m/s.

| $Q^h_{max}$ | $Q^{\dot{h}}_{max}$ | $Q^{\alpha}_{max}$ | $Q^{\dot{\alpha}}_{max}$ | $R_{Pitch}$ |
|---|---|---|---|---|
| 0 | 0 | 1 | 0 | 1 |
| | | | | 5 |
| | | 5 | | 1 |
| | | 0.5 | | 1 |

### 5.1.1 Discrete-Time LQR: Free-stream Velocity at 6 m/s

The pitch response and control effort of the LQR controller with the $Q$ matrix defined using method 1 are portrayed in Figures 5.1 and 5.2 respectively. Results from the first and third set of $Q$ and $R$ matrices show larger damping and shorter settling times compared to the open-loop response. The third set has a slightly lower RMS error in pitch with the least control effort utilized in the process of regulating the pitch response to 0 degrees, as shown in Table 5.5. Hence, the discrete-time LQR controller with the third set of $Q$ and $R$ matrices is chosen to represent this controller design.

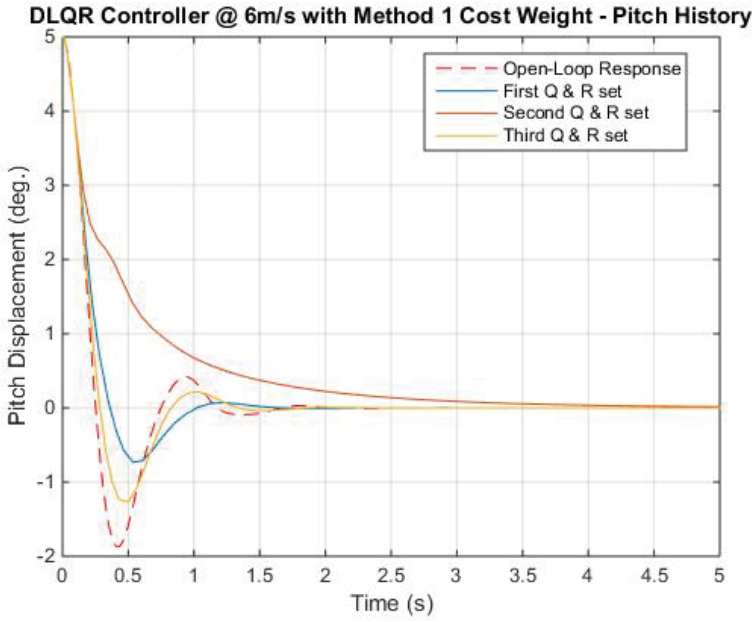


Figure 5.1. Pitch response for discrete-time LQR baseline controller on the nonlinear aeroelastic system with $Q$ chosen using method 1 at U = 6 m/s.

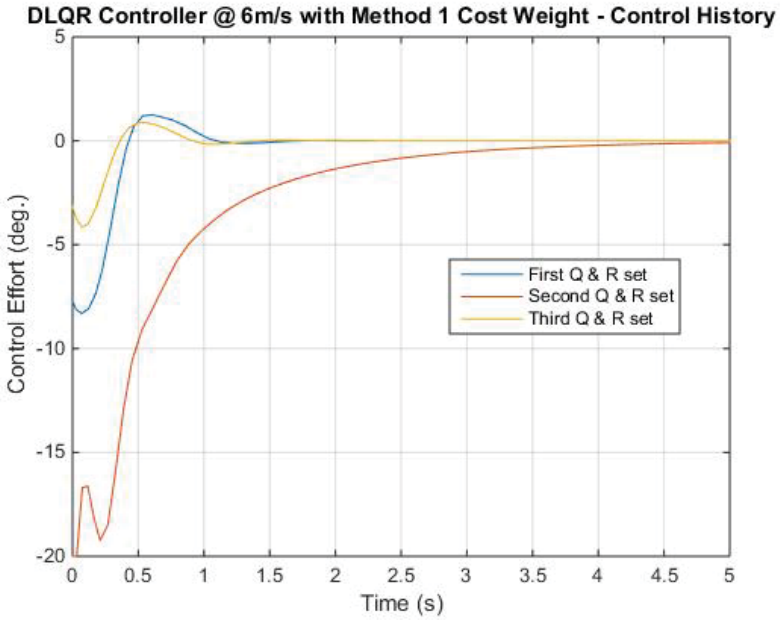


Figure 5.2. Control effort for discrete-time LQR baseline controller on the nonlinear aeroelastic system with $Q$ chosen using method 1 at U = 6 m/s.

Table 5.5. RMSE and control effort for the discrete-time LQR controller using method 1 to determine the $Q$ matrix on the nonlinear aeroelastic system at U = 6 m/s.

| **Sets** | $Q^h_{max}$ | $Q^{\dot{h}}_{max}$ | $Q^{\alpha}_{max}$ | $Q^{\dot{\alpha}}_{max}$ | $R_{Pitch}$ | **Pitch RMSE** | **Control Effort** |
|---|---|---|---|---|---|---|---|
| 1 | 1 | 1 | 1 | 1 | 1 | 1.755 | 3.191 |
| 2 | | | 10 | | 10 | 2.052 | 9.484 |
| 3 | | | | | 0.5 | 1.722 | 1.360 |

The pitch response from the controllers using the second method to define the $Q$ matrix had similar performance and time to settle as the open-loop response, which is depicted in Figures 5.3 and 5.4. Based on the RMSE presented in Table 5.6, the controller with $Q^{\alpha}_{max} = 0.5$ and $R_{Pitch} = 100$ (light green) yielded the best performance with pitch RMS error and control effort of 1.746 and 2.290 respectively.

Table 5.6. RMSE and control effort for the discrete-time LQR controller using method 2 to determine the $Q$ matrix on the nonlinear aeroelastic system at U = 6 m/s.

| $Q^h_{max}$ | $Q^{\dot{h}}_{max}$ | $Q^{\alpha}_{max}$ | $Q^{\dot{\alpha}}_{max}$ | $R_{Pitch}$ | **Pitch RMSE** | **Control Effort** |
|---|---|---|---|---|---|---|
| 0 | 0 | 1 | 0 | 50 | 1.782 | 2.072 |
| | | | | 100 | 1.762 | 2.243 |
| | | 5 | | 50 | 1.780 | 0.946 |
| | | | | 100 | 1.781 | 1.519 |
| | | 0.5 | | 100 | 1.746 | 2.290 |

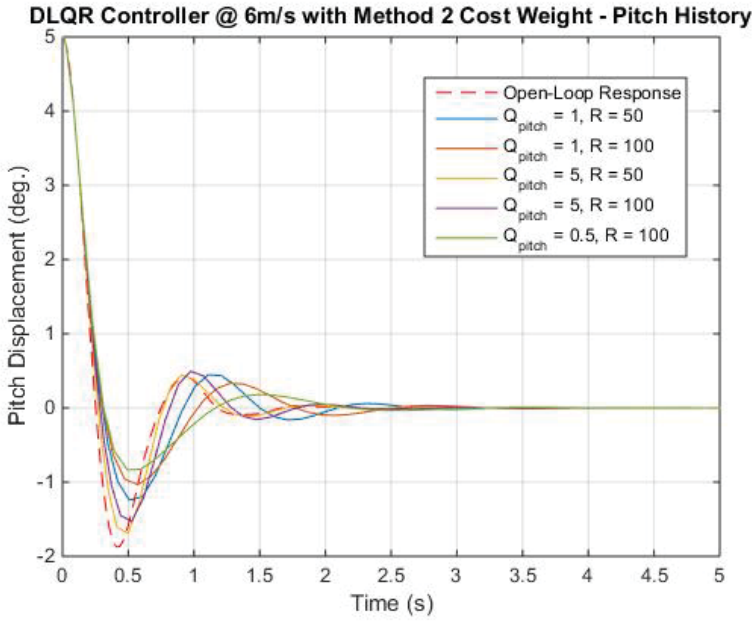


Figure 5.3. Pitch response for discrete-time LQR baseline controller on the nonlinear aeroelastic system with $Q$ chosen using method 2 at U = 6 m/s.

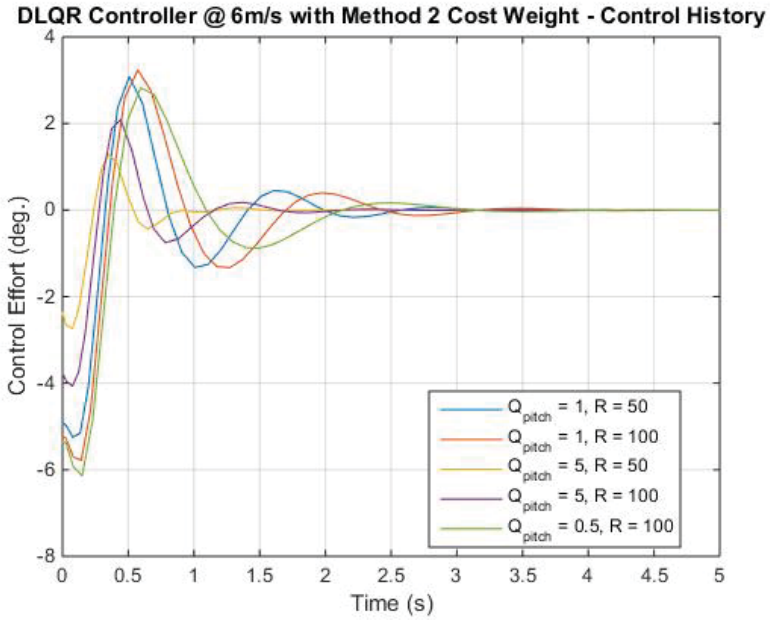


Figure 5.4. Control effort for discrete-time LQR baseline controller on the nonlinear aeroelastic system with $Q$ chosen using method 2 at U = 6 m/s.

### 5.1.2 Discrete-Time LQR: Free-stream Velocity at 12.5 m/s

All discrete-time LQR controller designs successfully stabilized the nonlinear aeroelastic system, which enters a bounded limit cycle oscillation in the open-loop. Figures 5.5 and 5.6 show that the controllers with the first and third set of $Q$ and $R$ matrices have a similar pitch response and control effort, while the same comment can be made for the controllers with the second and fourth set of $Q$ and $R$ matrices. The first and third set of $Q$ and $R$ matrices yielded a pitch response with settling time at around 1.5 seconds and minimal overshoot. The cost of having a better transient response is more control action is required. This observation is validated by the RMSE and control effort shown in Table 5.7. Based on these results, the controller with the third set of $Q$ and $R$ matrices yields the best performance among the other designs with a pitch error and control effort of 1.836 and 1.131 respectively.

Table 5.7. RMSE and control effort for the discrete-time LQR controller using method 1 to determine the $Q$ matrix on the nonlinear aeroelastic system at U = 12.5 m/s.

| **Sets** | $Q^h_{max}$ | $Q^{\dot{h}}_{max}$ | $Q^{\alpha}_{max}$ | $Q^{\dot{\alpha}}_{max}$ | $R_{Pitch}$ | **Pitch RMSE** | **Control Effort** |
|---|---|---|---|---|---|---|---|
| 1 | 1 | 1 | 1 | 1 | 0.1 | 1.836 | 1.135 |
| 2 | | | | | 0.05 | 1.915 | 0.735 |
| 3 | | | 5 | | 0.1 | 1.836 | 1.131 |
| 4 | | | | | 0.05 | 1.916 | 0.732 |

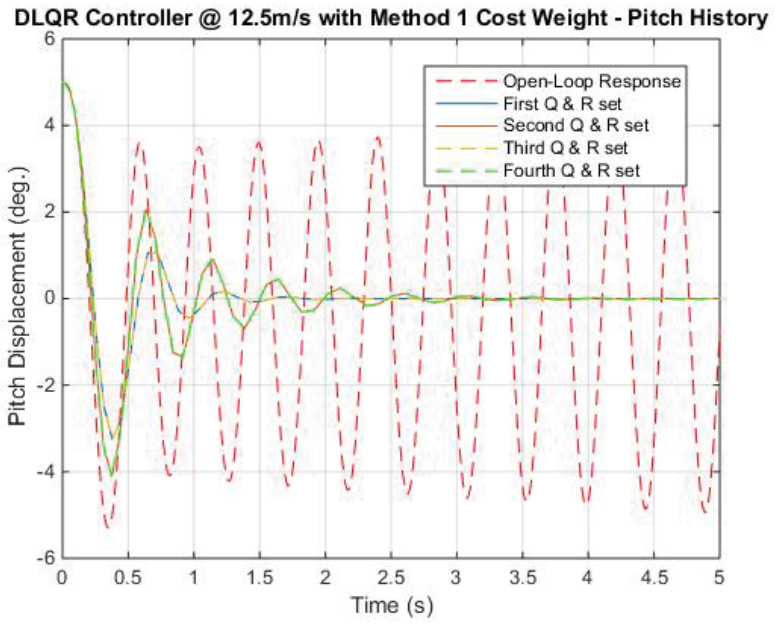


Figure 5.5. Pitch response for the discrete-time LQR baseline controller on the nonlinear aeroelastic system with $Q$ chosen using method 1 at U = 12.5 m/s.

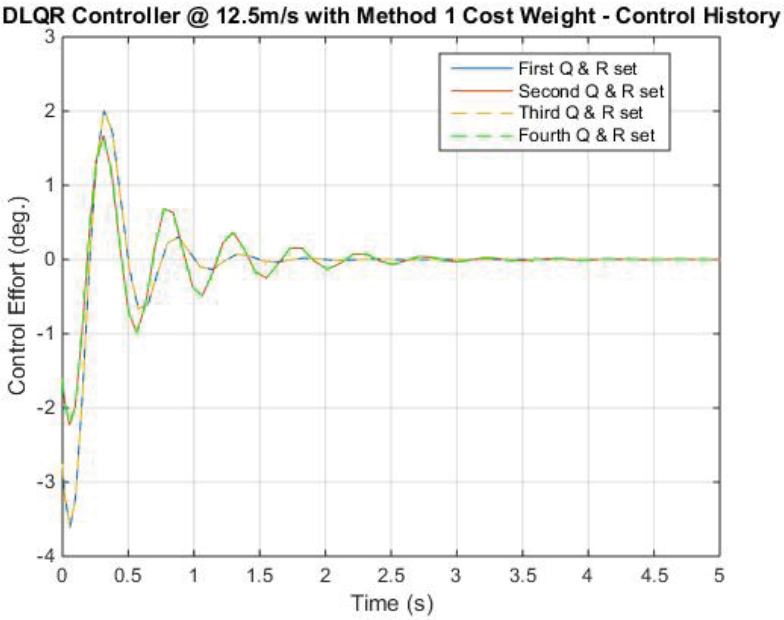


Figure 5.6. Control effort for the discrete-time LQR baseline controller on the nonlinear aeroelastic system with $Q$ chosen using method 1 at U = 12.5 m/s.

Figures 5.7 and 5.8 depict the pitch response and control effort of the LQR controllers using the second method to define the $Q$ and $R$ matrices. The controllers stabilized the nonlinear aeroelastic system and regulated the pitch response to 0 degree. Although the controller with $Q^{\alpha}_{max} = 5$ and $R_{Pitch} = 1$ required the least control action, it provided the worst transient performance as the pitch response oscillated about 0 for more than 4 seconds before converging to 0 degrees. The controller with $Q^{\alpha}_{max} = 0.5$ and $R_{Pitch} = 1$ (purple) yielded the least RMS error in pitch and control effort according to Table 5.8, and it obtained the best transient performance as the time to settle is around 1.25 seconds while the maximum trailing edge flap deflection required is slightly less than -4 degrees.

Table 5.8. RMSE and control effort for the discrete-time LQR controller using method 2 to determine the $Q$ matrix on the nonlinear aeroelastic system at U = 12.5 m/s.

| $Q^{h}_{max}$ | $Q^{\dot{h}}_{max}$ | $Q^{\alpha}_{max}$ | $Q^{\dot{\alpha}}_{max}$ | $R_{Pitch}$ | **Pitch RMSE** | **Control Effort** |
|---|---|---|---|---|---|---|
| 0 | 0 | 1 | 0 | 1 | 1.896 | 1.191 |
| | | | | 5 | 1.986 | 2.555 |
| | | 5 | | 1 | 2.013 | 0.450 |
| | | 0.5 | | 1 | 1.890 | 1.717 |

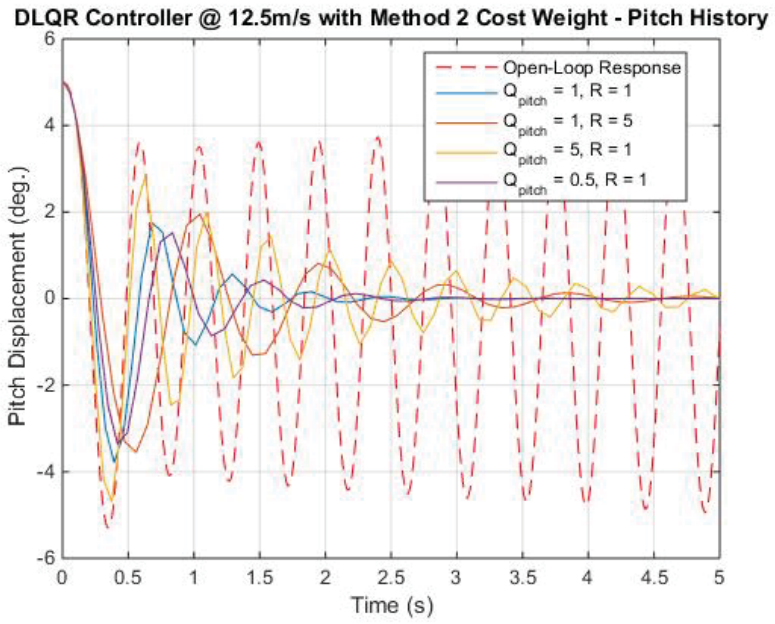


Figure 5.7. Pitch response for the discrete-time LQR baseline controller on the nonlinear aeroelastic system with $Q$ chosen using method 2 at U = 12.5 m/s.

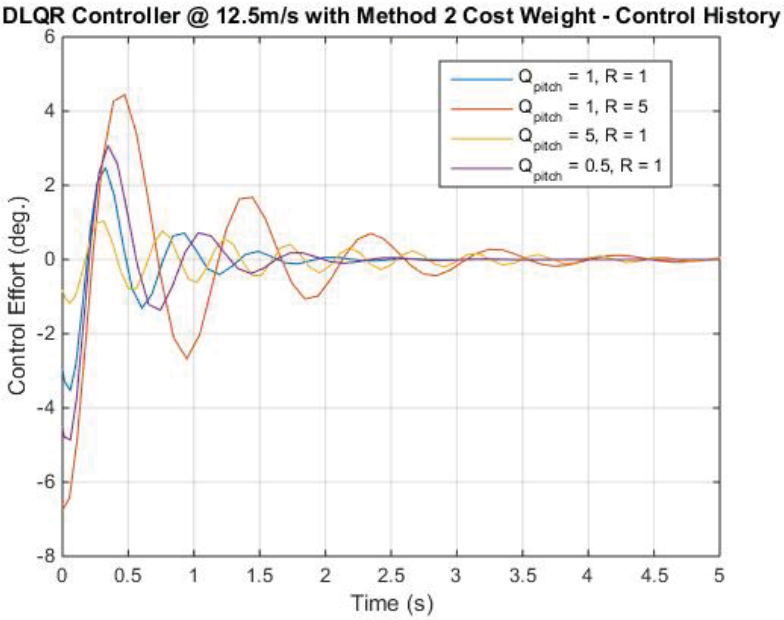


Figure 5.8. Control effort for the discrete-time LQR baseline controller on the nonlinear aeroelastic system with $Q$ chosen using method 2 at U = 12.5 m/s.

## 5.2 NMPC Stability

Closed-loop stability of NMPC controllers is an important consideration. Different methods to achieve closed-loop stability using a finite horizon strategy have been proposed in numerous papers (Mayne & Michalska, 1990; Mayne et al., 2000; Rawlings & Muske, 1993; Findeisen & Allgöwer, 2002). Most of the methods require modifying the NMPC controller setup such that closed-loop stability can be guaranteed independently of the plant and the performance of the controller. Approaches mentioned in the papers can be categorized into the following three approaches and presented in the order of increasing complexity:

1. Suitable tuning of controller design parameters
2. Modify constraints requirement
3. Quasi-infinite horizon MPC scheme

### 5.2.1 Method 1: Tuning Design Parameters

NMPC does not necessarily guarantee closed-loop stability even when the predictive model perfectly represents the plant. The simplest method to achieve closed-loop stability is by suitable tuning of controller design parameters, namely prediction horizon, control horizon, weighting matrices and constraints (Zhao, Diehl, Longman, Bock, & Schlöder, 2004). If the prediction horizon is chosen to be large compared with the settling time of the plant, then the stability properties of an infinite horizon

are achieved (Mayne et al., 2000). The objective function with an infinite horizon control is expressed as follows:

$$J = \frac{1}{2}\int_0^\infty (x^T Q x + u^T R u) dt \tag{5.1}$$

where $Q$ and $R$ are symmetric positive definite weighting matrices. If the plant is stable, then the receding horizon controller with the objective function presented in Eq.(5.1) is stabilizing (Rawlings & Muske, 1993). Moreover, for a stabilizable $\{A, B\}$, the receding horizon controller with the above objective function is stabilizing if the open-loop plant is unstable.

### 5.2.2 Method 2: Modify Constraints Requirement

The remaining approaches require modification of the setup of the MPC controller. With these modifications, the controller will achieve guaranteed closed-loop stability independent of the controller performance. Hence, there is no guarantee of acceptable performance from the controller. Closed-loop stability can be enforced by adding a terminal constraint of the form:

$$x(T_H) = 0$$

This terminal constraint ensures that the state will reach the desired final state at the end of the prediction horizon. Linear systems with terminal constraints were thoroughly investigated by Kwon and Pearson (1977). Mayne and Michalska (1990) showed that under certain reasonable conditions and assumptions, closed-loop stability of nonlinear systems using a MPC controller can be realized. They proposed

10 different assumptions throughout the paper and these assumptions are used in the following two theorems. Furthermore, the proof for both theorems treated the objective function as a Lyapunov function as $Q$ is positive definite.

**Theorem 1(Mayne & Michalska, 1990):** *If assumptions 1 to 9 are satisfied, then the closed-loop system using the receding horizon strategy is (locally) asymptotically stable (i.e. there exists a ball, such that for any initial condition the solution of the closed-loop system tends to zero as time goes to infinity).*

**Theorem 2(Mayne & Michalska, 1990):** *If assumptions 1 to 10 are satisfied, then the closed-loop system using the receding horizon strategy is (globally) asymptotically stable (i.e. for every initial condition the solution of the closed-loop system tends to zero as time goes to infinity).*

### 5.2.3 Method 3: Quasi-Infinite Horizon NMPC Scheme

The last approach to ensure closed-loop stability is to employ the quasi-infinite horizon NMPC scheme presented by Chen and Allgöwer (1997) on a system modeled as a general nonlinear set of ordinary differential equations (ODEs) expressed in the following form, subject to $x(0) = x_0$:

$$\dot{x}(t) = f(x(t), u(t))$$

The general idea of the quasi-infinite horizon NMPC scheme is to use a terminal region ($\Omega$) and terminal penalty matrix ($P$) that are determined off-line to ensure the nonlinear system is led into the region about the end point (origin) where the

model can be linearized. If the linearized system is stabilizable, then the terminal penalty matrix is adjusted in the cost function to satisfy an equality, which states the finite horizon cost function will transform into an infinite horizon cost function where asymptotic closed-loop stability is achieved. In this scheme, a terminal regional constraint is added and the objective function (J) is modified to include a terminal penalty term, as defined below.

Terminal Regional Constraint:

$$x(T_H) \in \Omega$$

where the compact and convex terminal set $\Omega$ is defined as

$$\Omega = \{x \in \mathbb{R}^n \mid x^T P x \leq \alpha\}$$

Objective Function with Terminal Penalty Term:

$$J = \frac{1}{2} \int_0^{T_H} [x^T(t) Q x(t) + u^T(t) R u(t)] dt + x^T(T_H) P x(T_H) \tag{5.2}$$

The following assumptions are made for this approach (Johansen, 2004):

A1: $Q$, $R$, $P > 0$

A2: $y_{min} < 0 < y_{max}$ and $u_{min} < 0 < u_{max}$

A3: The function $\boldsymbol{f}$ is twice continuously differentiable with $f(0,0) = 0$

Consider the Jacobian linearization at the origin:

$$A = \frac{\partial f}{\partial x}(0,0) \qquad\qquad B = \frac{\partial f}{\partial u}(0,0)$$

and make the following assumption:

A4: $\{A, B\}$ is stabilizable

Let $K$ be the optimal gain matrix from the linear state feedback control, $u = -Kx$, such that $AK = A - BK$ and $AK$ is asymptotically stable. The following Lemma can be stated (H. Chen & Allgöwer, 1997):

**Lemma 1.** If assumptions A1-A4 are satisfied, then the following Lyapunov equation is defined

$$(A_K + \kappa I)^T P + P(A_K + \kappa I) = -Q^* \tag{5.3}$$

where $Q^* = Q + K^T RK$ is a symmetric positive definite matrix and $\kappa > 0$ satisfies

$$\kappa < -\lambda_{max}(A_K)$$

Furthermore, there exists a constant $\alpha > 0$ such that $\Omega$ defined above satisfies the following points:

i. The linear feedback controller respects the input constraints in $\Omega$

ii. $\Omega$ is positively invariant. Hence, the nonlinear system with linear feedback control $u = -Kx$ is asymptotically stable for all $x(0)$.

iii. The infinite horizon cost function subject to the nonlinear system controlled by the linear feedback controller is bounded by the terminal penalty term.

$$J^\infty = \frac{1}{2}\int_0^\infty (x^T Qx + u^T Ru)dt \leq x^T(T_H)Px(T_H) \tag{5.4}$$

The following procedure (Findeisen & Allgöwer, 2002) can be used to determine the terminal region ($\Omega$) and the terminal penalty matrix ($P$).

*Step 1.* Solve the linear control problem based on the Jacobian linearization model to get a locally stabilizing linear state feedback control gain ($K$).

*Step 2.* Choose a constant $\kappa$ that satisfies $\kappa < -\lambda_{max}(A_K)$ and solve the following Lyapunov equation to get a symmetric positive definite $P$.

$$(A_K + \kappa I)^T P + P(A_K + \kappa I) = -(Q + K^T R K)$$

*Step 3.* Find the largest possible $\alpha_1$ defining a region

$$\Omega_{\alpha_1} = \{x \in \mathbb{R}^n \mid x^T P x \leq \alpha_1\}$$

such that $Kx \in U$, for all $x \in \Omega\alpha_1$.

*Step 4.* Find the largest possible $\alpha$ defining a terminal region,

$$\Omega_\alpha = \{x \in \mathbb{R}^n \mid x^T P x \leq \alpha\}$$

such that the optimal value of the following optimization problem is non-positive:

$$\max_x \{x^T P \phi(x) - \kappa \cdot x^T P x \mid x^T P x \leq \alpha\}$$

where $\phi(x) := f(x, Kx) - A_K x$.

## 5.3 Nonlinear Volterra-Based MPC

The Volterra-based model predictive control strategy was implemented to control the pitch response of the nonlinear aeroelastic system at two different free-stream velocities, namely at U = 6 m/s and U = 12.5 m/s. The first free-stream velocity is chosen at 6 m/s as it corresponds to the stable region of the system, while the second value is chosen at 12.5 m/s, which corresponds to a limit cycle condition for the nonlinear aeroelastic system. At each free-stream velocity condition, the Volterra model was used to predict the pitch response and the MPC algorithm was utilized to regulate the pitch response to zero and also to drive the pitch response to track a constant reference value.

### 5.3.1 NMPC: Free-stream Velocity at 6 m/s

The NMPC algorithm was first implemented to regulate the pitch response from an initial pitch angle of 5 degrees to 0 degrees, then it was utilized to track a step input with a specific pitch angle value. It should be noted that, as the system is stable at this free-stream velocity condition, the pitch response will naturally decay to zero without any control effort. For each regulator and tracking case, discussion is provided on how the pitch response and control effort were affected by different MPC controller parameters and the Volterra model.

### 5.3.2 The Effect of Control Discretization and Predictive Model

Volterra models were used as predictive models within the NMPC strategy. In all the examples provided, the cost function weights were chosen as $w_\alpha = 100$ and $w_\beta = 0$ unless otherwise stated. This means the cost function did not penalize the control effort and was simply designed to regulate the pitch response to zero. Implementation of the MPC algorithm requires the selection of the cost (or optimization) horizon, $T_H$, the control horizon, $T_C$ (i.e. the portion of the computed control history that is applied before a new optimization is performed), and the control discretization $\Delta T_D$. Since the zero- and first-order kernels have 4 seconds memory (i.e. the kernels decay to zero in 4 seconds) and the second- and third- order kernels only have 2 seconds memory at this flight condition, the largest possible and reasonable value for the optimization horizon, $T_H$, for the linear and nonlinear predictive models would be 4 and 2 seconds respectively.

Figures 5.9 and 5.10 depict the pitch response and control effort obtained using the linear MPC algorithm with $T_H = 4$ seconds and $T_C = 2$ seconds using several different control discretization values. The open-loop pitch response was also plotted for comparison. The results showed that with finer control discretization, the pitch responses were attenuated faster with larger control deflections from the trailing edge flaps. This trend is clearly seen as the control discretization is reduced from 1 second (light blue) to 0.1 seconds (purple). The control effort increased significantly and showed higher frequency oscillations while the pitch response improved marginally.

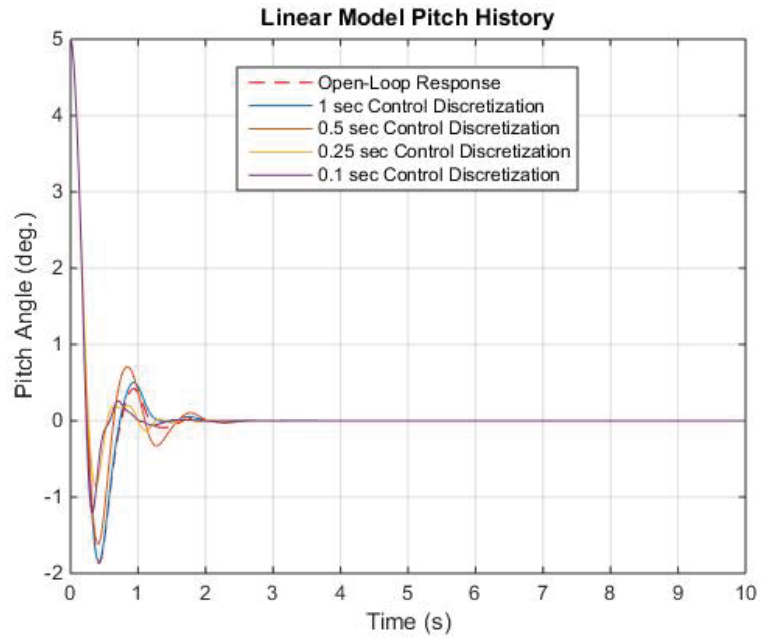


Figure 5.9. Pitch response for nonlinear regulator case using the linear predictive model with different control discretizations with $T_H = 4$ *sec* and $T_C = 2$ *sec*.

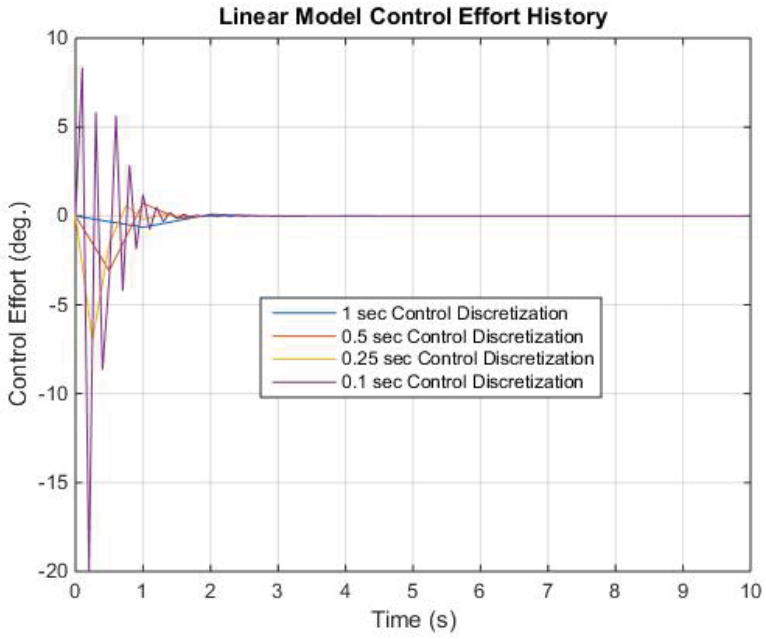


Figure 5.10. Control effort for nonlinear regulator case using the linear predictive model with different control discretizations with $T_H = 4$ *sec* and $T_C = 2$ *sec*.

This trend is also demonstrated in the RMSE analysis presented in Table 5.9. These results imply that 0.5 second and 0.25 second control discretizations would be the better choices in this case based on pitch RMS error and control effort.

Table 5.9. RMSE and control effort for Linear MPC regulator case with $T_H = 4$ *sec* and $T_C = 2$ *sec* for various control discretizations ($\Delta T_D$).

| **Cost Horizon** ($T_H$) | **Control Horizon** ($T_C$) | **Control Discretization** ($\Delta T_D$) | **Pitch RMSE** | **Control Effort** |
|---|---|---|---|---|
| **Open-Loop Response** | | | | |
| N/A | | | 0.588 | N/A |
| **Linear MPC Controller - ($V_0 + V_1$)** | | | | |
| 4 | 2 | 1 | 0.608 | 0.160 |
| | | 0.5 | 0.596 | 0.543 |
| | | 0.25 | 0.552 | 0.975 |
| | | 0.1 | 0.553 | 1.780 |

The MPC algorithm with the same choice of parameters was then applied to track a predefined pitch angle reference value ($\alpha_{ref} = 1$ degree). The resulting pitch response and control effort are shown in Figures 5.11 and 5.12 respectively. For all control discretization values, the controller did not successfully drive the pitch response of the nonlinear aeroelastic system to the desired pitch reference angle as there was a steady state error of roughly 0.06 degrees.

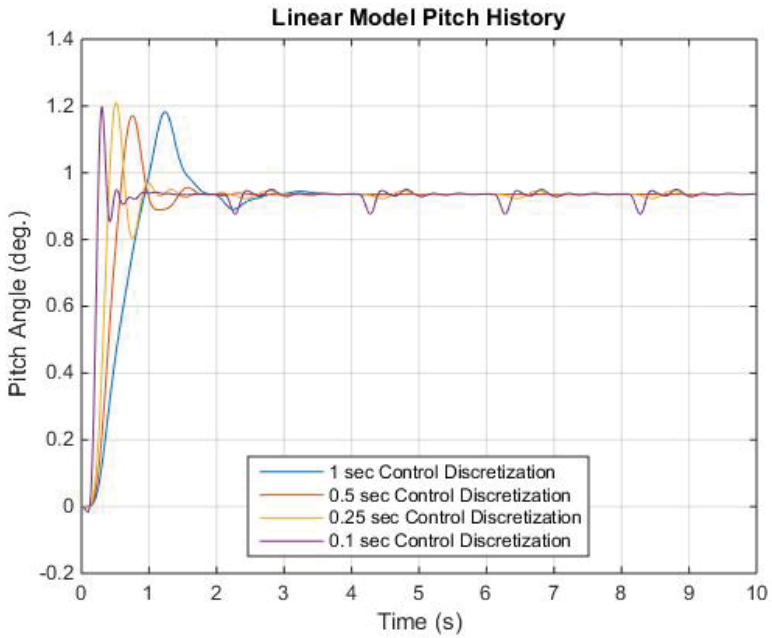


Figure 5.11. Pitch response for nonlinear tracking case using the linear predictive model with different control discretizations with $T_H = 4$ *sec* and $T_C = 2$ *sec*.

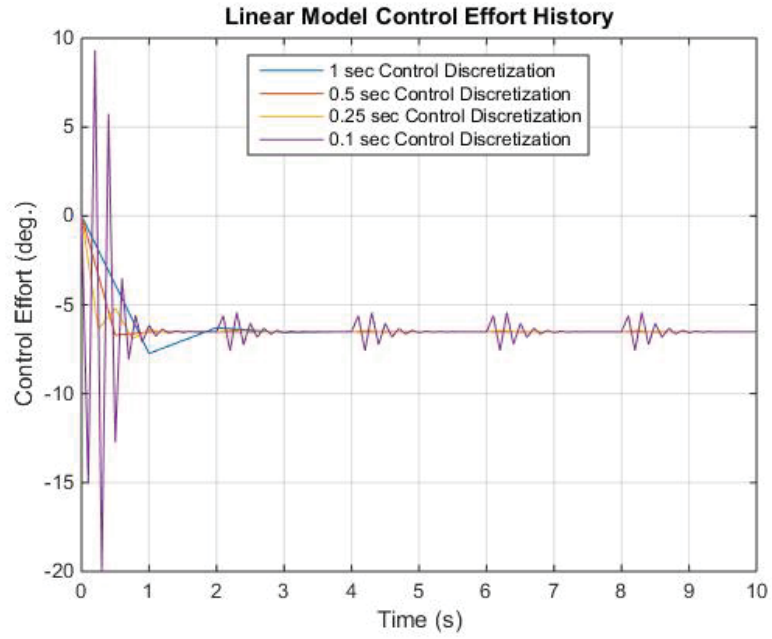


Figure 5.12. Control effort for nonlinear tracking case using the linear predictive model with different control discretizations with $T_H = 4$ *sec* and $T_C = 2$ *sec*.

Table 5.10. RMSE for Linear MPC tracking case at $T_H = 4$ *sec* and $T_C = 2$ *sec* with various control discretizations ($\Delta T_D$).

| **Cost Horizon** ($T_H$) | **Control Horizon** ($T_C$) | **Control Discretization** ($\Delta T_D$) | **Pitch RMSE** | **Control Effort** |
|---|---|---|---|---|
| **Linear MPC Controller - ($V_0 + V_1$)** | | | | |
| 4 | 2 | 1 | 0.223 | 6.348 |
| | | 0.5 | 0.196 | 6.413 |
| | | 0.25 | 0.181 | 6.436 |
| | | 0.1 | 0.154 | 6.646 |

Although there was steady state error within the pitch response, the pitch response leveled to a constant value within 4 seconds. For the finest discretization level of $\Delta T_D$ = 0.1 seconds, the control effort becomes very large and oscillatory in nature, with a control effort of 6.646, the largest control effort out of all the designs. Both the performance plots and error analysis suggest that a coarser discretization level, such as 1 second or 0.5 seconds, which result in a lower frequency control input, would be better choices for this case.

The Nonlinear MPC (NMPC) was then implemented on the nonlinear aeroelastic system and compared to the linear MPC results. The NMPC was implemented using the second-order Volterra model and the third-order Volterra model. The second-order nonlinear model includes the zero-, first- and second-order kernels (i.e. $V_0$ +

$V_1 + V_2$), while the third- order Volterra model also includes the third-order kernels (i.e. $V_0 + V_1 + V_2 + V_3$).

The pitch response and control effort for the regulator case are shown in Figures 5.13-5.16. Figures 5.13 and 5.14 depict the results using the second-order nonlinear predictive model, whereas Figures 5.15 and 5.16 show the results of using the third-order nonlinear predictive model.

Table 5.11. RMSE and control effort for second- and third-order NMPC regulator case with $T_H = 2$ *sec* and $T_C = 2$ *sec* with various control discretizations ($\Delta T_D$).

| **Cost Horizon** ($T_H$) | **Control Horizon** ($T_C$) | **Control Discretization** ($\Delta T_D$) | **Pitch RMSE** | **Control Effort** |
|---|---|---|---|---|
| **Second-Order MPC Controller - ($V_0 + V_1 + V_2$)** | | | | |
| 2 | 2 | 1 | 0.608 | 0.180 |
| | | 0.5 | 0.596 | 0.615 |
| | | 0.25 | 0.554 | 1.037 |
| | | 0.1 | 0.554 | 1.798 |
| **Third-Order MPC Controller - ($V_0 + V_1 + V_2 + V_3$)** | | | | |
| 2 | 2 | 1 | 0.608 | 0.180 |
| | | 0.5 | 0.596 | 0.609 |
| | | 0.25 | 0.554 | 1.034 |
| | | 0.1 | 0.554 | 1.794 |

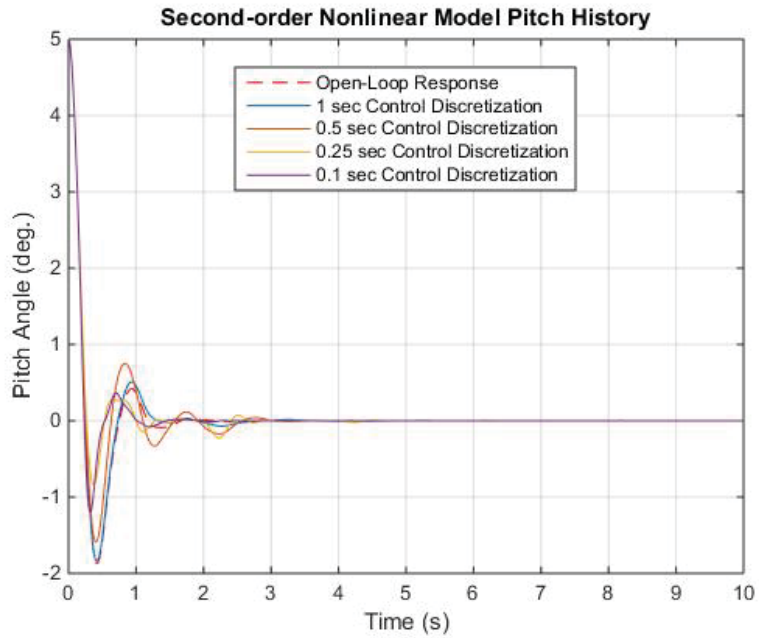


Figure 5.13. Pitch response for nonlinear regulator case using the second-order nonlinear predictive model with different control discretizations with $T_H = 2$ *sec* and $T_C = 2$ *sec*.

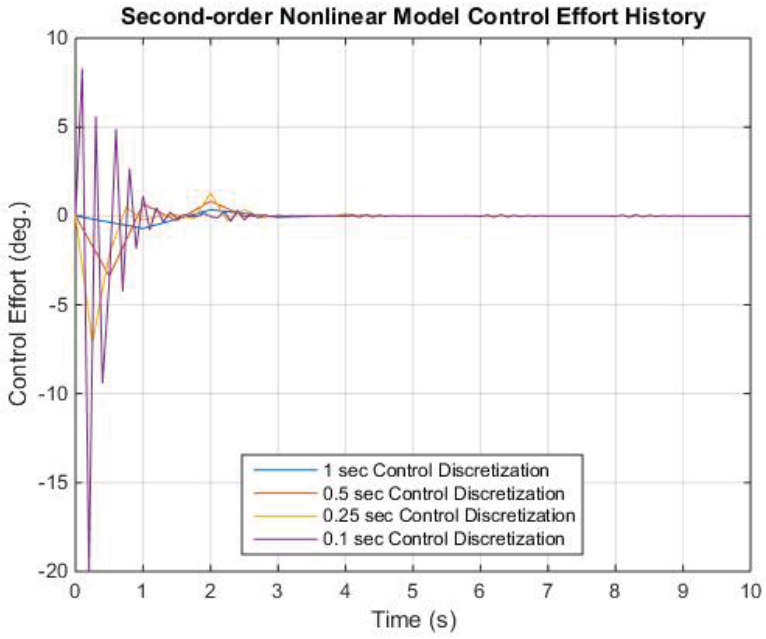


Figure 5.14. Control effort for nonlinear regulator case using the second-order nonlinear predictive model with different control discretizations with $T_H = 2$ *sec* and $T_C = 2$ *sec*.

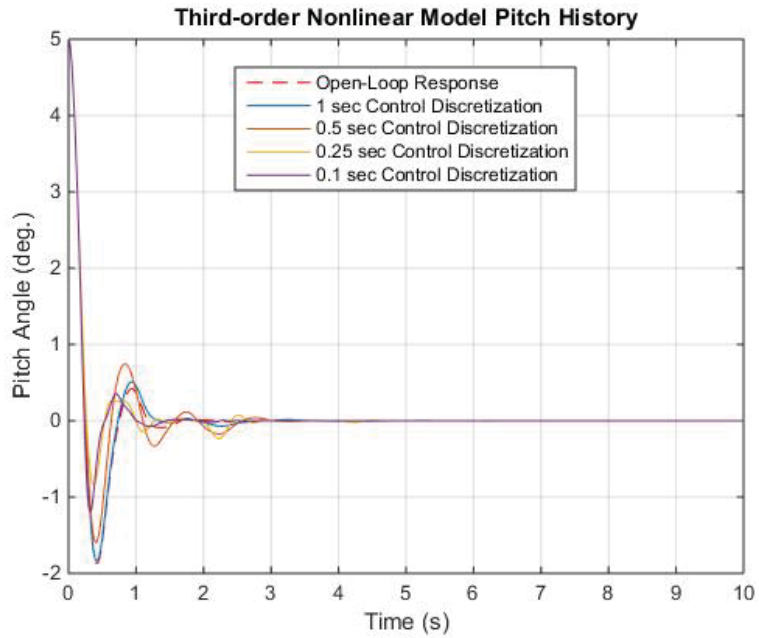


Figure 5.15. Pitch response for nonlinear regulator case using the third-order nonlinear predictive model with different control discretizations with $T_H = 2$ *sec* and $T_C = 2$ *sec*.

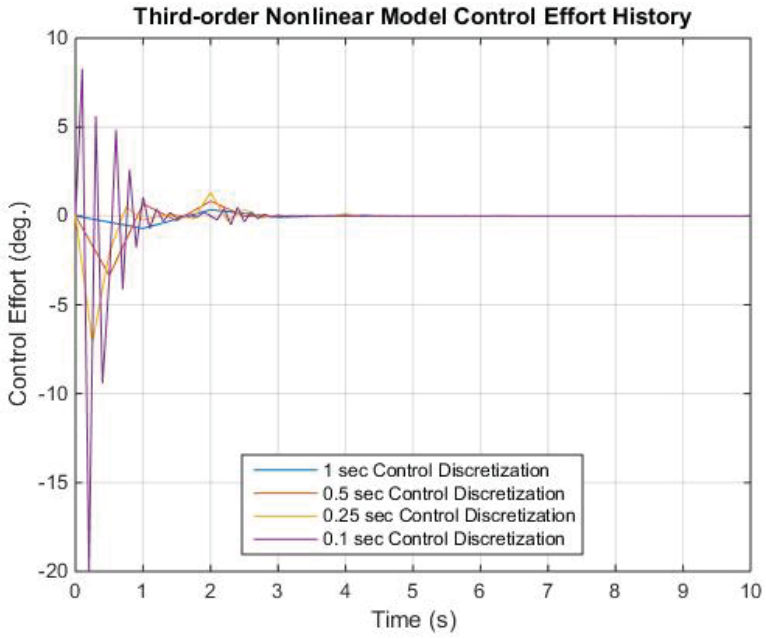


Figure 5.16. Control effort for nonlinear regulator case using the third-order predictive model with different control discretizations with $T_H = 2$ *sec* and $T_C = 2$ *sec*.

The pitch response and control effort from both nonlinear predictive models show the same trend as the results obtained using the linear predictive model in that control discretizations of 0.5 seconds or 0.25 seconds provide the best results. These observations from the plots are supported by the quantitative pitch RMS error and control effort analysis presented in Table 5.11. In general, the second-order NMPC has a slightly higher control effort compared to the third-order NMPC, while the pitch RMS error is the same in both cases.

The pitch response and control effort for the tracking case are shown in Figure 5.17-5.20. Figures 5.17 and 5.18 depict the results of the second-order nonlinear predictive model, whereas Figures 5.19 and 5.20 show the results of the third-order nonlinear predictive model. The pitch response and control effort from both nonlinear predictive models show the same trend as the regulator case. As the control discretization is reduced, more control effort is required and aggressive oscillations can be seen in the both the pitch response and control effort plots. In addition, the RMS error presented in Table 5.12 demonstrates that the third-order NMPC has a lower RMS error in pitch and control effort compared to the error analysis for the second-order NMPC. Therefore, the third-order NMPC with control discretization of 1 second or 0.5 seconds would be the best choice for the tracking case.

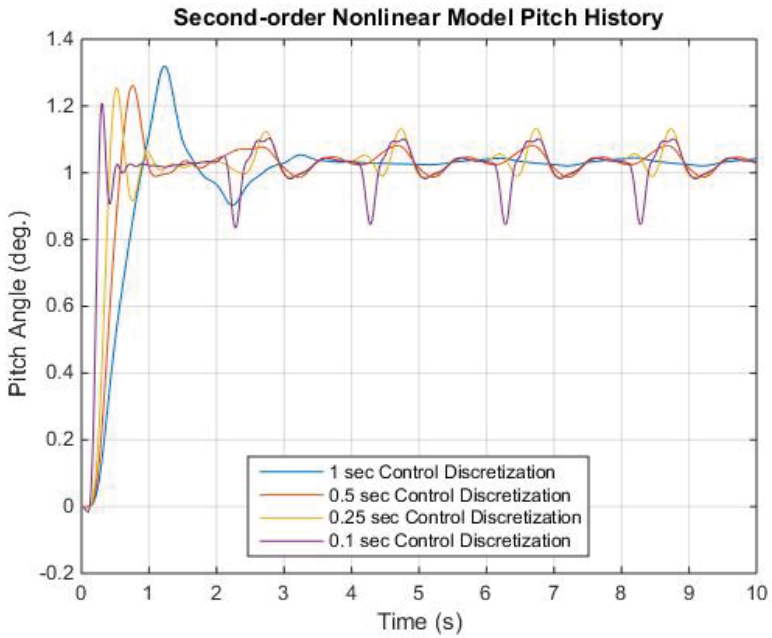


Figure 5.17. Pitch response for nonlinear tracking case using the second-order nonlinear predictive model with different control discretizations with $T_H = 2$ *sec* and $T_C = 2$ *sec*.

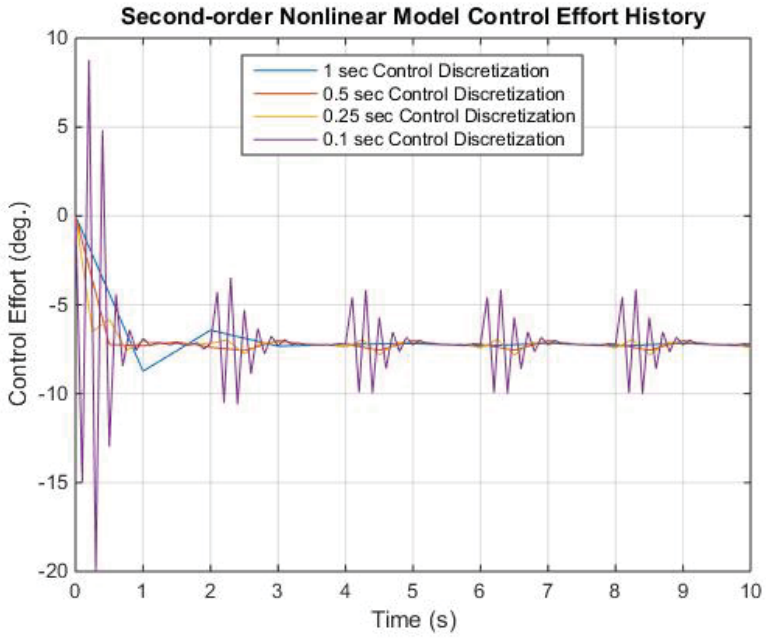


Figure 5.18. Control effort for nonlinear tracking case using the second-order nonlinear predictive model with different control discretizations with $T_H = 2$ *sec* and $T_C = 2$ *sec*.

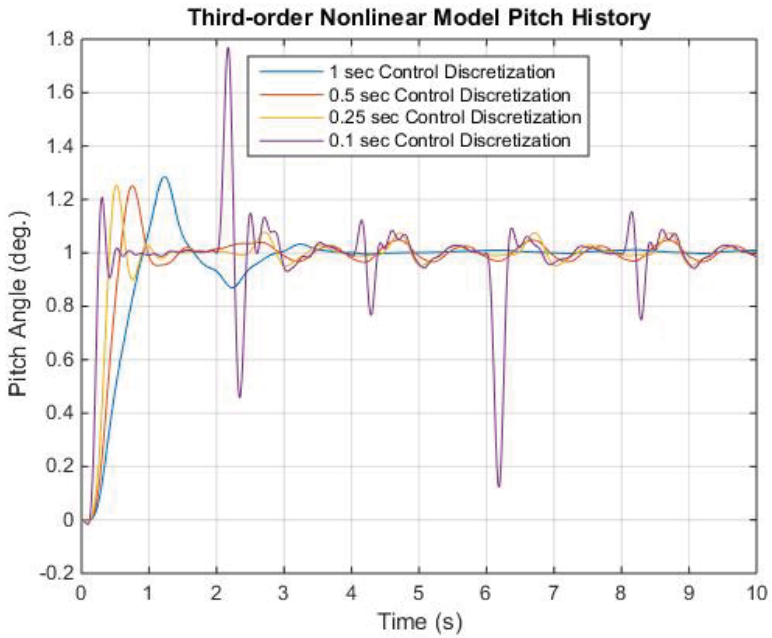


Figure 5.19. Pitch response for nonlinear tracking case using the third-order nonlinear predictive model with different control discretizations with $T_H = 2\ sec$ and $T_C = 2\ sec$.

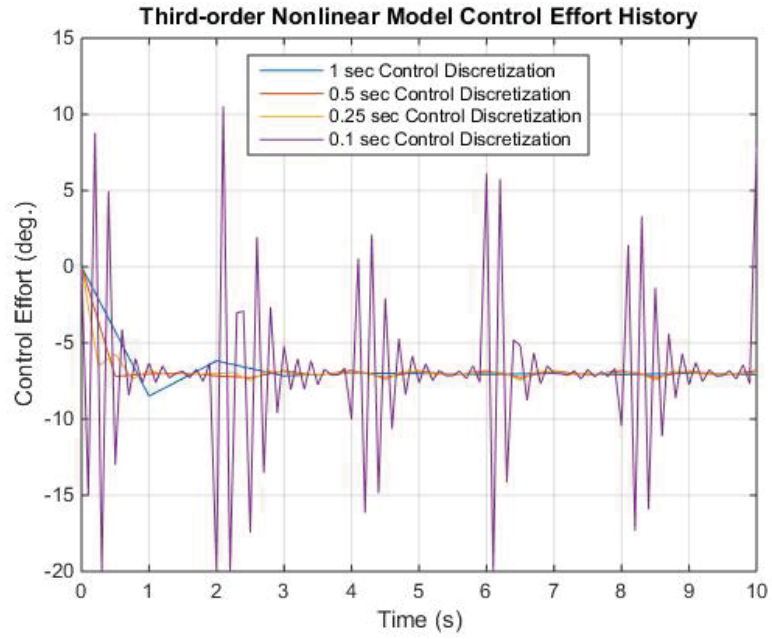


Figure 5.20. Control effort for nonlinear tracking case using the third-order nonlinear predictive model with different control discretizations with $T_H = 2\ sec$ and $T_C = 2\ sec$.

Table 5.12. RMSE and control effort for second- and third-order NMPC tracking cases with $T_H = 2$ *sec* and $T_C = 2$ *sec* with various control discretizations ($\Delta T_D$).

| **Cost Horizon** ($T_H$) | **Control Horizon** ($T_C$) | **Control Discretization** ($\Delta T_D$) | **Pitch RMSE** | **Control Effort** |
|---|---|---|---|---|
| **Second-Order MPC Controller - ($V_0 + V_1 + V_2$)** | | | | |
| 2 | 2 | 1 | 0.213 | 7.054 |
| | | 0.5 | 0.190 | 7.139 |
| | | 0.25 | 0.175 | 7.141 |
| | | 0.1 | 0.148 | 7.314 |
| **Third-Order MPC Controller - ($V_0 + V_1 + V_2 + V_3$)** | | | | |
| 2 | 2 | 1 | 0.212 | 6.849 |
| | | 0.5 | 0.187 | 6.914 |
| | | 0.25 | 0.171 | 6.933 |
| | | 0.1 | 0.198 | 7.687 |

To obtain a better understanding of how the linear and nonlinear predictive models affect the pitch response and control effort of MPC controllers applied to the nonlinear aeroelastic system, the results using all predictive models were directly compared. In the following examples, the cost (optimization) horizon and control horizon were both chosen to be 2 seconds while designing the linear and nonlinear MPC controllers.

According to Figures 5.21 and 5.22 similar trends can be seen in all predictive models as the nonlinear aeroelastic system is open-loop stable. The predictive models provide similar results for this nonlinear regulator case. The results obtained with a control discretization of 0.5 seconds has a smoother trend in attenuating the pitch response to zero and it requires less control effort. This conclusion is also supported by the RMS error analysis, as the results shown in Table 5.11 for a control discretization of 0.5 seconds show a good balance between pitch RMS error and control effort. Thus, 0.5 seconds was chosen as the value of the control discretization in the NMPC for the regulator case.

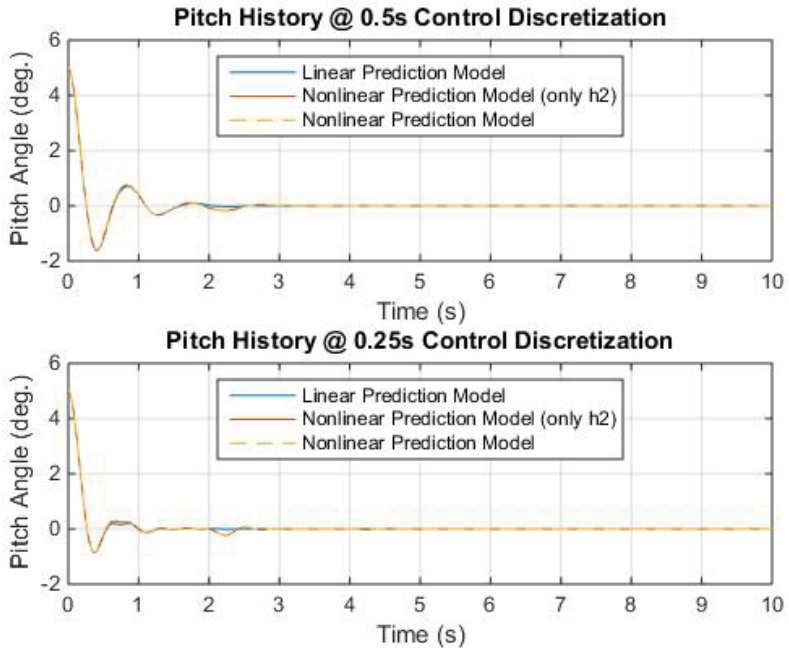


Figure 5.21. Pitch response comparison of different predictive models for nonlinear regulator case with 0.5 second and 0.25 second control discretizations.

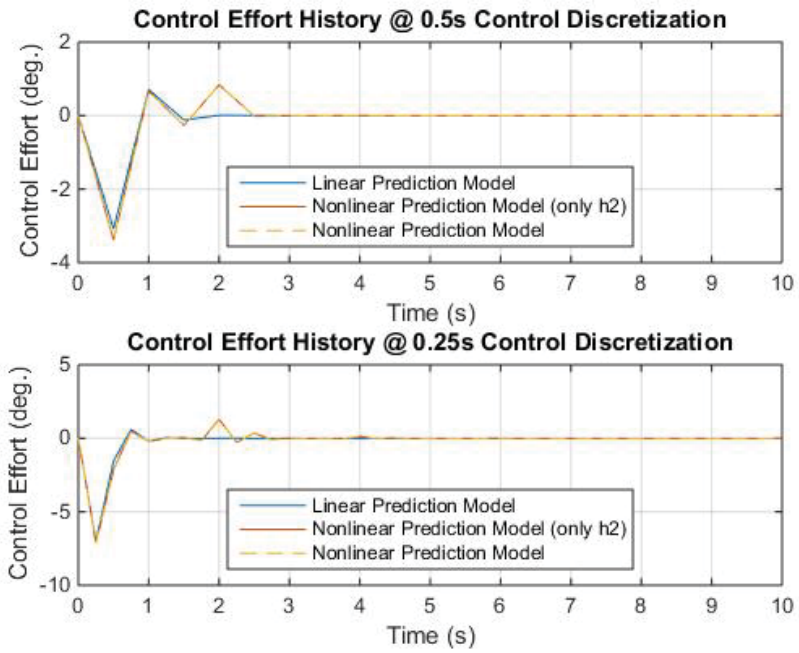


Figure 5.22. Control effort comparison of different predictive models for nonlinear regulator case with 0.5 second and 0.25 second control discretizations.

The same comparison study was performed for the nonlinear tracking case. The pitch response and control effort with 1 second and 0.5 seconds control discretizations are shown in Figures 5.23 and 5.24 respectively. In general, the third-order nonlinear predictive model shows the best performance in tracking the desired pitch angle with a minimal steady state error. Also, the 1 second control discretization provides better results as there are minimal oscillations while tracking the reference pitch angle. Although this case requires more control effort, the required amount is still within the trailing edge flap deflection limits. Therefore, a nonlinear predictive model with 1 second control discretization was used in the remaining simulation analysis for the tracking case.

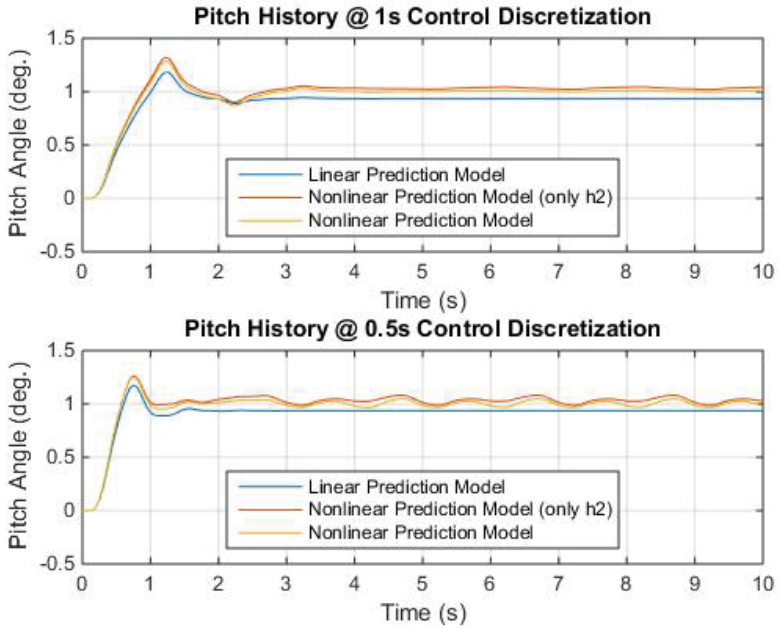


Figure 5.23. Pitch response comparison of different predictive models for nonlinear tracking case with 1 second and 0.5 second control discretizations.

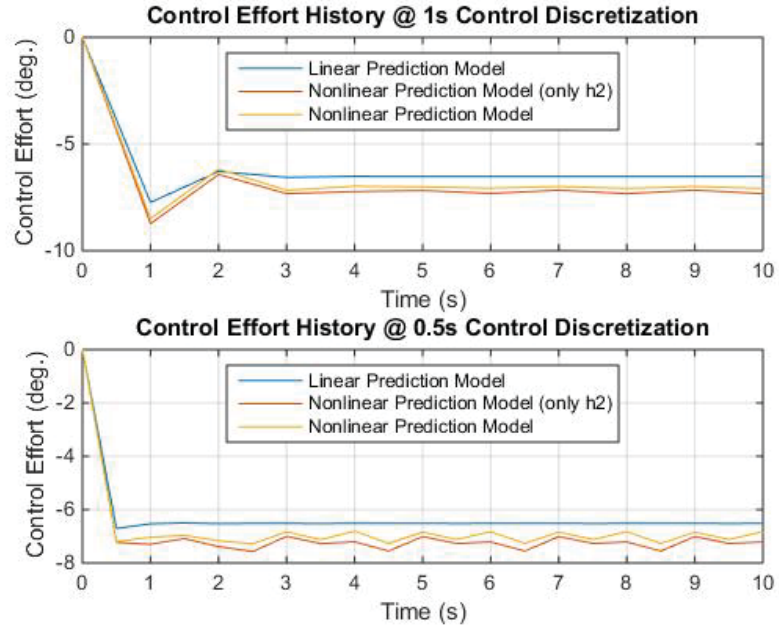


Figure 5.24. Control effort comparison of different predictive models for nonlinear tracking case with 1 second and 0.5 second control discretizations.

### 5.3.3 The Effect of Control Horizon

Control horizon ($T_C$) is another important parameter for designing a MPC controller. It determines how many seconds of the optimized control sequence are implemented on the actual nonlinear aeroelastic system. Therefore, the value of the control horizon must be less than or equal to the cost horizon ($T_H$). Based on results from the previous section, the third-order nonlinear predictive model with 0.5 seconds control discretization is implemented with varying control horizon parameter.

Figure 5.25 shows that the pitch response with a 2 seconds control horizon has a longer settling time and aggressive control deflection compared to the results of other control time horizons. The 1 second control horizon provides the best qualitative results because the pitch response has the least overshoot and the shortest settling time with minimal control effort, as depicted in Figure 5.26. Hence, the control horizon of 1 second is an appropriate choice for the regulator case NMPC controller.

Table 5.13. RMSE and control effort for nonlinear regulator case using NMPC with varying control time horizon.

| **Cost Horizon** ($T_H$) | **Control Horizon** ($T_C$) | **Control Discretization** ($\Delta T_D$) | **Pitch RMSE** | **Control Effort** |
|---|---|---|---|---|
| 2 | 2 | 0.5 | 0.596 | 0.609 |
| | 1 | | 0.607 | 0.069 |
| | 0.5 | | 0.595 | 0.593 |

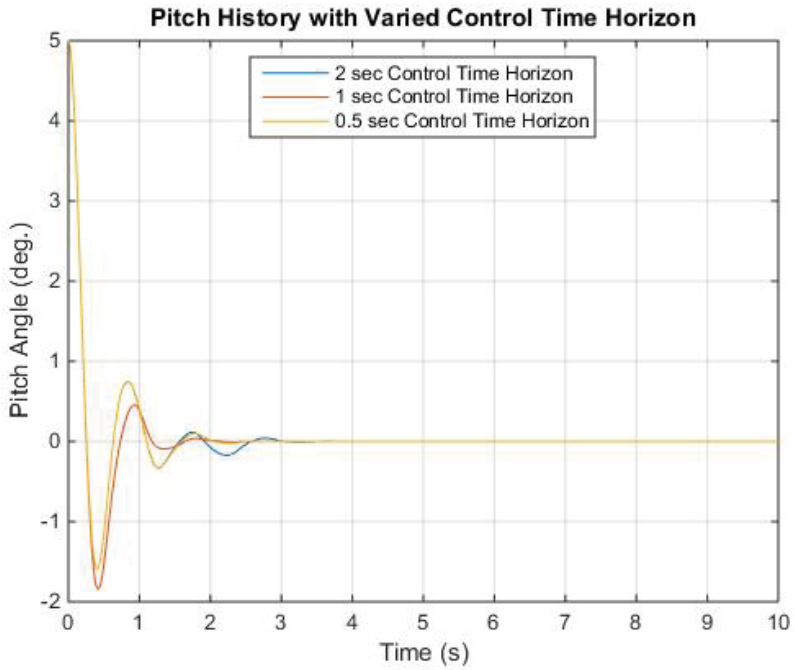


Figure 5.25. Nonlinear regulator case pitch response with $\Delta T_D = 0.5$ second at different control time horizons ($T_c$).

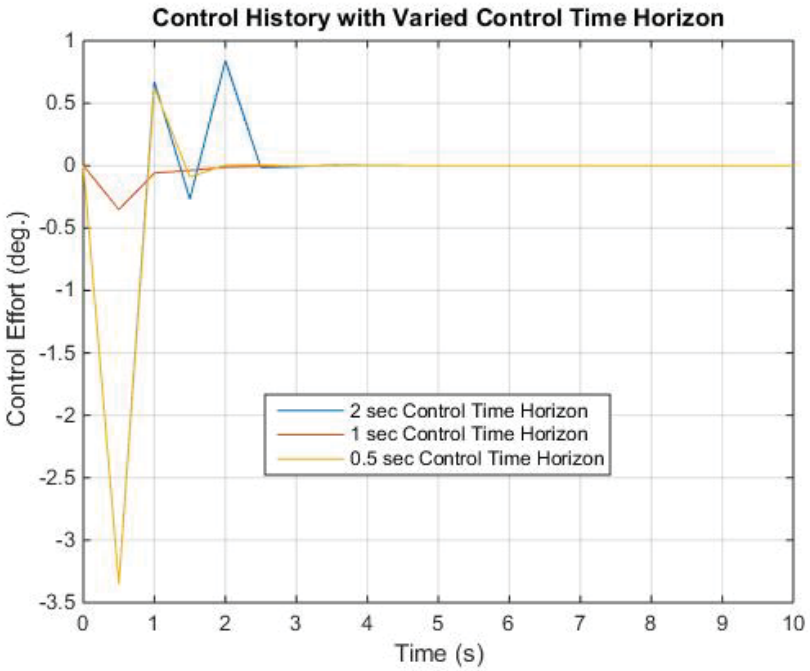


Figure 5.26. Nonlinear regulator case control effort with $\Delta T_D = 0.5$ second at different control time horizons ($T_c$).

Figures 5.27 and 5.28 present the pitch response and control effort for varying control time horizon for the tracking case. The 0.5 second control time horizon clearly yields the best qualitative performance as there is no overshoot and it tracks the desired pitch angle with minimal oscillation and control effort. According to the RMS error analysis presented in Table 5.14, it also yields the least pitch RMS error of 0.209 and control effort of 6.697. Thus, 0.5 second is the most suitable value for the control horizon parameter for the tracking case.

Table 5.14. RMSE and control effort for nonlinear tracking case using NMPC with varying control time horizon.

| **Cost Horizon** ($T_H$) | **Control Horizon** ($T_C$) | **Control Discretization** ($\Delta T_D$) | **Pitch RMSE** | **Control Effort** |
|---|---|---|---|---|
| 2 | 2 | 1 | 0.212 | 6.849 |
| | 1 | | 0.211 | 6.877 |
| | 0.5 | | 0.209 | 6.697 |

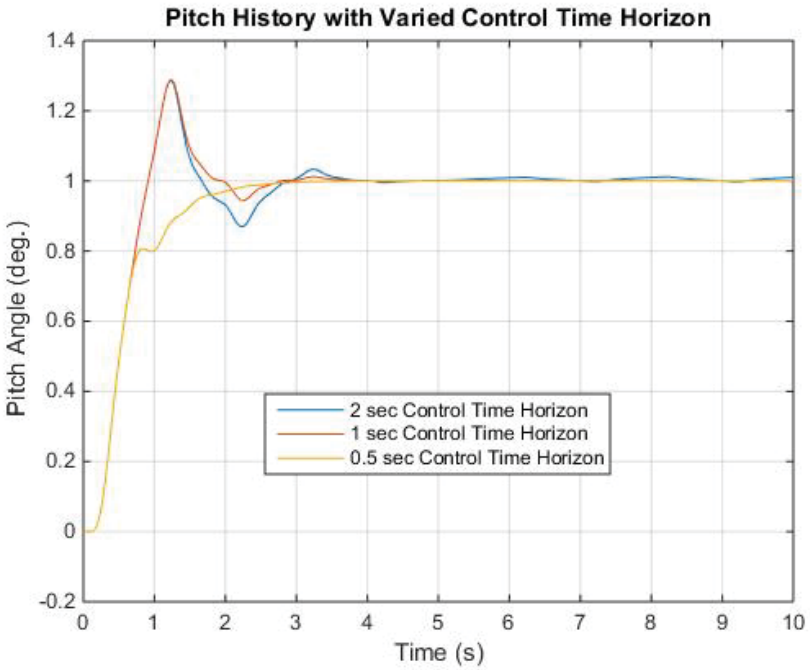


Figure 5.27. Nonlinear tracking case pitch response with $\Delta T_D = 1$ *sec* with different control time horizons ($T_c$).

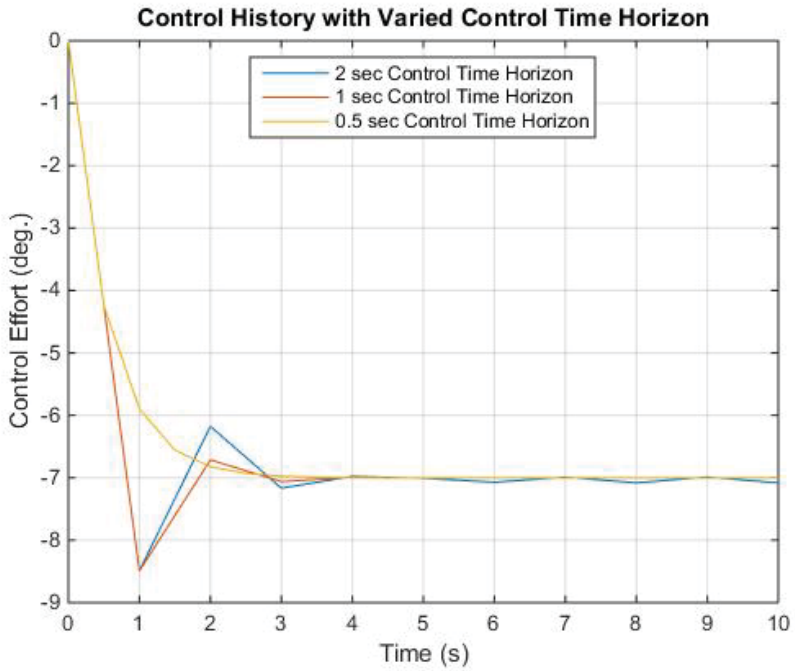


Figure 5.28. Nonlinear tracking case control effort with $\Delta T_D = 1$ *sec* with different control time horizons ($T_c$).

### 5.3.4 The Effect of Volterra Kernel Padding

As previously mentioned, the cost horizon for the linear MPC controller is set at 4 seconds while the nonlinear MPC controller horizon is set at 2 seconds. After analyzing the simulation results, it is clear that the third-order nonlinear predictive model provides a higher level of precision in predicting the response of the nonlinear aeroelastic system. However, results from the tracking case demonstrated that the linear predictive model can track the desired pitch angle accurately without any sudden oscillations after it settles at the reference value, while the nonlinear predictive model fails to do so. These results suggest that the full 4 seconds memory of the linear Volterra kernel should be used to improve the performance of the nonlinear MPC controller.

Kernel padding is used to increase the memory of second- and third- order Volterra kernels from 2 seconds to 4 seconds. The memory of the second- and third- order Volterra kernels was extended from 2 seconds to 4 seconds by padding zeros to the data set. This means the second- and third- order Volterra kernels will not contribute to the nonlinear predictive model after 2 seconds; however it will allow the nonlinear predictive model to utilize the remaining data in the zero- and first- order Volterra kernels to track the reference pitch angle. After padding, the cost horizon of the NMPC can be set to 4 seconds. With this approach, the pitch response performance improved for both regulator and tracking cases by shortening the settling time and tracking the target pitch angle with minimal control effort. This can be seen in Figures

5.29-5.32. The RMS error and control effort analysis in Table 5.15 also reveals the same observations.

Although more control effort is required for the tracking case, the required flap deflection is still within the deflection limits. The NMPC with padded Volterra kernels used for regulating the pitch response improved the performance by minimizing both the pitch error and control effort. This suggests that a longer cost horizon will improve the performance of the NMPC controller. In conclusion, Volterra kernel padding is required for all cases in order to obtain a lower pitch RMS error.

Table 5.15. RMSE and control effort for nonlinear regulator and tracking cases using NMPC with padded and non-padded Volterra kernels.

| **Cost Horizon** ($T_H$) | **Control Horizon** ($T_C$) | **Control Discretization** ($\Delta T_D$) | **Pitch RMSE** | **Control Effort** |
|---|---|---|---|---|
| **Regulator Case** | | | | |
| 2 | 2 | 0.5 | 0.666 | 0.681 |
| 4 | | | 0.665 | 0.662 |
| **Tracking Case** | | | | |
| 2 | 2 | 1 | 0.237 | 6.801 |
| 4 | | | 0.236 | 6.839 |

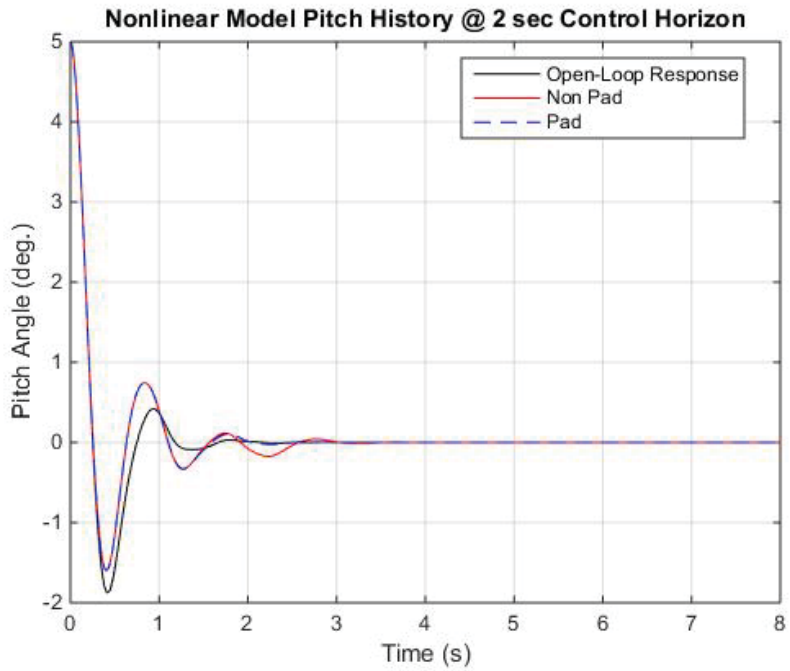


Figure 5.29. Nonlinear regulator case pitch responses with padded and non-padded NMPC at $T_C = 2$ *sec*.

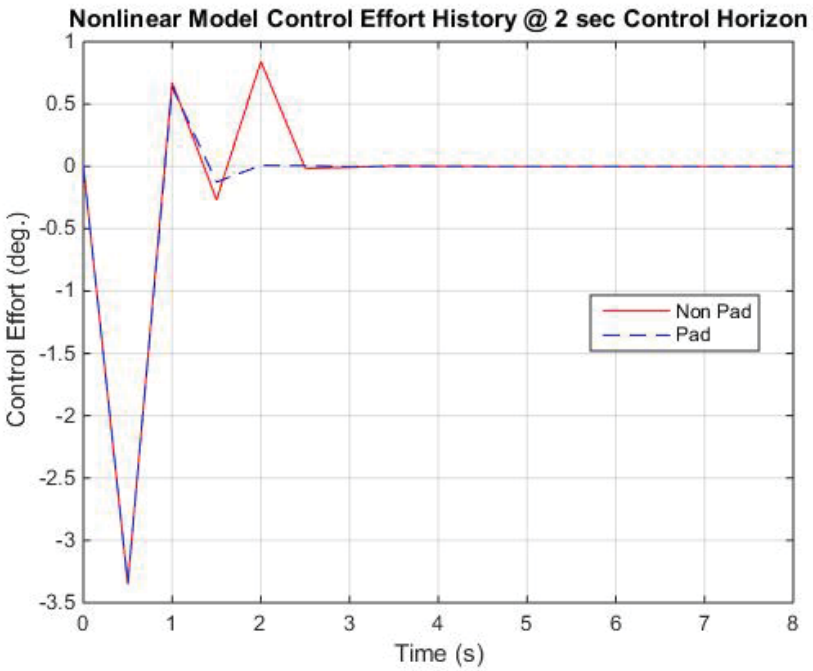


Figure 5.30. Nonlinear regulator case control effort with padded and non-padded NMPC at $T_C = 2$ *sec*.

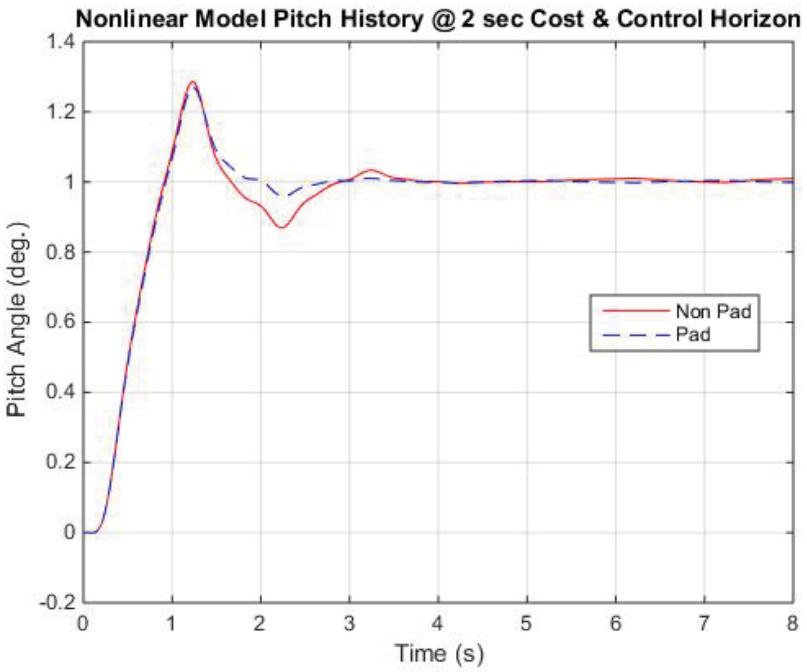


Figure 5.31. Nonlinear tracking case pitch responses with padded and non-padded NMPC at $T_C = 2$ *sec*.

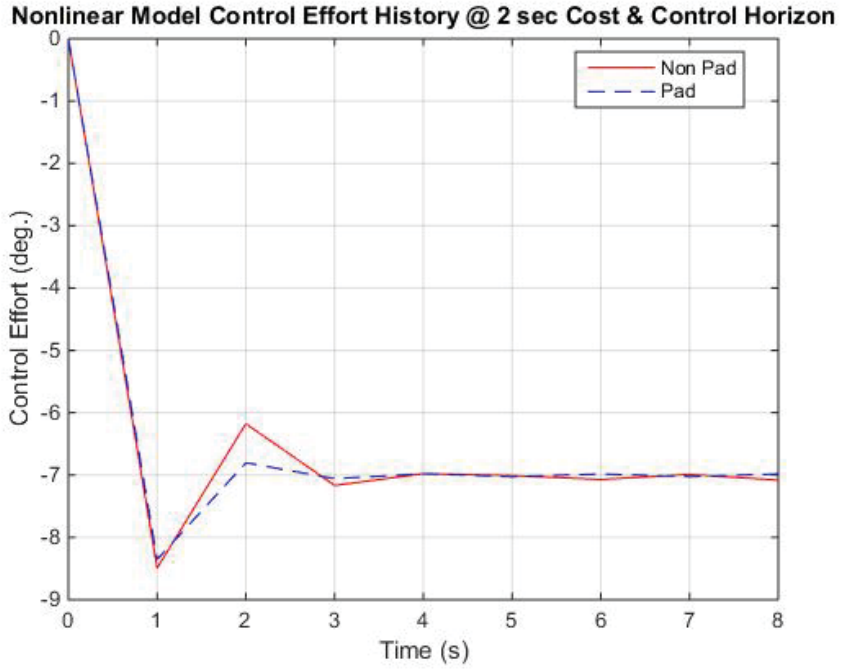


Figure 5.32. Nonlinear tracking case control effort with padded and non-padded NMPC at $T_C = 2$ *sec*.

### 5.3.5 The Effect of Cost Function Weighting

Weighting factors on pitch response ($w_\alpha$) and control effort ($w_\beta$) appear in the cost function ($J$), and they serve as MPC controller tuning parameters. The purpose of the weighting factors is to adjust the priority on minimizing the pitch error relative to minimizing the control effort. Figures 5.33 and 5.34 show the pitch response and control effort for both cases with multiple combinations of weighting factors.

Figures 5.33 and 5.34 show that there is an increase in the damping of the pitch response and the time to settle is reduced from 3 seconds to 2 seconds. In addition, it reduced the control effort by a significant amount. This can be seen in both the plots and the pitch RMS error and control effort analysis presented in Table 5.16. Although the pitch RMS error has a trend of increasing as the pitch error weighting is decreased in the cost function, the control effort is reduced significantly from 0.609 to 0.072. Hence, the weighting factor combination of 80% on pitch and 20% on control yields an acceptable pitch response with minimal control effort.

For the tracking case, on the other hand, the pitch response and control effort depicted in Figures 5.35 and 5.36 show that pitch error must have 100% weighting over the control effort. If not, the pitch response does not track the reference pitch angle as the control effort is not sufficient. The same conclusion can be made by analyzing the error given in Table 5.17 because the pitch RMS error increases dramatically as more penalty is given to the control effort.These results imply that the weighting combination of $w_\alpha = 100$ and $w_\beta = 0$ needs to be used for all NMPC tracking cases.

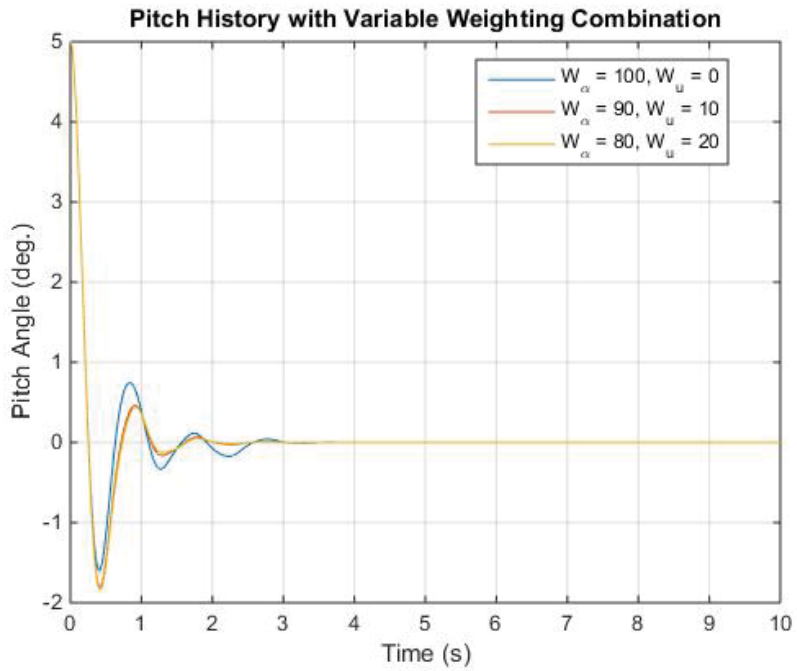


Figure 5.33. Regulator case pitch response with various combinations of weighting factors.

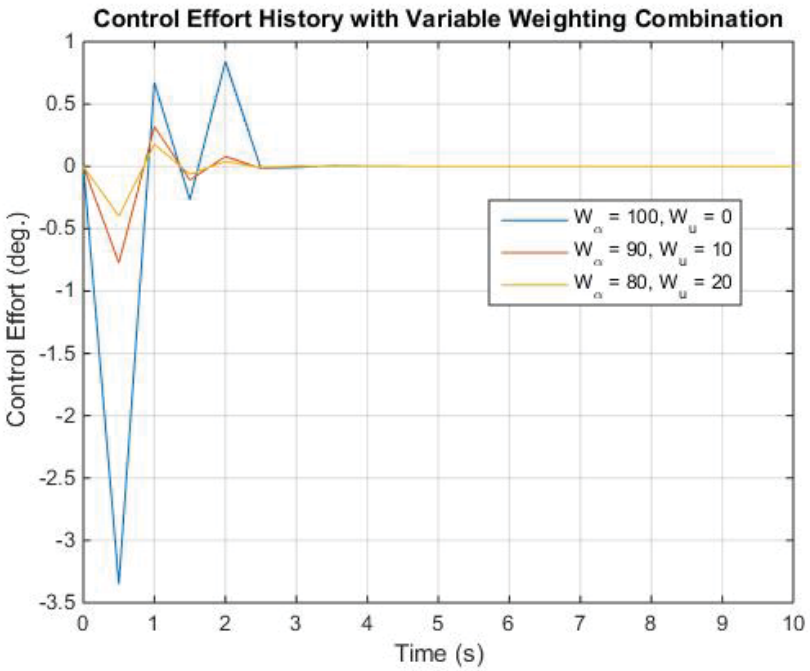


Figure 5.34. Regulator case control effort with various combinations of weighting factors.

Table 5.16. RMSE and control effort for nonlinear regulator case with various combinations of pitch and control weighting factors.

| **Pitch Weight** ($w_\alpha$) | **Control Weight** ($w_\beta$) | **Control Discretization** ($\Delta T_D$) | **Pitch RMSE** | **Control Effort** |
|---|---|---|---|---|
| 100 | 0 | 0.5 | 0.596 | 0.609 |
| 90 | 10 | | 0.604 | 0.138 |
| 80 | 20 | | 0.606 | 0.072 |

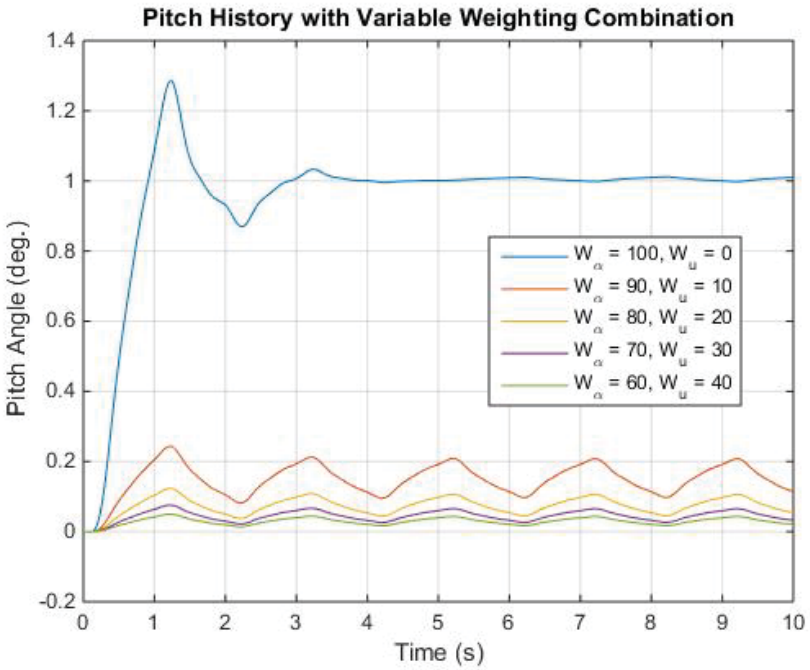


Figure 5.35. Nonlinear tracking case pitch response with various combinations of weighting factors.

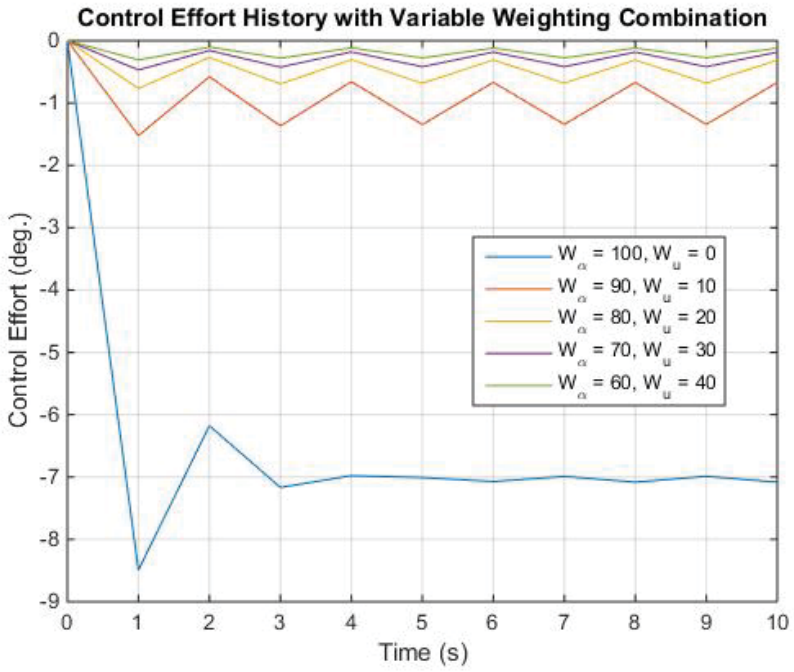


Figure 5.36. Nonlinear tracking case control effort with various combinations of weighting factors.

Table 5.17. RMSE for tracking case with various combinations of pitch and control weighting factors.

| **Pitch Weight** ($w_\alpha$) | **Control Weight** ($w_\beta$) | **Control Discretization** ($\Delta T_D$) | **Pitch RMSE** | **Control Effort** |
|---|---|---|---|---|
| 100 | 0 | 0.5 | 0.171 | 6.933 |
| 90 | 10 | | 0.853 | 1.070 |
| 80 | 20 | | 0.925 | 0.536 |
| 70 | 30 | | 0.954 | 0.327 |
| 60 | 40 | | 0.970 | 0.219 |

### 5.3.6 NMPC Design Summary at U = 6 m/s

After analyzing the effect of the MPC controller parameters on pitch response and control effort, two NMPC controllers were designed for nonlinear regulator and tracking cases with parameter values that yield the best pitch response and control effort in each case. Table 5.18 summarizes the final design parameter values and quantitative analysis results for both NMPC controllers.

Table 5.18. NMPC final design parameters with quantitative analysis results for both nonlinear regulator and tracking cases.

| **Description** | **Symbol** | **Value** | |
|---|---|---|---|
| | | Regulator | Tracking |
| Optimization Time Horizon | $T_H$ | 4 | 4 |
| Control Time Horizon | $T_C$ | 0.5 | 0.5 |
| Final Simulation Time | $T$ | 10 | 8 |
| Simulation Time Step | $\Delta T$ | 0.01 | 0.01 |
| Control Input Discretization | $\Delta T_D$ | 0.25 | 1 |
| Pitch Weighting Factor | $w_\alpha$ | 100 | 100 |
| Control Effort Weighting Factor | $w_\beta$ | 0 | 0 |
| Pitch RMSE | $\alpha_{RMSE}$ | 0.552 | 0.235 |
| Control Effort | CE | 1.025 | 6.622 |

For the regulator case shown in Figures 5.37 and 5.38, the pitch response is slightly damped with a short settling time of approximately 1.5 seconds with maximum control effort of 0.4 degree downward flap deflection. The nonlinear MPC controller achieved this performance with the help of adding weight factors on the control effort and reducing the priority on the pitch error.

The pitch response for the tracking case is depicted in Figure 5.39. It is shown that the nonlinear MPC controller performs well with no overshoot, a short settling time of approximately 2.5 seconds and tracks the reference pitch angle with zero steady-state error. As shown in Figure 5.40, the maximum control effort is 7 degrees downward flap deflection, which is within the flap deflection limits.

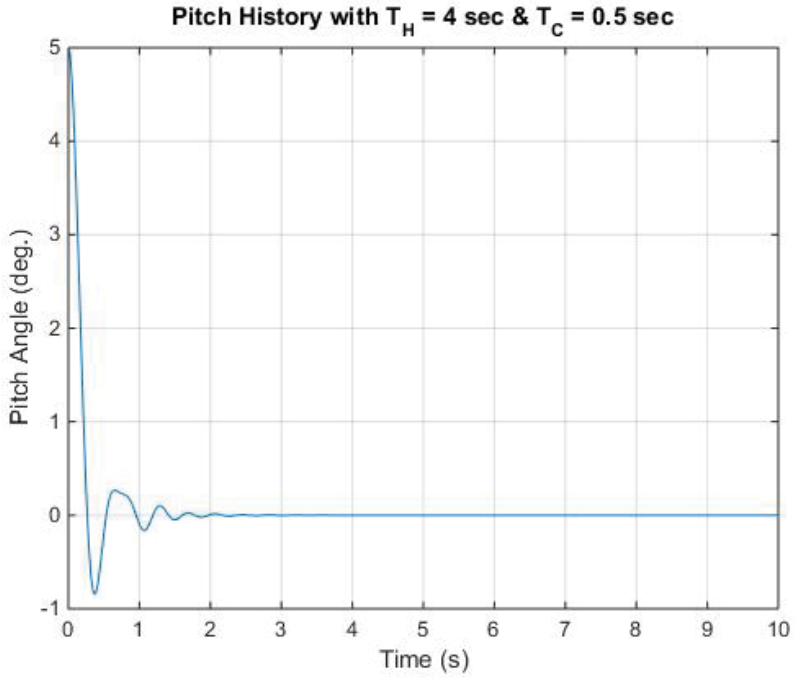


Figure 5.37. Pitch response from nonlinear regulator case NMPC controller with specific parameter values.

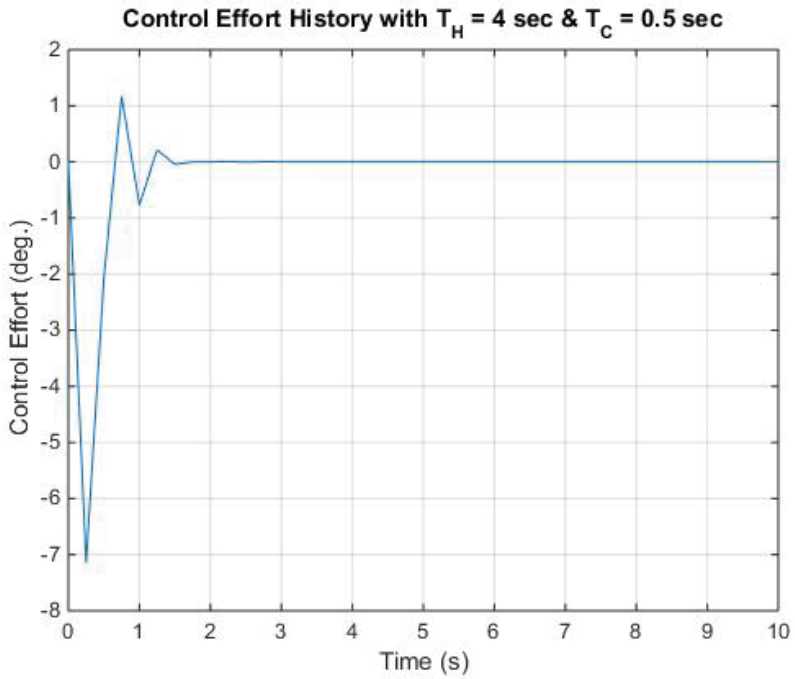


Figure 5.38. Control effort from nonlinear regulator case NMPC controller with specific parameter values.

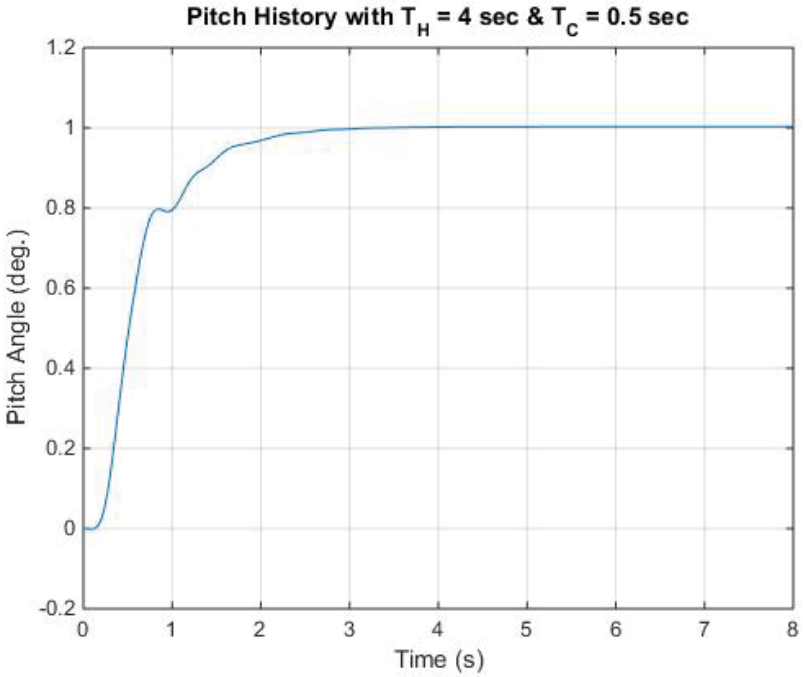


Figure 5.39. Pitch response from nonlinear tracking case NMPC controller with specific parameter values.

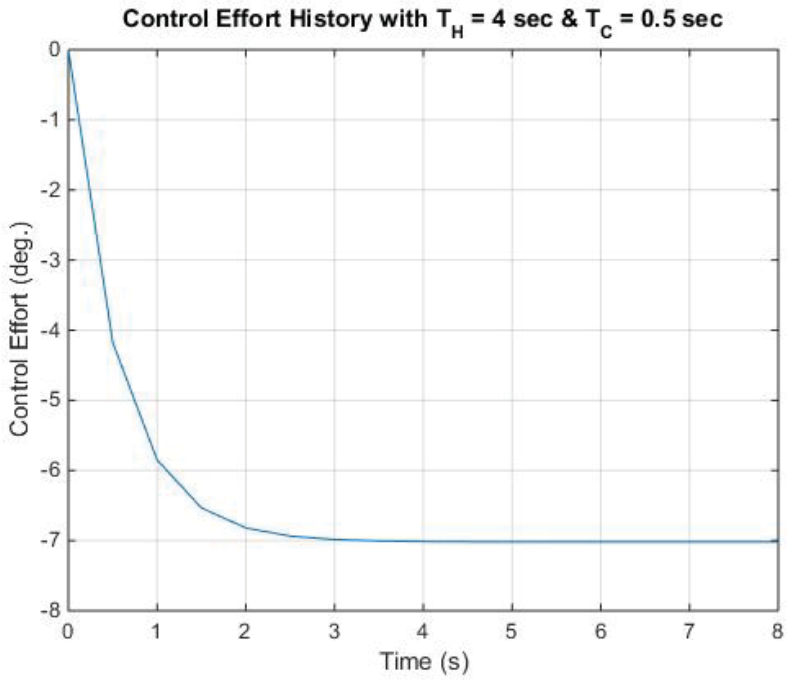


Figure 5.40. Control effort from nonlinear tracking case NMPC controller with specific parameter values.

Figures 5.41 and 5.42 compare the open-loop response with the pitch response produced by the LQR and NMPC controllers. It is clear that the discrete-time LQR controller has a similar settling time as the NMPC controller. The NMPC controller has the best qualitative pitch response as it has the least initial overshoot and the required control effort is minimal comparing to the DLQR controller, as shown in Table 5.19. Additional tuning of the parameters and weights may further improve the NMPC performance. With the current NMPC design, the controller outperforms the baseline discrete-time LQR controller qualitatively and quantitatively.

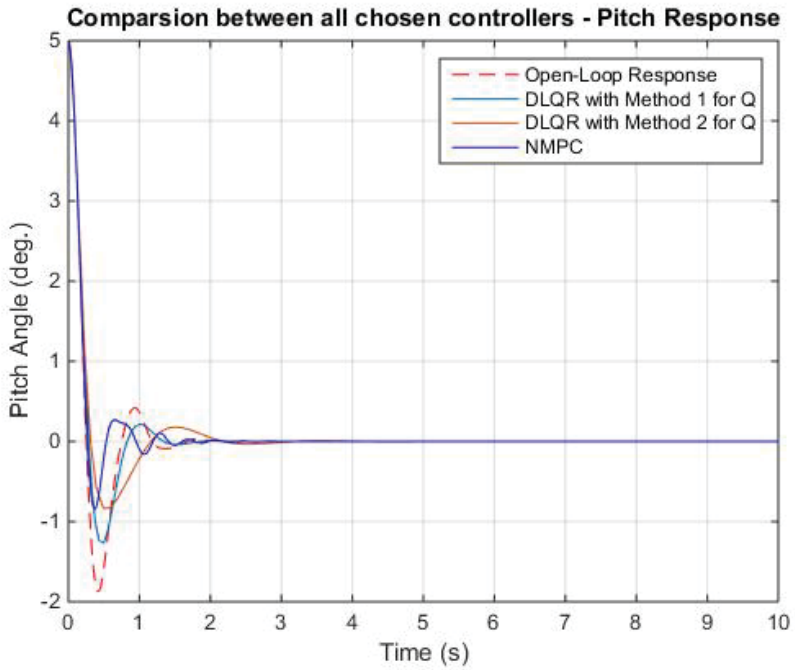


Figure 5.41. Nonlinear pitch response comparison between open-loop, DLQR and NMPC controllers at free-stream velocity of 6 m/s.

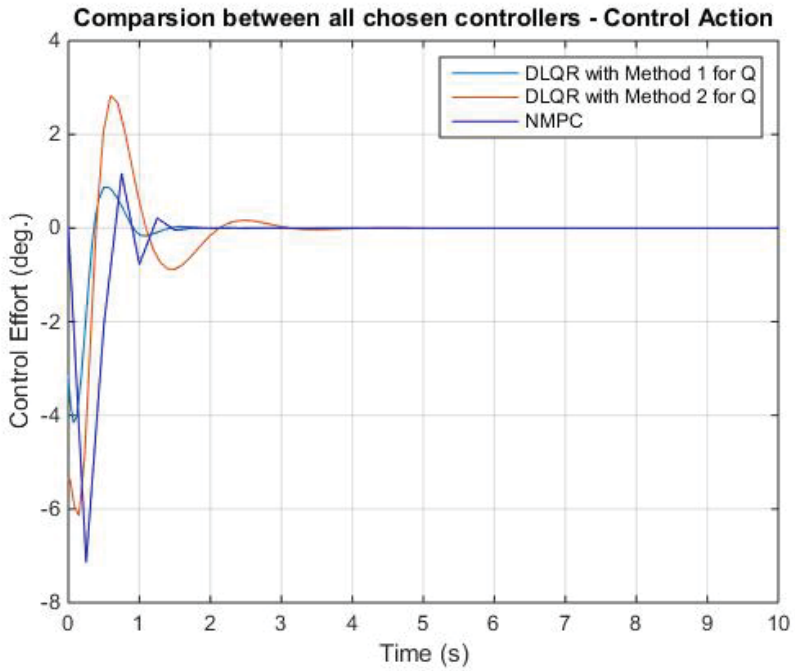


Figure 5.42. Control effort comparison between DLQR and NMPC controllers at free-stream velocity of 6 m/s.

Table 5.19. RMSE and control effort comparison between chosen controllers at U = 6 m/s.

| **Controller** | **Pitch RMSE** | **Control Effort** |
|---|---|---|
| Open-Loop Response | 0.588 | N/A |
| NMPC | 0.552 | 1.025 |
| DLQR (Q defined using Method 1) | 1.722 | 1.360 |
| DLQR (Q defined using Method 2) | 1.746 | 2.290 |

## 5.4 NMPC: Free-stream Velocity at 12.5 m/s

The MPC controllers are than applied to the nonlinear aeroelastic system at a free-stream velocity of 12.5 m/s, which corresponds to a limit cycle oscillation condition for the nonlinear system. In this case, the zero- and first- order Volterra kernels were identified over a 4 second window. As the flight condition is not asymptotically stable, the Volterra kernels have infinite memory meaning the kernels will not decay to zero in finite time. Hence, the only method to identify a Volterra model for this system is to identify kernels that the same duration as the training data set. In this case, a 4 second training input-output data set was used to extract kernels within a 4 second horizon.

Using the same approach as the U = 6 m/s case, the MPC controllers were employed to regulate the pitch response from an initial pitch angle of 5 degrees to zero. The open-loop pitch response is a limit cycle oscillation, corresponding to bounded oscillations. Since second- and third-order Volterra kernels were not identified at this

flight condition, the LMPC controller is implemented to stabilize and regulate the pitch response. The weighting factors within the cost function were chosen as $w_\alpha = 100$ and $w_\beta = 0$ unless otherwise stated. Since the first-order kernel was identified with a duration of 4 seconds, the largest feasible choice for the cost horizon is $T_H = 4$ *sec*.

### 5.4.1 Regulator Case

Figures 5.43 and 5.44 depict the pitch response and control effort that were obtained using the linear MPC controller with $T_H = 4$ *sec*, $T_C = 2$ *sec* and several values of the control input discretization $\Delta T_D$. The open-loop pitch response is also shown for comparison purposes. Since the open-loop response at this flight condition is characterized by a limit cycle with frequency of approximately 2 Hz, the Nyquist sampling criteria implies that the control input must be applied at a minimum of 4 Hz in order to be effective. This corresponds to a maximum control discretization (i.e. coarsest allowable) of 0.25 seconds. The results show that the linear MPC controller successfully stabilizes the pitch response and regulates to zero with a reasonable level of control effort. With a control discretization of 0.1 and 0.05 seconds, the pitch response is attenuated and settles more quickly at a cost of larger control effort, and saturates at the flap deflection limit.

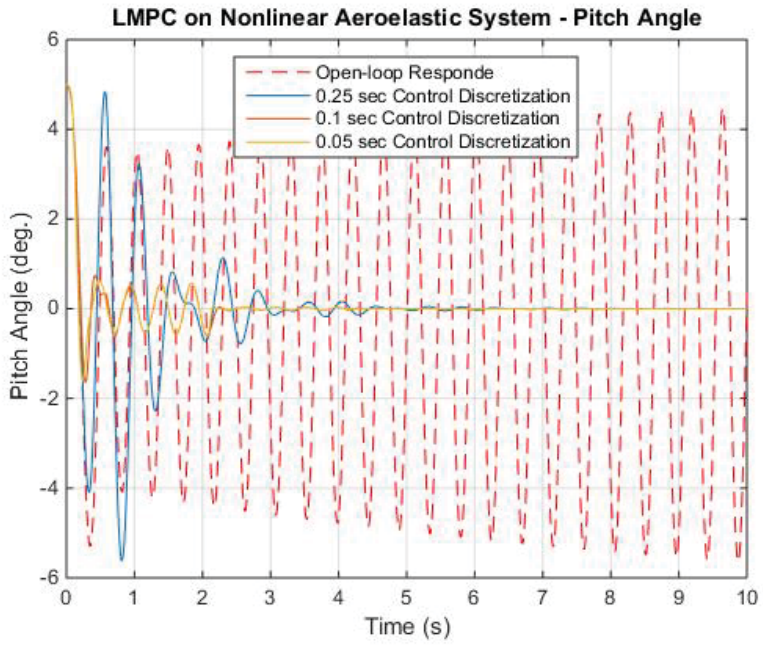


Figure 5.43. Regulator case pitch response for nonlinear aeroelastic system using the linear MPC controller with different control input discretizations.

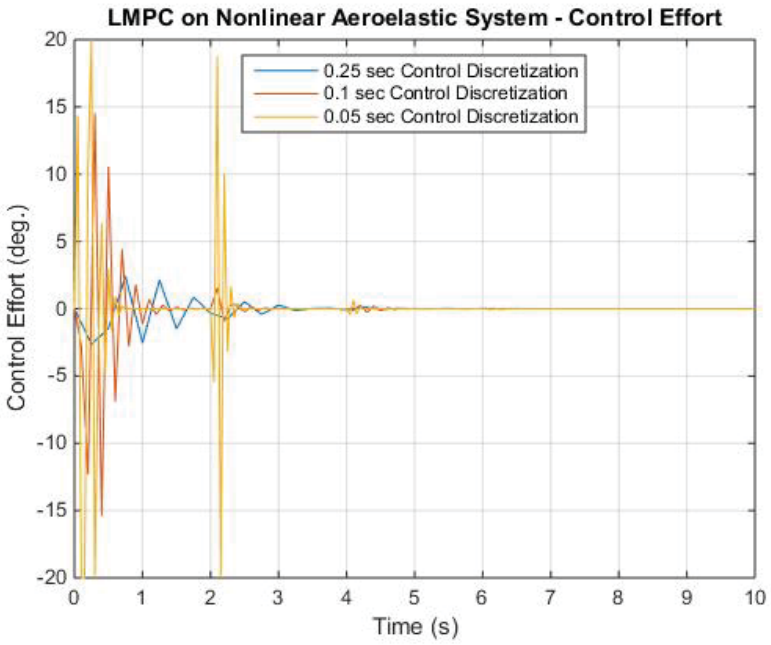


Figure 5.44. Regulator case control effort for nonlinear aeroelastic system at using the linear MPC controller with different control input discretizations.

Table 5.20. RMSE and control effort for regulator case at 12.5 m/s.

| **Cost Horizon** ($T_H$) | **Control Horizon** ($T_C$) | **Control Discretization** ($\Delta T_D$) | **Pitch RMSE** | **Control Effort** |
|---|---|---|---|---|
| **Open-Loop Response** | | | | |
| N/A | | | 3.272 | N/A |
| **Linear MPC Controller - ($V_0$ + $V_1$)** | | | | |
| 4 | 2 | 0.25 | 1.209 | 0.605 |
| | | 0.1 | 0.604 | 1.792 |
| | | 0.05 | 0.584 | 2.865 |

To further improve the performance of the MPC controller, different combinations of weights were used in the cost function to minimize the overshoot and oscillation in the pitch response. Results presented in Figures 5.45 and 5.46 demonstrate improvement in pitch response by reducing the overshoot and time to settle. The pitch response with weights of $w_\alpha = 90$ and $w_\beta = 10$ in the cost function showed the best qualitative performance with reasonable amount of control effort from the flap.

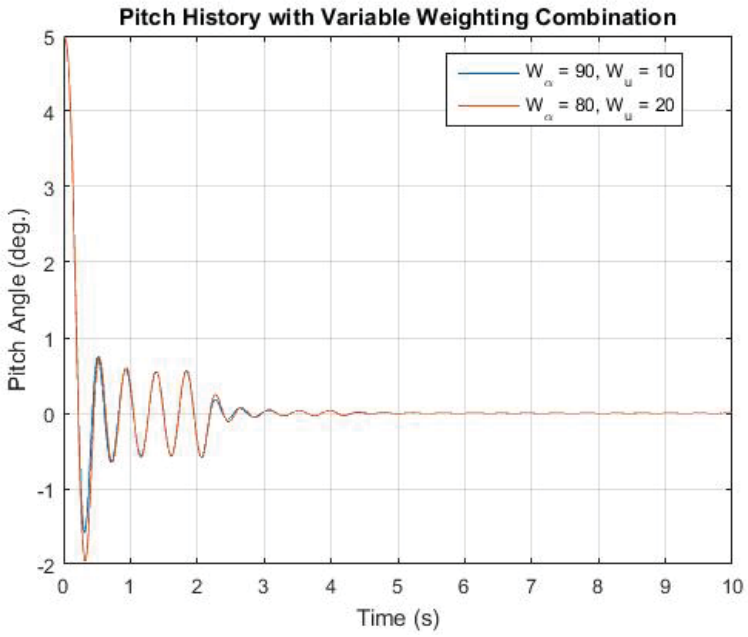


Figure 5.45. Regulator case pitch response for the nonlinear aeroelastic system using the linear MPC controller with different combinations of weights.

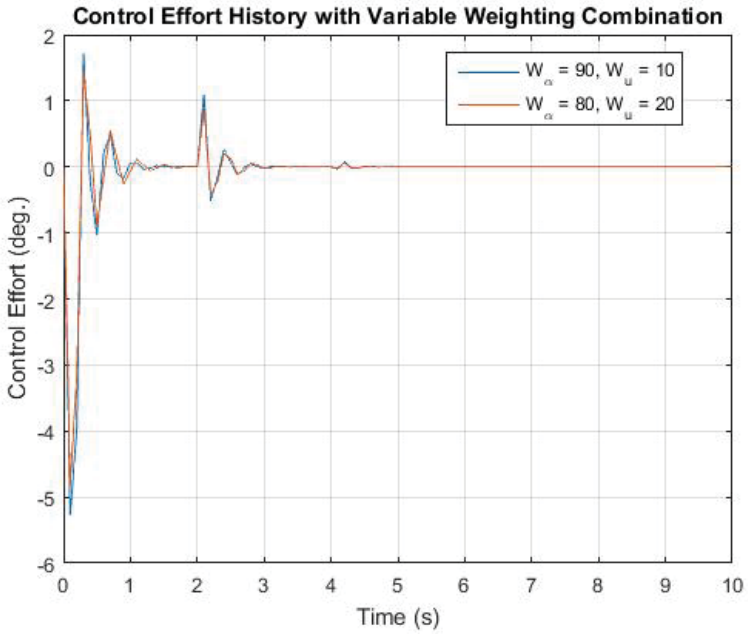


Figure 5.46. Regulator case control effort for the nonlinear aeroelastic system using the linear MPC controller with different combinations of weights.

Table 5.21. RMSE and control effort for regulator case at U = 12.5 m/s with various combinations of weights.

| **Pitch Weight** ($w_\alpha$) | **Control Weight** ($w_\beta$) | **Control Discretization** ($\Delta T_D$) | **Pitch RMSE** | **Control Effort** |
|---|---|---|---|---|
| 90 | 10 | 0.1 | 0.407 | 1.429 |
| 80 | 20 | | 0.583 | 0.985 |

Figures 5.47 and 5.48 show that all three controllers stabilize, the open-loop pitch response and result in pitch responses that converged within the first 5 seconds. The LQR controller accomplishes the task with better performance than the NMPC as the settling time is less than 2 seconds. The NMPC controller completed the task but with a longer settling time and minor oscillations with amplitude of 0.5 degrees within the first 2 seconds. Although further investigation and tuning is required on the NMPC to achieve better transient performance at this flight condition, the RMS error in Table 5.22 shows the NMPC controller performs better than the classical LQR controller quantitatively.

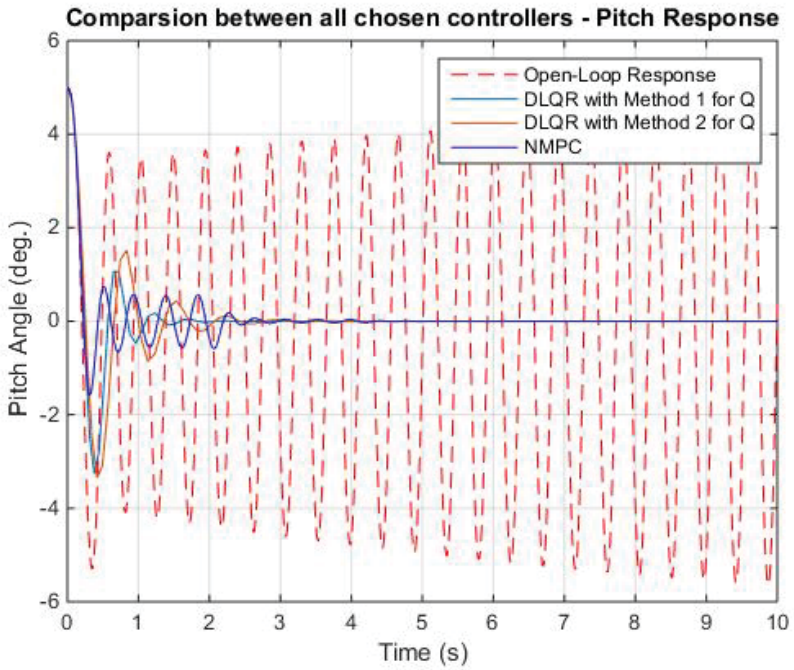


Figure 5.47. Nonlinear pitch response comparison between open-loop, DLQR and NMPC controllers at free-stream velocity of U = 12.5 m/s.

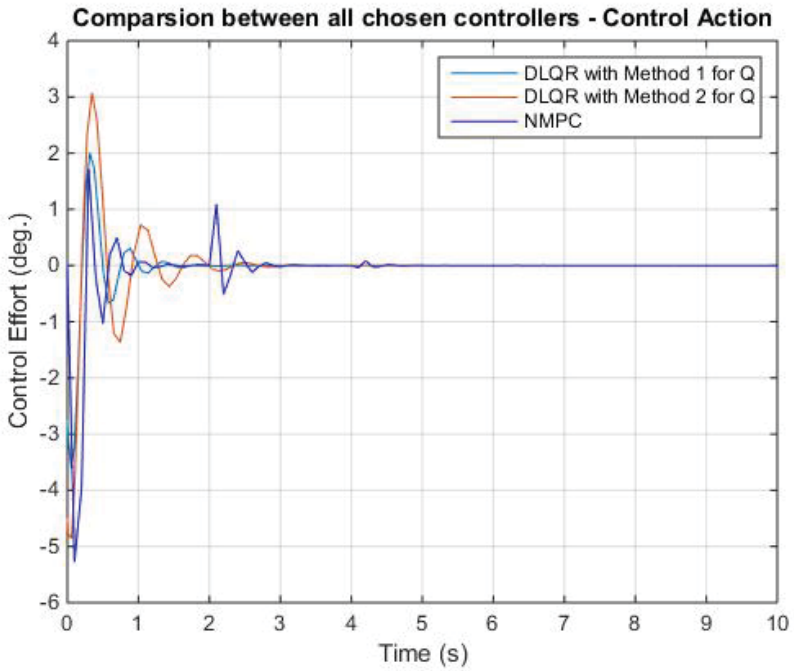


Figure 5.48. Control effort comparison between DLQR and NMPC controllers at free-stream velocity of U = 12.5 m/s.

Table 5.22. RMSE and control effort comparison between chosen controllers at U = 12.5 m/s.

| **Controller** | **Pitch RMSE** | **Control Effort** |
|---|---|---|
| Open-Loop Response | 3.272 | N/A |
| LMPC | 0.407 | 1.429 |
| DLQR (Q defined using Method 1) | 1.836 | 1.131 |
| DLQR (Q defined using Method 2) | 1.890 | 1.717 |

### 5.4.2 Tracking Case

Table 5.23. RMSE and control effort for tracking case at U = 12.5 m/s.

| **Cost Horizon** ($T_H$) | **Control Horizon** ($T_C$) | **Control Discretization** ($\Delta T_D$) | **Pitch RMSE** | **Control Effort** |
|---|---|---|---|---|
| 4 | 2 | 0.25 | 0.193 | 2.253 |
| | | 0.1 | 0.170 | 2.322 |

The linear MPC controller with the same choice of parameters was then applied to a tracking case, where the controller drives the pitch angle from zero initial condition to a constant pitch reference value of 1 degree. Figures 5.49 and 5.50 show the pitch response and control effort respectively. For both chosen control discretization values, the pitch response is drive to an average value that corresponds to the commanded value of 1 degree; however, the pitch response oscillates about this value with an

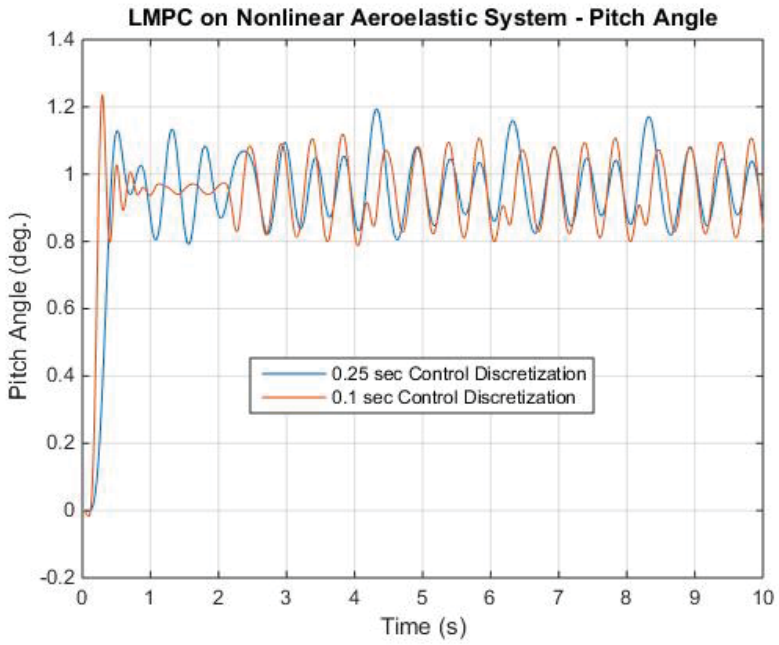


Figure 5.49. Tracking case pitch response for the nonlinear aeroelastic system using the linear MPC controller with different control input discretizations.

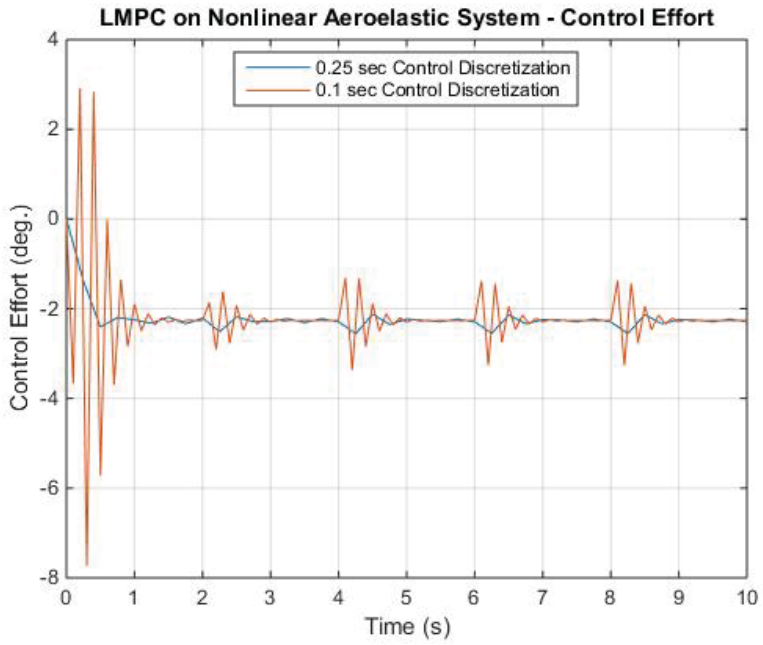


Figure 5.50. Tracking case control effort for the nonlinear aeroelastic system at using the linear MPC controller with different control input discretizations.

amplitude of 0.2 degrees. It appears that a linear MPC controller is not sufficient to control the nonlinear aeroelastic system to track a desired pitch reference value at the flutter speed. Thus, further investigation is required for the tracking case at this flight condition.

# 6. Conclusion and Future Work

## 6.1 Conclusion

The main objective of this research was to investigate the potential effectiveness of using Volterra-based MPC strategies to control an aeroelastic system and to evaluate the performance of these controllers. The results from the NMPC controller showed that the nonlinear predictive model using the first-, second- and third- order Volterra kernels was sufficient to model and compensate for the weak nonlinearities cause by the nonlinear spring within the aeroelastic system. This evaluation was performed through regulator and tracking cases at U = 6 m/s and U = 12.5 m/s. The latter case corresponds to the unstable flutter speed for the linear system and results in a bounded limit cycle oscillation in the nonlinear system. Classical LQR controllers were implemented on the linear and nonlinear aeroelastic systems in continuous and discrete-time as baseline controllers to evaluate the performance of the Volterra-based MPC controllers.

The results showed that all controllers successfully stabilized the linear aeroelastic system at the flutter condition and provided adequate tracking performance. Simulation results using the controllers implemented on the linear aeroelastic system demonstrated that the LMPC controller outperformed the classical LQR controller both qualitatively and quantitatively, in terms of the RMS error in the pitch angle

and the control effort required. For controllers implemented on the nonlinear aeroelastic system, the simulation results showed that the NMPC did not outperform the classical LQR baseline controller qualitatively in the regulator case, but did provide superior quantitative performance as demonstrated by the pitch RMS error and control effort. It is also shown that the incorporation of the second and third-order Volterra kernels in the nonlinear MPC controller provides superior tracking performance on the nonlinear aeroelastic system compared to the results obtained using only a linear model.

This study also investigated the effect of several MPC design parameters including the optimization horizon, the control horizon, and the control discretization. A kernel padding technique is used to prolong the memory of the Volterra kernels and extend the optimization horizon, which resulted in shorter settling time on the pitch response. Further tuning of the design parameters and cost function weights could potentially improve the closed-loop response of the system. In addition, the thesis discussed methods to achieve closed-loop stability using linear and nonlinear MPC strategies.

## 6.2 Future Work

This thesis provides the foundation for implementing Volterra-based MPC strategies to control a nonlinear aeroelastic system. Future work for this study could include determining an effective way to tune the MPC controllers, identifying the second- and third-order Volterra kernels at U = 12.5 m/s and implementing the NMPC stability strategy at this flight condition. Furthermore, online system ID can be implemented

to identify and update the Volterra kernels at different flight conditions. The MPC algorithm presented in this thesis can potentially be extended to other systems with fast dynamics. For example, MPC could be applied to control a UAV operating in complex environments with obstacle avoidance constraints.

# REFERENCES


Abyss, W. (2016). *Mcdonnell douglas av-8b harrier ii computer background.* Retrieved from `https://wall.alphacoders.com/big.php?i=75568`

*Anticipation.* (2016). Retrieved from `http://www.merriam-webster.com/dictionary/anticipation`

Bemporad, A. (2015). *Linear model predictive control.* Retrieved from `http://cse.lab.imtlucca.it/~bemporad/teaching/mpc/imt/1-mpc.pdf`

Bemporad, A., & Morari, M. (1999). Robust model predictive control: A survey. In *Robustness in identification and control* (pp. 207–226). Springer.

Beylkin, G., Coifman, R., & Rokhlin, V. (1991). Fast wavelet transforms and numerical algorithms i. *Communications on pure and applied mathematics*, *44*(2), 141–183.

Borys, A. (2001). *Nonlinear aspects of telecommunications: discrete volterra series and nonlinear echo cancellation.* CRC Press.

Campbell, C., & Maciejowski, J. (2009). Control and guidance of a highly-flexible micro air vehicle using model predictive control. In *Aiaa guidance, navigation, and control conference* (p. 5874).

Chao, H., Cao, Y., & Chen, Y. (2010). Autopilots for small unmanned aerial vehicles: a survey. *International Journal of Control, Automation and Systems*, *8*(1), 36–44.

Chao, Z., Zhou, S.-L., Ming, L., & Zhang, W.-G. (2012). Uav formation flight based on nonlinear model predictive control. *Mathematical Problems in Engineering*, *2012*.

Chen, H., & Allgöwer, F. (1997). A quasi-infinite horizon nonlinear model predictive control scheme with guaranteed stability. In *Control conference (ecc), 1997 european* (pp. 1421–1426).

Chen, X., & Wang, L. (2013). Cascaded model predictive control of a quadrotor uav. In *Control conference (aucc), 2013 3rd australian* (pp. 354–359).

Cherry, J. A., & Snelgrove, W. M. (1998). On the characterization and reduction of distortion in bandpass filters. *Circuits and Systems I: Fundamental Theory and Applications, IEEE Transactions on*, *45*(5), 523–537.

Chon, K. H., Chen, Y.-M., Holstein-Rathlou, N.-H., & Marmarelis, V. Z. (1998). Nonlinear system analysis of renal autoregulation in normotensive and hypertensive rats. *Biomedical Engineering, IEEE Transactions on*, *45*(3), 342–353.

Cutler, C., Morshedi, A., & Haydel, J. (1983). An industrial perspective on advanced control. In *Aiche annual meeting.*

Cutler, C. R., & Ramaker, B. L. (1980). Dynamic matrix control - a computer control algorithm. In *Proceeding of the joint automatic control conference* (p. 72).

Dai, L., Mahmoud, M. S., Fu, M., & Xia, Y. (2012). *Discrete-time model predictive control*. INTECH Open Access Publisher.

Deshmukh, S., & Sawarkar, S. (2015). Convergence analysis of model predictive control. *International Journal of Advance Research in Computer Science and Software Engineering*, *5*(3), 125–131.

Donovan, G. C., Geronimo, J. S., & Hardin, D. P. (1996). Intertwining multiresolution analyses and the construction of piecewise-polynomial wavelets. *SIAM Journal on Mathematical Analysis*, *27*(6), 1791–1815.

Du, J., Kondak, K., Bernard, M., Zhang, Y., Lü, T., & Hommel, G. (2008). Model predictive control for a small scale unmanned helicopter. *International Journal of Advanced Robotic Systems*, *5*(4), 433–438.

Dunbar, W. B., Milam, M. B., Franz, R., & Murray, R. M. (2002). Model predictive control of a thrust-vectored flight control experiment. In *15th ifac world congress on automatic control*.

Eklund, J. M., Sprinkle, J., & Sastry, S. (2005). Implementing and testing a nonlinear model predictive tracking controller for aerial pursuit/evasion games on a fixed wing aircraft. In *American control conference, 2005. proceedings of the 2005* (pp. 1509–1514).

Findeisen, R., & Allgöwer, F. (2002). An introduction to nonlinear model predictive control. In *21st benelux meeting on systems and control* (Vol. 11, pp. 119–141).

Franz, M. O., & Schölkopf, B. (2006). A unifying view of wiener and volterra theory and polynomial kernel regression. *Neural computation*, *18*(12), 3097–3118.

French, A. S., Sekizawa, S.-i., Höger, U., & Torkkeli, P. H. (2001). Predicting the responses of mechanoreceptor neurons to physiological inputs by nonlinear system identification. *Annals of biomedical engineering*, *29*(3), 187–194.

Froisy, J., & Matsko, T. (1990). Idcom-m application to the shell fundamental control problem. In *Aiche annual meeting* (Vol. 43).

Froisy, J. B. (1994). Model predictive control: Past, present and future. *ISA transactions*, *33*(3), 235–243.

Garcia, C. E., Prett, D. M., & Morari, M. (1989). Model predictive control: theory and practicea survey. *Automatica*, *25*(3), 335–348.

Goodwin, G. C., Graebe, S. F., & Salgado, M. E. (2001). *Control system design* (Vol. 240). Prentice Hall New Jersey.

Grosdidier, P., Froisy, B., & Hammann, M. (1988). The idcom-m controller. In *Proceedings of the 1988 ifac workshop on model based process control* (pp. 31–36).

Hafez, A. T., Givigi, S. N., Ghamry, K. A., & Yousefi, S. (2015). Multiple cooperative uavs target tracking using learning based model predictive control. In *Unmanned aircraft systems (icuas), 2015 international conference on* (pp. 1017–1024).

Hespanha, J. P. (2009). *Linear systems theory*. Princeton university press.

*Heuristic.* (2016). Retrieved from `www.merriam-webster.com/dictionary/heuristic`

Holkar, K., & Waghmare, L. (2010a). Discrete model predictive control for dc drive using orthonormal basis function. In *Control 2010, ukacc international conference on* (pp. 1–6).

Holkar, K., & Waghmare, L. (2010b). An overview of model predictive control. *International Journal of Control and Automation*, *3*(4), 47–63.

Iskandarani, M., Givigi, S. N., Fusina, G., & Beaulieu, A. (2014). Unmanned aerial vehicle formation flying using linear model predictive control. In *Systems conference (syscon), 2014 8th annual ieee* (pp. 18–23).

Iskandarani, M., Givigi, S. N., Rabbath, C. A., & Beaulieu, A. (2013). Linear model predictive control for the encirclement of a target using a quadrotor aircraft. In *Control & automation (med), 2013 21st mediterranean conference on* (pp. 1550–1556).

Johansen, T. A. (2004). Approximate explicit receding horizon control of constrained nonlinear systems. *Automatica*, *40*(2), 293–300.

Kalman, R. E. (1960a). Contributions to the theory of optimal control. *Bol. Soc. Mat. Mexicana*, *5*(2), 102–119.

Kalman, R. E. (1960b). A new approach to linear filtering and prediction problems. *Journal of basic Engineering*, *82*(1), 35–45.

Kang, Y., & Hedrick, J. K. (2006). Design of nonlinear model predictive controller for a small fixed-wing unmanned aerial vehicle. In *Aiaa guidance, navigation, and control conference.*

Kwon, W., Bruckstein, A., & Kailath, T. (1983). Stabilizing state-feedback design via the moving horizon method. *International Journal of Control*, *37*(3), 631–643.

Kwon, W., & Pearson, A. (1977). A modified quadratic cost problem and feedback stabilization of a linear system. *IEEE Transactions on Automatic Control*, *22*(5), 838–842.

Lee, Y., & Schetzen, M. (1965). Measurement of the wiener kernels of a non-linear system by cross-correlation. *International Journal of Control*, *2*(3), 237–254.

Luukkonen, T. (2011). Modelling and control of quadcopter. *Independent research project in applied mathematics, Espoo*.

Marasco, A. J., Givigi, S. N., & Rabbath, C. A. (2012). Model predictive control for the dynamic encirclement of a target. In *American control conference (acc), 2012* (pp. 2004–2009).

Marmarelis, V. Z. (1993). Identification of nonlinear biological systems using laguerre expansions of kernels. *Annals of biomedical engineering*, *21*(6), 573–589.

Marquis, P., & Broustail, J. (1988). Smoc, a bridge between state space and model predictive controllers: application to the automation of a hydrotreating unit. In *Proc. of the 1988 ifac workshop on model based process control* (pp. 37–43).

Marzocca, P., Librescu, L., & Silva, W. A. (2002). Aeroelastic response of nonlinear wing sections using a functional series technique. *AIAA journal*, *40*(5), 813–824.

Mathews, V. J., & Sicuranza, G. L. (2000). *Polynomial signal processing* (Vol. 27). Wiley-Interscience.

Mathisen, S. H., Fossen, T. I., & Johansen, T. A. (2015). Nonlinear model predictive control for guidance of a fixed-wing uav in precision deep stall landing. In *Unmanned aircraft systems (icuas), 2015 international conference on* (pp. 356–365).

Mathisen, S. H., Gryte, K., Fossen, T. I., & Johansen, T. A. (2016). Nonlinear model predictive control for longitudinal and lateral guidance of a small fixed-wing uav in precision deep stall landing. In *Aiaa infotech@ aerospace* (p. 0512).

Mayne, D. Q., & Michalska, H. (1990). Receding horizon control of nonlinear systems. *IEEE Transactions on automatic control*, *35*(7), 814–824.

Mayne, D. Q., Rawlings, J. B., Rao, C. V., & Scokaert, P. O. (2000). Constrained model predictive control: Stability and optimality. *Automatica*, *36*(6), 789–814.

Newcome, L. R. (2004). *Unmanned aviation: a brief history of unmanned aerial vehicles*. AIAA.

Nikolaou, M., & Mantha, D. (1998). Efficient nonlinear modeling using wavelets and related compression techniques. In *Nsf workshop on nonlinear model predictive control*.

Ogata, K., & Yang, Y. (1970). Modern control engineering.

Prazenica, R. J. (2014). Model predictive control of a nonlinear aeroelastic system using reduced-order volterra models. In *Aiaa atmospheric flight mechanics conference* (pp. 2188–2203).

Prazenica, R. J., & Kurdila, A. J. (2004). Volterra kernel identification using triangular wavelets. *Journal of Vibration and Control*, *10*(4), 597–622.

Prazenica, R. J., & Kurdila, A. J. (2006). Multiwavelet constructions and volterra kernel identification. *Nonlinear Dynamics*, *43*(3), 277–310.

Prazenica, R. J., Reisenthel, P. H., Kurdila, A. J., & Brenner, M. J. (2004). Volterra kernel identification and extrapolation for the f/a-18 active aeroelastic wing. In *Proceedings of the 45th aiaa/asme/asce/ahs/asc structures, structural dynamics & materials conference, palm springs, california* (pp. 1939–1957). AIAA.

Prett, D. M., & García, C. E. (2013). *Fundamental process control: Butterworths series in chemical engineering*. Butterworth-Heinemann.

Propoi, A. (1963). Application of linear programming methods for the synthesis of automatic sampled-data systems. *Avtomat. i Telemekh*, *24*(7), 912–920.

Qin, S. J., & Badgwell, T. A. (2003). A survey of industrial model predictive control technology. *Control engineering practice*, *11*(7), 733–764.

Rawlings, J. B., & Muske, K. R. (1993). The stability of constrained receding horizon control. *Automatic Control, IEEE Transactions on*, *38*(10), 1512–1516.

Reisenthel, P. H. (1999). Prediction of unsteady aerodynamic forces via nonlinear kernel identification. In *International forum on aeroelasticity and structural dynamics.*

Richalet, J., Rault, A., Testud, J., & Papon, J. (1976). Algorithmic control of industrial processes. In *Proceedings of the 4th ifac symposium on identification and system parameter estimation* (pp. 1119–1167).

Richalet, J., Rault, A., Testud, J., & Papon, J. (1978). Model predictive heuristic control: Applications to industrial processes. *Automatica*, *14*(5), 413–428.

Rossiter, A. (2014). *Predictive control 1 - introduction.* Retrieved from `https://www.youtube.com/watch?v=4kCcXGDvjU8&list=PLs7mcKy_nInFEpygo_VrqDFCsQVnGaoy-`

Schetzen, M. (1980). *The volterra and wiener theories of nonlinear systems.* {John Wiley & Sons}.

Scokaert, P. O., & Rawlings, J. B. (1998). Constrained linear quadratic regulation. *Automatic Control, IEEE Transactions on*, *43*(8), 1163–1169.

Seborg, D. E., Mellichamp, D. A., Edgar, T. F., & Doyle III, F. J. (2010). *Process dynamics and control.* John Wiley & Sons.

Shekhar, R. C., Kearney, M., & Shames, I. (2015). Robust model predictive control of unmanned aerial vehicles using waysets. *Journal of Guidance, Control, and Dynamics*, *38*(10), 1898–1907.

Shim, D. H., Kim, H. J., & Sastry, S. (2003). Decentralized nonlinear model predictive control of multiple flying robots. In *Decision and control, 2003. proceedings. 42nd ieee conference on* (Vol. 4, pp. 3621–3626).

Silva, W., Strganac, T. W., & Hajj, M. (2005). Higher-order spectral analysis of a nonlinear pitch and plunge apparatus. In *Proceedings of the 46th aiaa/asme/asce/ahs/asc structures, structural dynamics, and materials conference* (pp. 2005–2013).

Silva, W. A. (1993). Application of nonlinear systems theory to transonic unsteady aerodynamic responses. *Journal of Aircraft*, *30*(5), 660–668.

Singh, L., & Fuller, J. (2001). Trajectory generation for a uav in urban terrain, using nonlinear mpc. In *American control conference, 2001. proceedings of the 2001* (Vol. 3, pp. 2301–2308).

Slegers, N., Kyle, J., & Costello, M. (2006). Nonlinear model predictive control technique for unmanned air vehicles. *Journal of guidance, control, and dynamics*, *29*(5), 1179–1188.

Strganac, T. W., Ko, J., & Thompson, D. E. (2000). Identification and control of limit cycle oscillations in aeroelastic systems. *Journal of Guidance, Control, and Dynamics*, *23*(6), 1127–1133.

Subbarao, K., Tule, C., & Ru, P. (2015). Nonlinear model predictive control applied to trajectory tracking for unmanned aerial vehicles. In *Aiaa atmospheric flight mechanics conference* (p. 2857).

Volterra, V. (1887). Sopra le funzioni che dipendono da altre funzioni. *Atti della Reale Accademia dei Lincei*, *3*, 97–105.

Wang, Y., Wynn, A., & Palacios, R. (2016). Model predictive control of flexible aircraft using nonlinear reduced-order models. In *57th aiaa/asce/ahs/asc structures, structural dynamics, and materials conference* (pp. 711–722). AIAA.

Wiener, N. (1966). *Nonlinear problems in random theory.* The MIT Press.

Wray, J., & Green, G. G. (1994). Calculation of the volterra kernels of non-linear dynamic systems using an artificial neural network. *Biological Cybernetics*, *71*(3), 187–195.

Yousfi, C., & Tournier, R. (1991). Steady state optimization inside model predictive control. In *American control conference, 1991* (pp. 1866–1870).

Zhao, J., Diehl, M., Longman, R., Bock, H. G., & Schlöder, J. P. (2004). Nonlinear model predictive control of robots using real-time optimization. In *Proceedings of the aiaa/aas astrodynamics conference, providence, ri.*

## A. Numerical Values of A and B Matrices for the Aeroelastic System

At free-stream velocity of U = 6 m/s:

$$A_{U6} = \begin{bmatrix} 0 & 0 & 1 & 0 \\ 0 & 0 & 0 & 1 \\ -291.16 & -1.67 & -3.39 & 0.15 \\ 1847.66 & -40.57 & 20.22 & -6.67 \end{bmatrix} \qquad B_{U6} = \begin{bmatrix} 0 \\ 0 \\ -1.71 \\ 3.03 \end{bmatrix}$$

At free-stream velocity of U = 12.5 m/s:

$$A_{U12.5} = \begin{bmatrix} 0 & 0 & 1 & 0 \\ 0 & 0 & 0 & 1 \\ -291.15 & -13.36 & -4.02 & 0.05 \\ 1847.66 & 7.67 & 22.83 & -6.28 \end{bmatrix} \qquad B_{U12.5} = \begin{bmatrix} 0 \\ 0 \\ -7.44 \\ 13.15 \end{bmatrix}$$